MOLECULAR MECHANISMS OF GLI2 REGULATION IN OSTEOLYTIC BONE DISEASE

By

Rachelle Whitney Johnson

Dissertation

Submitted to the Faculty of the

Graduate School of Vanderbilt University

in partial fulfillment of the requirements

for the degree of

DOCTOR OF PHILOSOPHY

in

Cancer Biology

December, 2011

Nashville, Tennessee

Approved:

Professor Lynn M. Matrisian

Professor Julie A. Sterling

Professor Florent Elefteriou

Professor H. Charles Manning

Professor Ethan Lee

To my husband, Josh, I am truly undeserving,

To my son, Samuel, you have given new meaning to my life,

To my family and friends, thank you for your love and support,

and

To the Bone Center, where rigorous training helps students reach their full potential

ACKNOWLEDGEMENTS

This work was made possible through the financial support of the training grant "Microenvironmental Influences in Cancer" (Lynn M. Matrisian), Vanderbilt University Tumor Microenvironment Network grant (Lynn M. Matrisian), the Program Project "Tumor effects on the Skeleton" (Gregory R. Mundy), the RO1 "The Gli Family of Transcriptional Activators and Breast Cancer Mediated Osteolysis" (Gregory R. Mundy), and the VA Career Award "The Effect of the Tumor Microenvironment on Cancer Metastasis to Bone" (Julie A. Sterling).

I am grateful for the opportunity to have worked within the highly collaborative Department of Cancer Biology. I would like to thank the Cancer Biology administrative staff (particularly Tracy Tveit) and my committee members, as well as Drs. Charles Hong, Aubie Shaw, and Omar Franco for openly sharing their thoughts and reagents.

I would especially like to thank my mentors, Drs. Julie Sterling, Lynn Matrisian, and the late Greg Mundy for their continuous support and direction. I hope this dissertation advances the cancer and bone field that Dr. Mundy worked so hard to establish. I also thank Dr. Mundy for introducing me to Dr. Julie Sterling, who has provided advice, direction, and friendship for which I am truly grateful. I am also indebted to Dr. Lynn Matrisian, who graciously took me on as her student and provided resources, direction, and advice, without which, this dissertation would not be possible. I would also like to thank Alyssa Merkel, Javier Esparza, Barbara Rowland, and Dr. Dan Perrien for their wonderful technical expertise and support.

Lastly, I would like to thank my husband, parents and sister for their continuous support of my education. My parents and sister, for encouraging and supporting me throughout the years, and my husband, Josh, for making the ultimate sacrifice by leaving his home state and family to pursue this adventure with me, and for providing for me and our son, Samuel.

TABLE OF CONTENTS

LIST OF TABLES

Page

LIST OF FIGURES

Page

LIST OF ABBREVIATIONS

Hh	Hedgehog
Bmp	Bone morphogenetic protein
Tgf-β	Transforming growth factor-beta
PTH	Parathyroid hormone
PTHrP	Parathyroid hormone-related protein
Ihh	Indian hedgehog
LRP5/6	Low density lipoprotein receptor-related protein 5/6
RANKL	Ligand for receptor activator of NFκB
M-CSF	Macrophage-colony stimulating factor
OPG	Osteoprotegerin
IFNγ	Interferon gamma
TNF	Tumor necrosis factor
HHM	Humeral hypercalcemia of malignancy
PTHR1	PTH receptor 1
CaR	Calcium-sensing receptor
Ptch	Patched
SBE	Smad-binding element
TBE	TCF-binding element
Smo	Smoothened
SuFu	Suppressor of fused
GANT58/61	Gli antagonist
DNRII	Dominant negative TGF-β receptor type II
VEGF	Vascular endothelial growth factor
Tgf-α	Transforming growth factor-alpha
SCC	Squamous cell carcinoma
Dkk1	Dikkopf1
MM	Multiple myeloma
sFRP2	Secreted frizzled-related protein 2
IL-8	Interleukin-8
MMPs	Matrix metalloproteinases
ET-1	Endothelin-1
ECM	Extracellular matrix
ROCK	Rho kinase
SDF-1	Stromal derived factor-1
CXCR4	C-X-C chemokine receptor type 4
CXCL12	C-X-C chemokine ligand 12
IL-6	Interleukin-6
ER-α	Estrogen receptor-alpha
TβR-I	Tgf-β receptor type 1
TβR-II	Tgf-β receptor type 2
Fz	Frizzled
Dsh	Disheveled
APC	Adenomatous polyposis
GSK3-β	Glycogen synthase kinase-3-beta

CK1	Casein kinase 1
TCF	T-cell factor
LEF	Lymphoid enhancer factor
MMTV-LTR	Mouse mammary tumor virus-long terminal repeat
ALP	Alkaline phosphatase
β-TRCP	Beta-transducin repeat-containing protein
CaMKII	Calcium/calmodulin-dependent kinase II
MDSCs	Myeloid derived suppressor cells
H+E	Hematoxylin and eosin
TRAP	Tartrate-resistant acid phosphatase
ROI	Region of interest
GFP	Green fluorescent protein
PET	Positron emission tomography
RFP	Red fluorescent protein
NIR	Near-infrared
PBR	Peripheral benzodiazapene receptor
FMT	Fluoresence molecular tomography
microCT	Micro-computed tomography
FDG	^{18}Fluorin-fluorodeoxyglucose
microSPECT	Micro-single photon emission computed tomography
^{99m}TC-MDP	Technetium methylene diphosphate
MRI	Magnetic resonance imaging
ADC	Apparent diffusion coefficient
DCE	Dynamic contrast enhanced
MALDI	Matrix-assisted later desorption/ionization
6-TG	6-Thioguanine
RT-PCR	Reverse transcriptase-polymerase chain reaction
Q-PCR	Quantitative real-time RT-PCR
LiCl	Lithium chloride
DMSO	Dimethyl sulfoxide
PA	Polyacrylamide
TCPS	Tissue culture polysterene
Fbn	Fibronectin
CTNNB1	Catenin, beta 1 (β-catenin)
PBS	Phosphate buffered saline
Gli2-Rep	Gli2 repressor construct
HU	Hounsfield units
SEM	Standard error mean
fpVCT	Flat-panel detector-based volume computed tomography
RFU	Relative fluorescent units
BV/TV	Bone volume/total tissue volume
ZA	Zoledronic acid
SFM	Serum-free medium
WT	Wild-type GLI2 promoter
mSmad	GLI2 promoter with mutated SBE
mTCF	GLI2 promoter with mutated TBE

CHAPTER I

INTRODUCTION

Impact of solid tumor metastasis to bone

Cancer metastasis to bone is a common problem in patients with metastatic tumors such as breast, prostate, and lung cancers. For example, it is estimated that 70% of patients with metastatic breast cancer and 90% of patients with metastatic prostate cancer will develop tumors in bone (1), and while 5-year survival rates remain high for breast tumors confined to the primary site, these rates decline by a staggering 62% when patients develop distant metastases (2009, ACS Cancer Facts & Figures). Once tumors have established in bone they disrupt normal bone remodeling that can result in an excess of poorly formed bone (osteoblastic-prostate) or the destruction of bone (osteolytic-breast and lung), though most patients display a mixture of both. This disruption in normal bone homeostasis increases patient risk of developing fractures, bone pain, spinal cord compression, and hypercalcemia (2), resulting in a dramatic decrease in quality of life and poor clinical outcome. Hypercalcemia, which can lead to liver failure, coma and death (3), is of particular concern in these patients due to the extent of calcium resorption throughout the skeleton. The current standard of care for these patients is bisphosphonate treatment, which may cause such negative side effects as osteonecrosis of the jaw (4) and increased atypical fractures (5), emphasizing the importance of finding new therapeutic targets to treat bone metastases. Importantly, once tumor cells metastasize to bone they become incurable, and while treatments have improved, the patients will eventually die from the disease.

Normal bone remodeling

When breast tumor cells metastasize to bone, they disrupt normal bone remodeling, or the coupling of osteoblast-induced bone formation and osteoclast-mediated bone resorption. Bone remodeling is a continuous process that occurs over the entire skeleton and throughout a person's lifetime to regulate bone homeostasis (6). Although the exact mechanisms that initiate normal bone remodeling are unknown, it has been proposed that osteoclast precursors are recruited from the bone marrow or capillaries to initiate bone turnover, where they differentiate into mature osteoclasts and simultaneously begin resorbing bone and recruiting osteoblast precursors (osteoprogenitors) (6). Once differentiated, osteoblasts replace the resorbed section of bone with new matrix, and mineralization completes the process (6).

Osteoblasts

There are a number of signaling pathways which drive pluripotent mesenchymal stem cells within the bone marrow to differentiate into osteoblasts, including Hedgehog (Hh), bone morphogenetic protein (Bmp), transforming growth factor-beta (Tgf-β), parathyroid hormone-related protein (PTHrP) and Wnt signaling, which drive osteoblast maturation at various stages. Osteoblasts (bone forming cells) and chondrocytes (cartilage forming cells), share a common osteo-chondrogenic precursor. This precursor cell shifts toward the osteoblast lineage when osteoblast differentiation factors are turned on, such as Runx2, which is considered a "master switch" of osteoblast differentiation, since Runx2-/- mice lack osteoblasts throughout the skeleton (7), a phenotype that has yet to be matched when other factors driving differentiation are knocked out.

Indian hedgehog (Ihh) signaling has been identified as a major component of osteoblast differentiation in endochondral bone formation, since Ihh knockout mice lack osteoblasts in the

long bones (8, 9). Tgf-β and Bmps, which are members of the Tgf-β superfamily, signal through Smad proteins. Bmps are required for skeletal formation during development, and conditional knockout mice have shown that these mice have skeletal abnormalities (10). Tgf-β signaling in bone is a more complicated story, which mimics its biphasic role in cancer where Tgf-β is protective against metastasis at the primary site, but promotes invasion and metastasis in later stages of disease. Tgf-β signaling through activation of Smad3 has been shown to enhance bone mineralization (11), but others have found that Tgf-β inhibition using small molecule inhibitors results in enhanced bone formation (12, 13). In addition to Tgf-β signaling, PTHrP is critical for bone formation, and PTHrP knockout mice experience a postnatal death (14) and transgenic mice display shortened limbs due to defects in the growth plate (15). Wnt signaling defects have been widely associated with skeletal defects and alterations in osteoblast differentiation. Specifically, β-catenin has been identified as an important component in driving osteo-chondroprogenitor cells away from the chondrocyte lineage and toward osteoblast differentiation (16, 17), and mutations in the Wnt signaling receptor low density lipoprotein receptor-related protein 5 (LRP5) are associated with bone disease resulting in high or low bone mass (18-20). Importantly, most of the signaling pathways that regulate osteoblast differentiation and maturation form multiple signaling loops and crosstalk extensively, which highlights the frustration and complexity of targeting a single signaling pathway in bone disease.

Osteoclasts

Osteoclasts arise from monocytic precursors stimulated by two separate factors, the ligand for receptor activator of NFκB (RANKL) and macrophage-colony stimulating factor (M-CSF), which are sufficient to drive osteoclastogenesis. Another important factor regulating osteoclast formation is osteoprotegerin (OPG), which is a high affinity decoy receptor for RANKL

secreted by osteoblasts along with RANKL. There are a number of cytokines which have been identified as regulators of osteoclasts such as interferon γ (IFNγ), but much of the data is in conflict with previously published studies or those conducted in humans (21-23). 1,25-dihydroxyvitamin D regulation of the osteoclast is slightly more straight-forward, in that vitamin D up-regulates RANKL mRNA expression and inhibits OPG and PTH production (24, 25), but studies in humans indicate that high levels of vitamin D are osteolytic. It is also now evident that estrogen (E_2) affects T cell secretion of tumor necrosis factor (TNF) and RANKL, which is a member of the TNF superfamily (23).

Breast tumor cells can disrupt the tightly regulated process of osteoblast and osteoclast coupling by antagonizing differentiation and activity on multiple levels and at numerous skeletal locations, which may cause the normal bone remodeling process to preferentially favor bone resorption or bone formation. Although patients may have both increased bone formation (osteoblastic) and increased bone resorption (osteolytic) at different sites of skeletal metastasis, breast cancer patients most frequently present with primarily osteolytic metastases which result from tumor cell activation of osteoclasts by both direct and indirect mechanisms.

Concept of the vicious cycle

Dr. Gregory Mundy coined the term "vicious cycle" approximately 20 years ago to refer to the important interactions between tumor cells and the bone micro-environment. In this model, factors from the tumor stimulate osteoclast-mediated bone destruction, which results in growth factors being released from the bone to stimulate further growth of the tumor cells and thus the production of more tumor-derived osteolytic factors (Figure 1) (26).

While the concept is overly simplified in order to illustrate the hypothesis, the vicious cycle has held up well over the past 20 years with the mechanistic and clinical data collected.

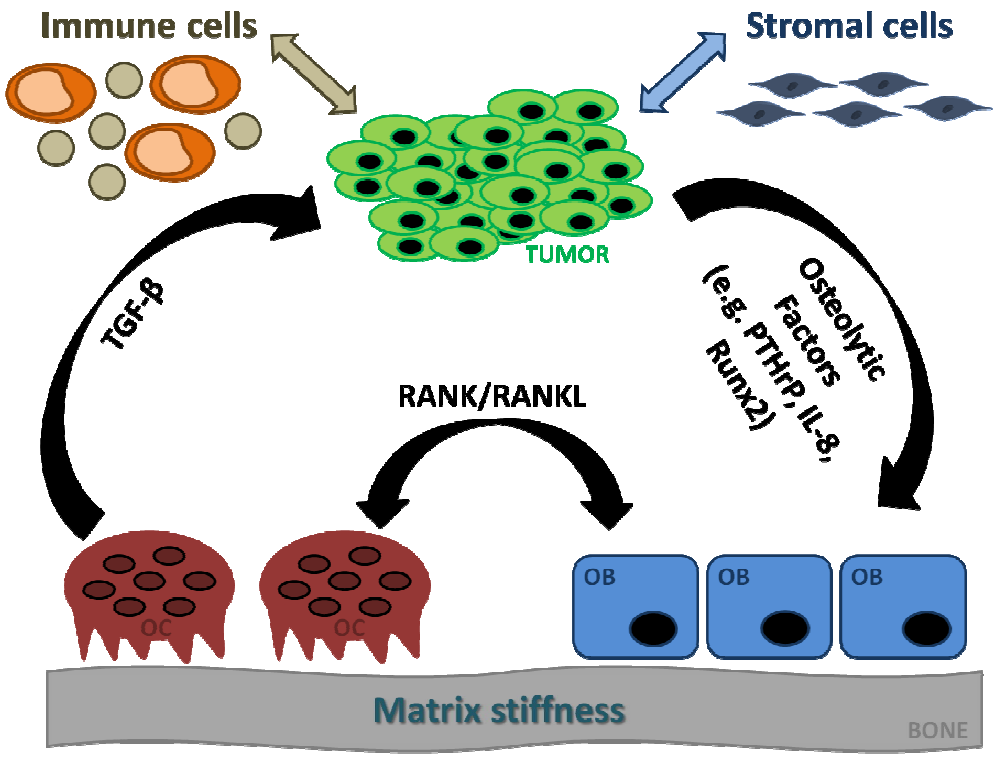

Figure 1. The vicious cycle of bone destruction. Tumor cells which metastasize to bone may secrete osteolytic factors which signal to osteoblasts to up-regulate expression of RANK. This results in increased osteoclastogenesis through RANK/RANKL signaling and the resorption of mineralized bone matrix, which releases active Tgf-β into the tumor-bone micro-environment and can result in enhanced proliferation of tumor cells and further secretion of osteolytic factors. Host stromal and immune cells further impact tumor cell behavior and their effects on bone.

This is especially true in studies using osteoclast inhibitors, such as bisphosphonates. These studies have demonstrated that inhibiting the bone resorption phase also reduces the tumor burden. While there is disagreement in the field as to whether bisphosphonates directly inhibit tumor cell growth, it is clear that inhibiting bone resorption inhibits tumor cell growth (4). Furthermore, inhibiting tumor-produced factors such as PTHrP inhibits bone destruction and further tumor growth (27, 28).

Our notion of the vicious cycle continues to emerge as we learn more about the interactions between tumor cells and the bone. It has become clear that many factors within the bone micro-environment interact with the tumor cells, and that these interactions are far more complicated than the original vicious cycle model alone can explain. For example, we now know that tumor cells can closely interact with osteoblasts (29-31), bone stroma (32), and immune cells (33, 34).

Molecular mechanisms of bone metastasis (osteolytic)

Breast and lung tumor metastasis to bone frequently results in significant osteolytic bone destruction through activation of osteoclasts in bone. Tumor cells which establish in bone up-regulate the expression and secretion of osteolytic factors which stimulate RANKL expression in osteoblasts and results in osteoclast activation through RANKL/RANK binding. PTHrP has been identified as a major osteolytic factor produced by tumor cells to activate bone destruction (26, 35), and our group has identified the developmental transcription factor Gli2, among other factors, as a key regulator of PTHrP transcription and secretion (36).

PTHrP discovery

PTHrP was originally identified as a novel mediator of humoral hypercalcemia of malignancy (HHM) when it was isolated from a human lung cancer cell line (37). The initial discovery of PTHrP identified a pre-pro-peptide and mature protein with homology to human PTH at the N-terminal end. However, the C-terminus differed significantly from PTH, suggesting an evolutionary mechanism of gene duplication. Indeed, the chromosomes on which PTH and PTHrP reside, chromosome 11 and 12, respectively, are evolutionarily related, and the authors believe that the more complicated primary structure of PTHrP suggests it is the original gene (37-41). In addition to its numerous introns and exons, PTHrP possesses three separate promoters which produce three isoforms of PTHrP (1-139),(1-141), and (1-173) (42, 43), which all have similar function, although isoform (1-139) appears to be the most potent inducer of osteolysis in a mouse model of breast cancer metastasis to bone (44). It should be noted that the gene expression assays utilized to complete this dissertation detect all three isoforms of PTHrP. All isoforms of PTHrP, as well as PTH, function through binding and activation of the G-protein coupled receptor PTH receptor 1 (PTHR1).

Shortly after the identification of PTHrP, immunohistochemical analyses of breast cancer patients found that PTHrP was present in 60% of tumors but not in matched normal breast tissue (45) and correlated positively with patient prognosis. Further analyses revealed that PTHrP was expressed in 92% of breast tumors in bone, compared with only 17% of breast tumors in non-bone sites (46). Taken together, these data indicated that PTHrP expression at the primary site is a positive prognostic indicator and negatively correlates with PTHrP expression in breast tumors in bone, where it may create a favorable niche for tumor growth. A

number of clinical studies have since confirmed the initial observations of differential PTHrP expression in cancer patients (47-50).

PTHrP in the growth plate

In addition to its role in breast cancer bone metastasis, PTHrP plays a significant role in bone formation through osteoblast regulation, as previously discussed, and growth plate chondrogensis downstream of Ihh signaling (51). As previously discussed, PTHrP knockdown results in shortened limbs and postnatal death (14), which is in large part due to altered chondrocyte differentiation. Immature proliferating chondrocytes normally secrete PTHrP in response to Ihh derived from differentiating hypertrophic chondrocytes, which express the PTHrP receptor PTHR1. PTHrP, having been stimulated by Ihh signaling, acts back on the proliferating and prehypertrophic cells to slow their differentiation into hypertrophic cells, creating a negative feedback loop (52). Thus, knockdown of PTHrP results in more chondrocyte hypertrophy and less cartilage formation.

PTHrP in mammary development

In relation to its involvement in bone, a significant role for PTHrP has been discovered in mammary development and lactation. PTHrP has been found both to be expressed in the lactating breast (53) and secreted into breast milk (54), and it is a critical component of mammary mesenchyme differentiation. Specifically, epithelial cells within the mammary bud express PTHrP, which signals via the PTHR1 to the surrounding mesenchyme that is responsible for ductal outgrowth (55). Accordingly, PTHrP knockdown mice lack mammary glands due to interrupted PTHrP/PTHR1 signaling (56). Interestingly, PTHrP that is secreted into breast milk is believed to promote bone resorption in order to supply enough calcium for milk production, as evidenced by decreased bone turnover in mice with mammary specific knockdown of PTHrP

(57). PTHrP-stimulated resorption is regulated through expression of the calcium-sensing receptor (CaR), which is also expressed in the lactating breast and inhibits PTHrP secretion in a feedback mechanism (58).

Gli2 signaling

PTHrP is regulated through a number of mechanisms, some of which include Gli2 and Tgf-β effects on PTHrP expression, activity, and stability. Recent studies have pinpointed the Hh transcription factor GLI2 as a major regulator of PTHrP. Specifically, chondrocytes in bones harvested from GLI2 embryonic lethal knockout mice showed decreased expression of Ihh, Patched (Ptch) and PTHrP (59). Based on these data and the involvement of PTHrP in tumor-induced osteolysis, the relationship between Gli2 and PTHrP was further explored in osteolytic and non-osteolytic breast cancer models (36). Interestingly, Gli2 was found to be up-regulated in osteolytic breast cancer cells which expressed PTHrP and metastasized to bone resulting in osteolytic lesions (36). Gli2 is regulated in large part by the Hh signaling pathway during development, and Dennler and colleagues have shown that the GLI2 promoter in keratinocytes and hepatocellular carcinoma contains a Smad-binding element (SBE) and TCF-binding element (TBE), implicating Tgf-β and Wnt signaling as co-regulators of GLI2 transcription (60). Additionally, we have shown that Gli2 expression in osteolytic tumor cells is regulated by a number of factors independent of Hh signaling, such as Tgf-β (61). Gli2 was found to be necessary for Tgf-β stimulation of PTHrP mRNA expression, and is therefore an excellent target in blocking osteolysis. Gli2 blockade has indeed been successful in blocking osteolytic bone destruction in a genetic model (61), and studies are underway to inhibit Gli proteins through small molecules, such as the GANT compounds (62) and *Excoecaria agallocha* (*E. agallocha*) extracts from Japanese herbals (63). The effectiveness of Gli2 blockade in decreasing osteolysis

introduces the possible involvement of Gli2 in metastasis; although there is currently no evidence to suggest that Gli2 regulates genes important for osteotropism (64), Tgf-β regulation of Gli2 opens up the possibility that Gli2 may still play a role in metastasis to bone.

Canonical Hh signaling occurs through Hh ligand binding to the membrane receptor Patched (Ptch), which releases inhibition of a second membrane receptor, Smoothened (Smo). This release initiates a downstream signaling cascade resulting in translocation of the Gli family proteins to the nucleus, where they can initiate transcription (65). Gli proteins have been demonstrated to be up-regulated in a number of tumor types, including medulloblastoma and those of the prostate, pancreas, and lung, suggesting that Gli may play an important role in tumorigenesis; however, the mechanisms resulting in Gli up-regulation can vary from inactivating mutations of Ptch to activating mutations of Smo or Suppressor of Fused (SuFu) (66).

Since Gli proteins are up-regulated in tumors of different origins, a number of screens have been developed to identify Hh signaling inhibitors. The most notable and widely-used of these inhibitors is cyclopamine, a potent Smo receptor antagonist reported to work in tumor models with varying levels of success (67, 68). More recently, a cell-based screen by Lauth and colleagues uncovered two antagonists of Gli signaling, GANT58 and GANT61, which have been shown to inhibit prostate cancer cell growth in a subcutaneous prostate tumor model which also expresses PTHrP (62) and can inhibit activation of Hh target genes despite potential upstream mutations in the signaling pathway. While the mechanism is unclear, these compounds are believed to block Gli1 translocation to the nucleus, and may therefore also block Gli2 since it is similar in structure to Gli1. The success of Gli antagonists in primary xenograft tumor growth suggests that GANT molecules may also be beneficial in treating osteolytic bone metastases by

both blocking tumor-induced bone destruction and inhibiting cell growth. Furthermore, the investigation of these small molecule inhibitors on tumor-induced bone disease may provide a novel therapeutic target for blocking osteolysis.

Tgf-β signaling

We and others have shown that Tgf-β impacts PTHrP expression both *in vitro* and *in vivo* (61, 69). Specifically, MDA-MB-231 human osteolytic breast tumor cells made unresponsive to Tgf-β signaling through expression of a dominant negative TGF-β receptor type II (DNRII) showed a significant reduction in PTHrP secretion and exhibited significantly smaller osteolytic lesions in a mouse model of breast cancer metastasis to bone (69). Accordingly, our data has shown that in addition to regulating PTHrP secretion, Tgf-β alters PTHrP mRNA expression and, furthermore, that its effects are mediated through Gli2 (61). Our group has also found that Tgf-β inhibition using a neutralizing antibody against the Tgf-β ligands blocks tumor-induced osteolysis and reduces PTHrP activity and mRNA expression, although these data are not yet published (Biswas et al., *submitted*).

Tgf-β and mRNA stability

In addition to regulating PTHrP mRNA expression and secretion, Tgf-β signaling is known to play a significant role in messenger RNA stabilization and turnover (70). Newly transcribed RNA is subjected to a number of post-transcriptional modifications before leaving the nucleus, such as 5' methyl-capping, splicing, cleavage, and polyadenylation to prevent proteasomal degradation (71), where the modified transcript then enters the cytoplasm and interacts with mRNA binding proteins, including Tgf-β.

Regulators of PTHrP mRNA stability include 1,25 Dihydroxyvitamin D_3, the hormonally active form of Vitamin D, which decreases both PTHrP mRNA expression and stabilization through a vitamin D response element in prostate cancer (72), and von Hippel-Lindau tumor suppressor protein, which negatively regulates PTHrP mRNA stability through the RNA binding protein HuR, which is also known to bind and stabilize VEGF, Tgf-α, and Tgf-β (73, 74). Previous reports have suggested that Tgf-β signaling may play a crucial role in regulating PTHrP mRNA stability (75-77); however, there are conflicting published data concerning Tgf-β stabilization of PTHrP transcript (78). For example, when SCC2/88 cells were treated with Tgf-β1, PTHrP production was increased, but there was no effect on mRNA stability; however, when the 3'-UTR of PTHrP transcript was truncated, Tgf-β treatment stabilized the message due to decreased binding to the coding region (79, 80). Conversely, when PTHrP mRNA stability was examined in keratinocytes following treatment with exogenous Tgf-β, PTHrP mRNA stability was significantly up-regulated (76). Therefore, it is likely that Tgf-β effects on PTHrP message stability is highly dependent on the cell type being used and the precise processing of PTHrP in these cells.

Wnt signaling

Deregulated Wnt signaling has been implicated in the pathogenesis of a number of different tumor types, including tumors of the breast and prostate. However, there is little data on Wnt signaling in these tumor types once they have reached the bone marrow. Conversely, Wnt signaling components, in particular Dkk1, have been identified as key regulators of Multiple Myeloma (MM)-induced bone disease. MM is a malignancy of the plasma cells with significant bone involvement and osteolytic disease, resulting from a combination of suppressed bone formation and enhanced bone resorption. Dkk1 inhibits Wnt signaling, which is important in osteoblast differentiation. Studies have shown that inhibition of Dkk1 reduces tumor burden

and enhances bone formation in mouse models of MM (81). In addition to Dkk1, secreted frizzled-related protein 2 (sFRP2) is produced by MM cells and blocks osteoblast differentiation (82). Interestingly, very recent data has indicated that sFRP1, 2, 4 and 6 are also produced by MM cells, and that hypermethylation of their respective promoters frequently occurs in patients. Indeed, this epigenetic regulation of sFPR2 occurs in up to 52.6% of patients with MM (83). However, considering that up to 70% of MM patients have skeletal involvement and that Wnt signaling inhibition in mouse models results in increased bone formation (84), the dual roles of Wnt signaling in MM remains to be sorted out.

Other osteolytic factors (MMPs, RANKL, IL-8, Runx2)

PTHrP remains the most well studied of the osteolytic factors produced by bone metastatic tumor cells, but there are other molecules which contribute significantly to tumor-induced bone destruction, such as RANKL, IL-8, Runx2, and the matrix metalloproteinases (MMPs). Interleukin-8 (IL-8) expression in tumor cells has been shown to correlate with increased bone metastases in human breast cancer cells (85) and stimulate osteoclastogenesis independent of osteoprotegerin (OPG) (86) and RANKL (87). Runx2, which is required for normal bone formation, is elevated in breast and prostate tumors and cells which metastasize to bone, and inhibition of Runx2 in breast tumor cells inhibits tumor-induced bone destruction (88). This inhibition is in part due to alterations in MMP-9 signaling, which is downstream of Runx2, and is important for tumor cell invasive properties (89). There is also evidence to support significant involvement of MMPs in regulating tumor-bone interactions. For example, MMP-7 has been shown to enhance osteolysis through solubilization of osteoblast-derived RANKL in the PC-3 prostate cancer model of bone destruction (90), and was found to play a similar role in breast tumor-induced osteolysis (91).

Molecular mechanisms of bone metastasis (osteoblastic)

Some cancers such as prostate, and less frequently breast, induce osteoblastic bone disease upon metastasis to bone. The mechanism driving the formation of osteoblastic lesions is unclear, but bone resorptive markers are often elevated in these patients, suggesting that osteoclast activation may still be necessary for the formation of osteoblastic lesions. Similar to patients with primarily osteolytic bone metastases, prostate cancer patients frequently present with mixed lesions throughout the skeleton. It is believed that at least in some cases, osteoblastic metastases begin with a heavy resorption component then switch to blastic lesions. This is further supported by the successful use of bisphosphonates, which inhibit osteoclast activity, in the treatment of prostatic bone metastases and associated bone pain (92).

The molecular mechanisms which stimulate bone formation in osteoblastic metastases remain largely undiscovered, but there is evidence to suggest that endothelin-1 (ET-1) and the Wnt signaling pathway make significant contributions. Dkk1 is a downstream target and inhibitor of the Wnt signaling pathway, and has been shown to inhibit prostate tumor-induced osteoblastic metastases when over-expressed in prostatic tumor cells by inhibiting TCF activity in osteoblast precursors (93); conversely, Dkk1 has been identified as a mediator of tumor-derived ET-1-induced bone formation (94), suggesting an autocrine loop in which Dkk1 and ET-1 up-regulate one another. Differences here may be attributable to cell-line specificity, since Thudi et al utilized ACE-1 prostate tumor cells, and Clines et al did not test his model in tumor cells. More data is needed to determine the extent of ET-1 regulation of Wnt signaling.

Tumor micro-environment regulation of bone disease

Certain tumor types rely heavily on autocrine signaling, but cancer cells are not as autonomous as once thought. In recent years, increasing emphasis has been placed on tumor

micro-environment influence on tumor cell behavior and the interactions between tumor cells and the stroma in particular. It has become evident that the micro-environment plays a tremendous role in both promoting and hindering tumor progression at different sites of the disease. While the host micro-environment significantly impacts tumor cell evolution, cancer cells may also influence host cells at the site of metastasis in addition to systemic alterations. This is particularly evident in the vicious cycle of bone destruction which requires extensive interactions and complex signaling between tumor cells, bone, and the bone marrow stroma. While there are numerous interactions occurring within the bone micro-environment, some of the micro-environmental factors which have been identified as significant mediators of tumor host interactions include matrix stiffness, the reactive stroma surrounding the tumor, Tgf-β, Wnt signaling, and Ephrins.

Stiffness and the extracellular matrix

The extracellular matrix (ECM) has long been thought of as a structural scaffold on which tumor cells could rely on for support, but there is now substantial evidence to suggest that breast tumor cells modify their behavior in response to ECM signaling and the changing stiffness of the ECM at the primary site (95). In the primary site of breast cancer, tumor progression has been connected with increased collagen crosslinking as well as integrin activation (96), and our group has shown that the rigidity of bone modulates tumor cell gene expression in a ROCK-dependent mechanism (97). These data show that osteolytic tumor cells detect the rigidity of the substrate upon which they are plated, and up-regulate gene expression as rigidity increases (97). These are key data in identifying the point at which tumor cells "turn on" PTHrP expression, since they demonstrate that osteolytic tumor cells require stiffness on the order of magnitude of bone in order to secrete biologically significant amounts of PTHrP.

The response of tumor cells to the physical micro-environment is complex and still actively being explored.

Stroma and fibroblasts

Much of the signaling which modulates tumor cell behavior in bone originates from the surrounding stroma. The contribution of the reactive stroma in tumor cell evolution has been well established, particularly in prostate cancer through studies conducted by the Cunha and Hayward groups (98, 99), but the impact of bone stroma in particular on tumor cell behavior is becoming appreciated. Most of the published data supports a significant role for bone-derived growth factors and chemokines (e.g. Tgf-β, SDF-1/CXCR4) (32, 100, 101), and an emerging role for immune cells such as MDSCs. It is well established that stromal derived factor-1 (SDF-1/CXCL12) is involved in tumor cell homing to bone (102), where it has been shown that bone metastatic breast cancer cells express elevated levels of the SDF-1 receptor CXCR4 (64, 103), and conditioned media from primary human bone marrow contains CXCL12 (103), which presumably promotes metastasis to bone. Indeed, tumor cell migration can be blocked when the CXCR4/CXCL12 interactions are blocked by a neutralizing antibody against CXCR4 (103).

Fibroblasts isolated from common sites of breast cancer metastasis (e.g lung, liver and bone) have also been shown to promote tumor cell growth more effectively than skin fibroblasts and do so in an IL-6-dependent manner (104), which strongly supports the idea of the pre-metastatic niche. These data are further supported by data from Bob Weinberg's group, showing that bone marrow-derived mesenchymal stem cells increase the aggressiveness of weakly metastatic breast carcinoma cells (105). Interestingly, fibroblasts appear to have the largest impact on breast cancer cell lines which are estrogen receptor-alpha (ER-α) positive (106), despite most breast cancer cells which metastasize to bone being ER negative. This is

suggestive of distinctive and separate properties of fibroblasts in the primary site of disease and the bone marrow. Accordingly, there is evidence that stromelysin-3, which facilitates tumor cell metastasis, is induced by Tgf-β in fibroblasts to promote tumor cell homing to the bone (107).

Tgf-β signaling

Tgf-β signaling is known to regulate such cell autonomous events as proliferation, migration, apoptosis, and tumor invasion (108), and has been shown to directly promote tumor cell growth in bone following release from the mineralized bone matrix (26). Interestingly, these same processes are controlled during development in part by the Wnt signaling pathway (109), which has been identified as an important stromal component in metastatic prostate cancer (110). Convergence of Tgf-β and Wnt signaling has been repeatedly demonstrated at the transcriptional level on the Gli proteins, which are downstream of the Hh signaling pathway during development. Previous reports have indicated that Wnt signaling can both regulate and be regulated by Gli proteins (111), although most publications place Hh signaling upstream of Wnt during development (112, 113). Likewise, Hh and Tgf-β signaling have been reported to crosstalk (108), and our group as well as others has reported that GLI2 transcription is regulated at least in part by Tgf-β signaling through Smads (61, 114), indicating the importance of this crosstalk for regulating bone destruction.

Tgf-β signaling involves three separate isoforms (Tgf-β1, 2 and 3) and two distinct serine/threonine kinase receptors, type I Tgf-β receptors (TβR-I) and type II Tgf-β receptors (TβR-II). The signaling cascade initiates when Tgf-β1 ligand binds the TβR-II, and TβR-I is then recruited to the complex. TβR-II phosphorylates TβR-I, which in turn phosphorylates and activates the Smad2 and Smad3 molecules. These activated Smads then bind Smad4, which facilitates nuclear translocation and activation of transcriptional targets (70).

Canonical Wnt signaling

Human osteolytic MDA-MB-231 breast cancer cells, which are frequently used as a model of breast cancer metastasis to bone when inoculated by cardiac injection, are both Tgf-β responsive and active Wnt signalers. Canonical Wnt signaling is activated when one or more Wnt ligands bind to the cell surface receptors frizzled (Fz) and low-density lipoprotein receptor-related protein 5 or 6 (Lrp5/6) and trigger a downstream signaling cascade. In the absence of signal, disheveled (Dsh), Axin, tumor suppressor adenomatous polyposis coli (APC) and glycogen synthesis kinase-3-β (GSK3-β) complex together in the cytoplasm, which facilitates GSK3-β and casein kinase 1 (CK1) phosphorylation of β-catenin and its subsequent proteasomal degradation (115). Once Wnt signaling is turned on, Axin is recruited to Lrp5/6 at the cell membrane and the Dsh-Axin-APC-GSK3-β complex is dispersed, causing β-catenin stabilization and translocation to the nucleus to activate the transcription factors T-cell factor (TCF)and lymphoid enhancer factor (LEF) and initiate transcription (115, 116).

Aberrant Wnt signaling has been implicated in a number of tumor types, including breast cancer, but genetic mutations which result in Wnt activation are rarely found in breast cancer patients (117). Conversely, β-catenin stabilization is often found in breast cancer, and still results in activation of Wnt target genes (117). There are a number of genetic mouse models which result in Wnt activation and/or β-catenin stabilization. For example, the MMTV-LTR model, which drives the expression of activated β-catenin in the mouse mammary gland, results in the development of mammary carcinoma similar to tumors observed in MMTV-Wnt mice (118). More recently, Wnt signaling has been identified as a key regulator of cancer stem cell proliferation, making it a promising target in breast cancer therapy (119).

Importantly, Wnt signaling plays a significant protective role in bone homeostasis. Mouse genetic models in particular have demonstrated its importance, showing that LRP5-/- mice exhibit a low bone mass phenotype and decreased pre-osteoblast proliferation (120). Even more valuable than the mouse genetic studies are the clinical data documenting patients with LRP5 activating mutations resulting in a high bone-mass phenotype and enhanced osteoblast proliferation (18, 19). These phenotypes are likely due to alterations in normal Wnt signaling, since it has been shown that canonical Wnt signaling also up-regulates osteoblast production of OPG, a decoy receptor for RANKL, and down-regulates RANKL, indirectly affecting osteoclastogenesis (121). Indeed, Wnt signaling activation through APC inactivation results in increased bone formation and a dramatic reduction in osteoclasts (122). Further studies have shown that Bmp2 promotes new bone formation in part by targeting alkaline phosphatase (ALP) and activating a Wnt signaling autocrine loop in pre-osteoblasts (123), and Bmp2 crosstalks with Wnt signaling to promote osteoblast differentiation by stimulating LRP5 expression and inhibiting β-TRCP, the ubiquitin ligase which targets β-catenin for degradation (124). Canonical Wnt signaling has also been shown to target ALP in the presence of Bmp4 (125), as well as up-regulate Runx2 expression and activity, which are critical for osteoblast differentiation and normal skeletal development (126).

Non-canonical Wnt signaling

The non-canonical Wnt signaling pathway, which can be broken down into several branches including the Planar Cell Polarity and Wnt/Ca^{2+} pathways, signals through Fz independent of Lrp5/6 and leads to activation of Dsh. In the Planar Cell Polarity pathway, Dsh activates the small GTPases Rho and Rac downstream, which can activate Rho kinase (ROCK) and myosin to mediate effects on the actin cytoskeleton. The Wnt/Ca^{2+} pathway is mediated

through trimeric G proteins and Dsh induction of Ca^{2+} release and activation of protein kinase C (PKC) and calcium/calmodulin-dependent kinase II (CamKII) (127). Interestingly, the non-canonical Wnt signaling pathway has also been identified as a positive regulator of bone formation. For example, mice that are heterozygous for Wnt5a, a Wnt more commonly associated with non-canonical Wnt signaling activation, exhibit decreased bone mass and a reduction in osteoblast number. This phenomenon appears to be tightly correlated with the extent of adipogenesis in the bone marrow, since Wnt5a+/- mice have elevated adipocyte numbers (128). Further data indicate that Wnt5a represses PPARγ-induced adipogenesis in MSCs, tilting MSC differentiation toward Runx2 activation and osteoblastogenesis (128). There is an overwhelming consensus that non-canonical Wnt signaling has a significant impact on bone formation, but much of the data supporting this has yet to be discovered. Based on the current data, it appears that non-canonical Wnt signaling has a considerable effect on MSC fate and differentiation, which will likely have a significant effect on osteoblast biology.

Ephrins

Ephrin/Eph signaling has been identified as an important mediator in tumor promotion and angiogenesis, and preclinical studies have shown soluble EphB4 and EphB4 neutralizing antibody to be efficacious treatment in breast and prostate solid tumors (129, 130); however, disruption of Ephrin/Eph family signaling results in skeletal abnormalities and increased bone resorption by disrupting coupling between osteoblasts and osteoclasts which is required for normal bone modeling (131-133). Further studies are needed to determine whether blockade of Ephrin/Eph signaling is detrimental in patients with potential bone metastatic disease, but it remains possible that Ephrin/Eph signaling, similar to Tgf-β, may play a biphasic role in tumor metastasis.

Immune cells

Immune cells such as myeloid derived suppressor cells (MDSCs) have been implicated in tumor promotion and metastasis to distant organs (33), and more recently these cells have been suspected to play a key role in tumor metastasis to bone (134). For example, it has been previously demonstrated that Gr-1^{+} CD11b^{+} MDSCs are capable of differentiating into osteoclasts in the 5T model of multiple myeloma (134), but further studies are needed to determine if this same potential exists in solid tumor metastasis to bone. More recent data examining CD8+ T cells in breast tumor metastasis to bone suggests that immune cells influence tumor cell metastasis independent of tumor effects on bone, specifically showing that osteoclast activation of T cells reduces tumor burden but increases osteolysis (135). As indicated by Fowler et al, the B cell population may be an important factor in the development of myeloma, since RAG-2-deficient mice which lack B cells develop 5T myeloma while nude mice, which have an intact B cell population, do not (136); however, it was also suggested that the elevated natural killer cell population in nude mice may contribute to this phenomenon. More studies are required to determine if these cell populations are significant in solid tumor metastases to bone, but the evidence from MDSCs and T cell promotion of osteolysis is compelling.

Animal models for studying bone metastases

Breast cancer models

Some of the most common models of tumor-induced bone disease include tail vein (137-139), cardiac (36, 69, 140), and intratibial (141-143) inoculation of breast tumor cells. Many breast cancer models rely on cardiac injections, in which tumor cells are inoculated directly into the left cardiac ventricle. This allows for tumor cells to disperse throughout the body, but

bypasses the direct blood flow to the lungs. Other tumor-bone models, such as the myeloma models, rely on tail vein injections, which for breast cancer cells result in large tumor burden and premature death due to lung metastases. In certain cases tumors are inoculated directly into the tibia. While not a model of metastasis, this approach is extremely important for prostate models which do not readily metastasize to bone when injected intravenously. In addition, for certain breast cancer models, intratibial injections can indicate how alterations in gene expression of a tumor cell alter tumor growth in bone separately from metastasis. While these models are the primary models available for the study of human metastasis to bone, the ideal models are those that spontaneously metastasize from the mammary fat pad. Unfortunately, there are currently no human tumors that metastasize from the fat pad in mouse models. There are mouse models, such as the 4T1/BalbC model, which can metastasize to bone from the primary site (144, 145), but this model lacks the clinical significance that can only be achieved through human metastasis models.

Prostate cancer models

Prostate models of bone metastasis are particularly challenging. The only metastatic models available utilize PC-3 cells, which unlike most prostate tumors in patients are purely osteolytic. Therefore, these cells are rarely used for tumor-bone models. Instead the field mostly relies on orthotopic models developed by Leland Chung's group from LNCaP C4-2 cells derived from a lymph node metastasis (146, 147) and numerous cell lines isolated by the Vessella group from their rapid autopsy program (148). These cells can also be directly injected into bone, where they develop into strongly osteoblastic tumors.

Lung cancer models

The most popular models of cancer metastasis to bone have traditionally focused on breast or prostate, primarily since these cancers tend to be the most prevalent in the population; however, a recent shift in the prevalence of lung cancer metastases to bone has stimulated the use of the RWGT2 model of lung carcinoma, which was generated by the Mundy group (149). This surge can be largely attributed to advancements in the treatment of lung tumors at the primary site, which extends patient survival from the primary tumor, but appears to facilitate the opportunity for tumor cells to metastasize to bone. The RWGT2 intracardiac model causes significant bone destruction, similar to the clinical disease.

Conventional techniques for imaging tumor in bone

In order to fully investigate these animal models, numerous imaging techniques have been applied with most focusing on imaging either the tumor cells or changes in bone. Radiography using Faxitron analysis has been the central tool for researchers monitoring bone disease for over 20 years, but other techniques have recently developed that allow for more comprehensive analysis, which will be discussed in the next section.

Radiography

Faxitron (Faxitron X-Ray, LLC) first developed their imaging equipment as a tool for micro-radiography in the 1960s and became popular as a method to perform *ex vivo* radiography on patient samples at higher magnification (150). This equipment was later applied to small animal imaging, where over the past 20 years it has maintained its status as the primary method for monitoring cancer bone disease in small animal models (151). While this approach has been very successful, in our experience it is difficult to accurately view the entire skeleton,

and small, early stage lesions are undetectable by planar radiography at such low resolution (141). However, Faxitron analysis has remained popular because it allows for inexpensive, fast, and reproducible imaging. The relative low price of the equipment and limited prep of animals before imaging still makes it an ideal imaging technique. Faxitron imaging is primarily performed now using digital formats which are used to calculate lesion number and lesion area using software from Metamorph (141). While the analysis is relatively basic in comparison to new more complex imaging techniques, the analysis is quick and reliable (36, 152, 153). As new technologies emerge it is unlikely that Faxitron imaging will ever fully be replaced, since it is the only technology that allows many samples to be processed quickly.

Histology

Perhaps the most standard imaging technique for all cancer and bone studies is histology. Histology allows for cellular detail that even new and advanced imaging techniques cannot give. In bone and cancer studies, researchers usually embed specimens in paraffin and stain with Hematoxylin and Eosin (H+E) to detect tumor burden in bone and Tartrate-Resistant Acid Phosphatase (TRAP) to quantify the osteoclast population as a parameter of osteolytic bone disease. H+E sections are also useful in determining bone volume and gross physiological features. Plastic embedding is also frequently used, especially for fluorescent staining, but is not preferred in tumor-bone samples since the difference in density between the bone and tumor can make clean sectioning difficult.

Various different programs are used to quantitatively measure tumor burden, parameters of bone, and perform cell counts. The most popular are Metamorph (36, 141, 152, 153) and Osteomeasure (136, 138, 154), which both rely on region of interest (ROI) analysis.

Both essentially perform the same analyses and their use mostly depends on availability and the preference of the investigator.

Fluorescence and luminescence

The development of fluorescent proteins for transfection into tumor cells in 1997 (155) has revolutionized tumor cell detection and has become one of the standard techniques for monitoring tumor growth *in vivo* in a high throughput and quantitative manner. As with many cancer fields, green fluorescent protein (GFP) imaging became the standard method for imaging tumors in bone as it gave us the ability to follow tumor cell growth without sacrificing the animal or performing more expensive and time consuming techniques, such as positron emission tomography (PET) imaging. For example, Oyajobi et al recently published GFP imaging techniques suitable for imaging myeloma in bone (153). Our group also uses GFP imaging as a standard practice for monitoring tumor growth in bone. This approach gives us the option of imaging weekly, where we normally begin to see tumors growing in bone after 2-3 weeks, but also allows us to perform post-mortem *ex vivo* imaging or immunohistochemistry on tissue sections.

Due to problems with background fluorescence and low depth of field of the green wavelength, other fluorescent proteins have been developed with longer wavelengths. The most popular of these are the red fluorescent protein (RFP) vectors. However, in our and others' experience, these proteins all are associated with increased cell death.

There are numerous systems available to detect the fluorescent proteins, many of which are very affordable (156). However, in our experience the Maestro technology (Cambridge Research and Instrumentation, Inc.) has been the best for imaging fluorescence in bone. This system allows us to eliminate background and examine specific peaks of fluorescence. This

ability also allows us to image multiple fluorescent colors/wavelengths at the same time. Furthermore, this system allows for basic ROI quantification. In addition to *in vivo* imaging, the Nuance multi-label imaging system (CRi) can be performed *ex vivo* on frozen sections. These images can be re-constructed into a 3D image and co-registered with other imaging modalities and histology (157).

Although in our experience GFP imaging has been very beneficial and successful, we are still unable to detect tumors in bone earlier than 2 weeks, which we believe is a limit of the technology and not that the tumors are not present in bone by 2 weeks after cardiac injection. For this reason many groups have switched to bioluminescence imaging (158-161). In this system, tumor cells are transfected with a luciferase vector which enzymatically cleaves the substrate D-luciferin. Upon imaging, full length luciferin is injected into the mice and given time for cleavage to occur at *in vivo* sites of luciferase expression. Luciferase imaging allows for the detection and quantification of smaller tumors. While the detection limit of luciferase imaging is superior to GFP, we find that the luciferase image peaks to maximum saturation early in some cases, making longitudinal quantification of larger tumors difficult. While luciferase imaging can detect tumors in bone earlier than GFP imaging, it still cannot detect very small tumors in bone. Furthermore, luciferase imaging can be more cumbersome and lacks definition to the bone region, which prevents more detailed analysis by histomorphometry. We have found that there is a reduction in metastasis to bone in tumor cells expressing the luciferase vector, but the reason for this is unclear. Unlike the fluorescent proteins, which can induce a T-cell response (162), luciferase expression is not known to induce an immune response or cause toxicity (163). Despite the drawbacks, this is the best option for many models. This is especially true in prostate cancer and other models that rely on mice with hair, which interferes with the GFP signal. The most common system for luciferase imaging is the IVIS system (Xenogen). This

system is relatively easy to use and performs basic quantification and is available at many institutions. Again, this makes luciferase imaging ideal for many laboratories.

There are benefits and draw-backs to both GFP and luciferase. We suggest that in systems where luciferase and/or GFP expression do not interfere with cell growth or metastasis, that both be used to obtain maximum information. GFP expression will allow for later analyses and more detailed *ex vivo* analyses, while luciferase will allow for early detection of relatively small numbers of tumor cells. If they cannot be used together, than the investigator needs to determine which to use based on what information is most critical. For example, if early detection in live animals is a necessity than luciferase is the better option.

The limitations of these conventional imaging techniques and others has driven the field to develop novel imaging modalities that allow us to better explore tumor-induced bone disease by enhancing resolution, sensitivity and the ability to examine molecular mechanisms *in vivo*.

Innovations in tumor-bone imaging (Figure 2)

Near-infrared proteins and antibodies

Because of their long wavelengths, proteins in the red and Near-infrared (NIR) wavelength can penetrate deeper into tissues, allowing better visibility of tumors in deeper tissues, such as within the bones. One group developed mKatuska (emission=588), eqFP650 (emission=650), and eqFP670 (emission=670) for the expression of far red/NIR (164), which they describe as having low toxicity. While they have not been tested extensively, these proteins should have all the benefits of GFP. However, because they are in the NIR range, tumors should be able to be visualized deeper in tissues, and importantly, since there is no background fluorescence at the NIR wavelengths, lower signals should be more easily detected (164).

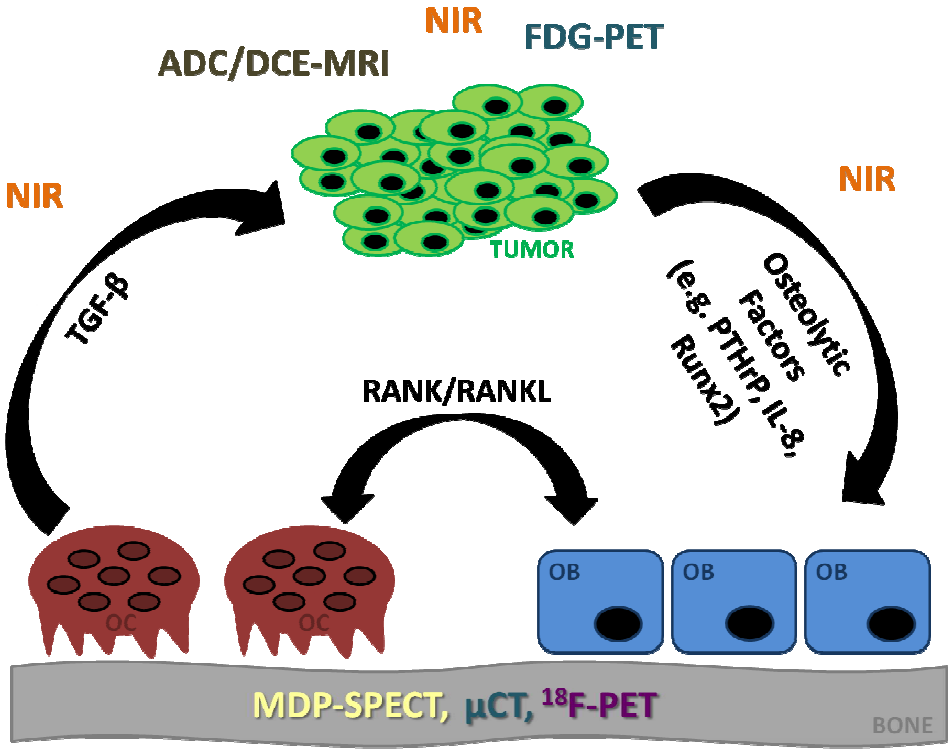

Figure 2. Emerging imaging techniques and their application in tumor-induced bone destruction.

Another promising application of the NIR wavelength has been the conjugation of NIR dyes with antibodies or small molecules. In this case NIR-labeled drugs can be targeted to specific proteins, allowing researchers to monitor the expression of the protein of interest in live animals. This technology has been applied to monitoring several proteins in different tumor models (165-167). For example, one group imaged colon cancer tumors using a small molecule targeted to peripheral benzodiazepine receptor (PBR), a receptor that is up-regulated in late-stage colon cancer. This technique allowed them to accurately, rapidly, and inexpensively detect colon cancer. This technology should be highly applicable to bone metastases and many other tumor types. From our group's pilot data, the NIR small molecules are highly visible in bone, and are likely to become a standard imaging approach in the future.

NIR imaging relies on much of the same equipment required for standard GFP imaging provided that the proper filters are available. Otherwise, several companies have developed stand-alone systems for imaging and image analysis. Additionally, an exciting new system, Fluorescence Molecular Tomography (FMT), was developed to perform 3D NIR imaging. Similar to fluorescent imaging, the Nuance system can be used to perform more detailed *ex vivo* imaging of frozen sections.

In vivo and ex vivo micro-computed tomography (microCT)

In recent years, micro-Computed Tomography (microCT) has gained tremendous popularity due to its ability to obtain both high resolution 3D images of trabecular and cortical bone and yield accurate quantification within specified parameters. To date, the highest degree of accuracy has been achieved using *ex vivo* scanners such as the Scanco microCT (SCANCO Medical) (141, 168-171), which is likely due to diminished tissue deformation and

contamination. However, recent optimization of scanner protocols has enabled the use of *in vivo* microCT to accurately detect changes in bone volume in a single mouse over time (141).

Since its establishment, microCT technology has been adapted significantly to more accurately detect specific models of disease. As is the case for breast tumor-induced bone disease, *ex vivo* microCT is becoming increasingly popular as a method for detecting murine bone volume post-mortem. Initial reports of microCT in monitoring tumor-induced bone disease were conducted in a rat model of breast cancer bone disease and utilized an *ex vivo* microCT similar to those used today (172). Accordingly, numerous publications since that study have utilized microCT as a primary method of reporting changes in bone volume and structure as a result of tumor burden (173-176).

While the utility of *ex vivo* microCT in detecting bone volume has not been refuted, its degree of efficacy has been obviously limited to end-point analyses. Until recently, the use of *in vivo* microCT to monitor changes in tumor-induced bone disease in a longitudinal study was considered unlikely due to concerns of radiation affecting tumor cell growth or the health of the animals, and therefore low-resolution Faxitron analyses have been the conventional method for monitoring tumor-induced bone disease *in vivo*. Indeed, Cowey and colleagues (2007) reported that nude mice exposed to microCT radiation exhibited an increase in tumor burden by histological analyses, but not by bioluminescent imaging, and that exposure to CT radiation may enhance the potential for metastasis to specific skeletal locations (177). Conversely, Johnson et al. reported that modifications to the scanner protocol which optimize resolution with scan time and intensity do not yield significant differences in tumor burden *in vivo* (141). Furthermore, the modified protocol enabled longitudinal analyses of bone volume in individual mice throughout the study.

Despite the advances in *ex vivo* and *in vivo* microCT, the low throughput of these systems in both scan time and analysis remains a serious limitation to the technology. This is in part due to the nature of microCT analysis, which is both cumbersome and time-consuming, and requires significant training for accurate analyses. Recently, however, Hojjat et al reported a method for automating microCT analyses of the vertebrae and trabeculae in tumor-bearing rats with metastatic bone disease using an automated algorithm created from a combination of registration and thresholding techniques (178, 179). These techniques are similar to published analyses, but increase throughput by automation. While this automated technique has not been extensively tested, it may be a potential avenue for increasing throughput for large-scale microCT analyses.

Micro-positron emission tomography (microPET)

^{18}Fluorin-fluorodeoxyglucose (FDG) positron emission tomography (PET) imaging is commonly used clinically to measure the size of a tumor and to determine if a tumor is responding to therapy. This technology relies on the greater metabolic activity of the tumor cells over normal cells, which causes the cancer cells to uptake the FDG prior to normal cells (180). FDG-PET imaging is not ideal for all tumor types, since some tumors do not preferentially uptake FDG-PET (181-183), but PET imaging is highly successful clinically in breast cancer patients with bone metastases (184, 185).

In addition to FDG, many other PET probes are used both clinically and pre-clinically to detect changes in cellular proliferation, angiogenesis, hypoxia, and other cellular events (180). One of the appeals of PET imaging in pre-clinical models is that often times identical approaches are taken clinically, making the translation of findings more applicable (186). Over the past decade, FDG-PET imaging has become more popular for use in animal models of tumor

metastasis to bone (187, 188) since it allows for the detection of relatively small tumors, but many other PET probes are available and frequently used in other cancer models.

Because of the nature of the imaging, tumors should be detectable regardless of their depth, and tumor cells do not need to be altered in order to visualize them *in vivo*. FDG-PET and other PET imaging techniques are highly promising for monitoring the growth of tumor in bone over time. However, mainstream use of the technology is likely to be severely limited by the expense of the equipment, the requirement of highly skilled individuals to run the equipment and analysis, and the length of time required for both the image acquisition and the analysis. Despite these issues, PET remains a very promising technique for detecting tumors early.

In addition to being used to detect tumors, PET imaging using ^{18}F-Fluoride can be utilized to image bone directly. Unlike MDP (discussed in detail in the next section), Fluoride binds directly to the bone matrix, but similarly it preferentially binds to areas of high bone turnover (186). However, due to the slower imaging time requirements (compared to scintigraphy), PET imaging is not the standard approach clinically.

More recently, investigators at Vanderbilt University have used PET imaging with TSPO (translocator protein), which was previously known as PBR, to detect solid tumors since it is expressed at elevated levels in the mitochondria of tumor cells (165, 166, 189, 190). Our group has preliminary data to suggest that PET imaging with TSPO is more sensitive than FDG in detecting tumors in bone, and we intend to pursue PET imaging using TSPO to monitor tumor cells in bone in the future.

Micro-single photon emission computed tomography (microSPECT)

Clinically, bone scans using ^{99m}TC-MDP (technetium methylene diphosphonate) scintigraphy have commonly been used to determine the presence of tumor in bone. In this technique, the uptake of MDP is greatest at sites of high bone turnover (191). This technology detects alterations in normal bone remodeling, which makes it a very successful tool for diagnosing tumor bearing areas of bone; however, slow growing tumors and tumors that do not alter normal bone remodeling will not be detected. Furthermore, as with planar radiography, certain areas of the skeleton, such as the spine, are difficult to diagnose with this imaging modality (191). Because of this, the clinical use of SPECT (Single Photon Emission Computed Technology) technology is more commonly being used to specifically detect tumor cells that are affecting bone. Additionally, recent studies have indicated that combined SPECT/CT imaging significantly improves the ability of doctors to diagnose tumors in bone above either technology alone (192).

^{99m}TC-MDP-SPECT has been utilized in a number of animal studies of bone metastases (177, 193). This technique can be very successful in some cases, but the animal imaging equipment tends to be less sensitive and lower resolution than the human scanners. Due to this, radiotracers need to be more specific and frequently require greater specific radioactivity (186). However, much like microPET imaging, microSPECT is very time consuming for animal models, and its use is therefore usually limited to only a few animals per group. Also, detecting lesions in younger mice can be difficult, since they have high bone turnover in the distal femur and proximal tibia, which also corresponds to where tumors seem to metastasize most frequently.

Magnetic resonance imaging (MRI)

Magnetic Resonance Imaging (MRI) has been used for decades clinically, especially for the diagnosis of brain tumors. One clinical benefit to this technology over PET and SPECT is that it does not rely on ionizing radiation. It has been highly successful in the diagnosis of tumor and other diseases in soft tissue, but until recently it has not been applied readily to the examination of bone. This is primarily due to the fact that MRI relies on visualizing differences in the relaxation times of water (194). While like all tissues bone contains some water, it contains little in comparison to soft tissues, making it difficult to gain information from MRI, especially in animal models where the resolution needs to be greater. Despite these limitations, many clinical groups are beginning to apply MRI technology to patients with bone metastases with great success. Some studies even suggest that MRI is more sensitive than ^{18}FDG-PET or bone scintigraphy for detecting bone metastases in patients (195). There are many different MRI techniques, but perhaps the most applicable to bone are ADC (Apparent Diffusion Coefficient) and DCE (Dynamic Contrast Enhanced). While both of these techniques have been used to image soft tissue tumor and the brain in mouse models, imaging mouse skeletal components is much more complicated due to the small size of the mouse bones (196-199). Despite this, we and other bone groups are working closely with imaging center personnel to apply MRI technology to mouse models of bone metastases. However, one group has successfully applied Diffusion Weighted MRI to monitor the treatment response of prostate tumor bearing mice with skeletal metastasis (200). Other groups have had more success using the nude rat model for MR imaging of tumor-bearing bones. For example, one group used longitudinal DCE MRI to measure changes in tumor vasculature with drug treatments (201, 202).

Co-registration of multiple imaging modalities

Since each technology tells only part of the story, the use of multiple modality imaging will provide a more comprehensive view of both the bone micro-environment and tumor properties. Surprisingly, co-registration of imaging modalities can actually give researchers more information than the simple combination of the individual modalities. In other words, the sum of these imaging modalities is greater than their individual parts. For example, probably one of the easiest images to co-register is PET or SPECT with CT, since they can be performed on the same instrument. The combination has allowed the detection of lesions that would not have otherwise been detectable with either technology alone (203, 204). However, it is feasible to combine images not acquired on the same apparatus. For example, the Vanderbilt Imaging Center has co-registered Matrix-Assisted Laser Desorption/Ionization (MALDI), which is acquired using tissue sections, with whole body MRI in a mouse model (205). Another group has co-registered MRI, CT, and PET images using patient data, and at the time cautioned against improper registration leading to biased information (206). However, co-registration procedures are continuing to improve, and in the future will likely be able to provide abundant information both in small animal models and clinically.

Current promising clinical targets

Despite decades of research focusing on the treatment of bone metastases, they remain incurable. Bisphosphonates are currently the clinical standard of care for treating patients with bone metastases, and have been highly effective in patients to reduce fractures and improve quality of life (207). However, they are not a permanent cure and are not without risk. Severe side-effects are rare, but include severe muscle pain, and osteonecrosis of the jaw and atypical subtrochanteric fractures in patients with long term high-dose treatments (208-210). Because

of these risks, newer drugs are currently of great interest. The emerging drug for clinical use, Denosumab or XGEVA™ (Amgen), which targets RANKL has been demonstrated to reduce bone turnover and increase bone density in clinical studies (211). Interestingly, this drug seems to have the capability of inhibiting tumor growth, yet this seems likely to be an indirect effect (212). However, XGEVA™ also presents safety risks, including hypocalcemia and osteonecrosis of the jaw, though the prevalence is unclear due to limited clinical data (208). Despite the clinical success of these drugs, they do not target the tumor, and therefore do not address the root of the disease and are not a cure for tumors growing in the bone. Therefore, other groups are investigating drugs that can target the tumor cells.

Tgf-β inhibition

One such approach is by inhibiting Tgf-β. Tgf-β is thought to affect both the tumor cells and the micro-environment, suggesting that an inhibitor of this pathway may be able to block bone destruction through multiple targets. Thus far, Tgf-β inhibitors have been very successful with several groups demonstrating that they can inhibit metastasis to soft tissues (213, 214) and bone (215). In addition to direct effects on the tumor, they appear to have positive effects on bone in non-tumor bearing mice. It has been reported by two independent groups that Tgf-β inhibitors 1D11 (Genzyme, Cambridge, MA) and SD-208 (Scios, Inc., Sunnyvale, CA) increase bone density and biomechanical properties as well as numerous measures of bone quality (e.g., trabecular bone architecture and mineral:collagen ratio) (12, 13). These studies also demonstrate an increase in osteoblast number and a decrease in osteoclast number in the bone marrow of healthy mice. Taken together, these data suggest that Tgf-β inhibition may be an ideal drug for bone metastases, since it can both inhibit tumor growth and improve bone quality. Despite their promise in pre-clinical models, their use may be complicated in patients

due to the biphasic effects of Tgf-β in tumor growth and its effects throughout the body on normal cells (216), with particular concerns in patients with residual primary tumor or multiple metastases.

Tumor growth inhibition

It is clear that more specific drugs are needed to target tumors growing in bone. Some potential pathways are being studied by multiple groups to block metastasis and establishment in bone through inhibition of integrins (217), SDF-1/CXCR4 (218), and ROCK (97, 219). Other groups have specifically targeted certain cell types, such as inhibiting osteoclasts using Src inhibitors (220, 221) and stimulating osteoblasts using Dkk1 inhibitors, while still others are investigating inhibitors of the tumors themselves. Some current promising approaches include the histone deacetylase inhibitor vorinostat, which inhibits tumor growth in bone, but can stimulate bone loss (222), suggesting possible combination treatments to protect bone. Erlotinib, an inhibitor against EGFR tyrosine kinase, has been successfully tested in a preclinical model of non-small-cell lung cancer metastasis to bone, and effectively inhibited release of osteolytic factors such as PTHrP and IL-8 (223). In our studies and others', inhibiting the transcription factor GLI2 appears promising in melanoma (152) and breast cancer metastasis (36, 61). Inhibitors to this pathway are currently under investigation in pre-clinical models of prostate cancer and are promising for treatment of primary tumor burden (62). For bone they are an attractive target since Gli2 has limited expression in adult tissues, suggesting minimal side-effects.

Guanosine nucleotides

Other inhibitors aimed at blocking tumor release of osteolytic factors include guanosine metabolites, which have been clinically utilized with varying degrees of success for many years

in cancer patients, primarily as the second or third line of treatment for acute leukemia. These purine analogs compete with endogenous purines for incorporation into DNA and disrupt DNA replication and subsequent cellular proliferation (224), which has a modest antitumor effect. 6-Thioguanine (6-TG) was initially identified during a cell-based screen for low-molecular weight compounds that inhibit PTHrP promoter activation, and has been reported to elicit specific inhibitory effects on PTHrP expression at low doses and with little cytotoxicity (27). This same publication also reported that 6-TG inhibits PTHrP activity in human breast cancer cells *in vitro* and inhibits tumor burden and tumor-induced bone destruction *in vivo* in a murine model of breast cancer metastasis to bone (27), and we have published that the inhibitory effects of 6-TG on PTHrP are mediated through GLI2 transcription regulation (Johnson et al., *in press*).

CHAPTER II

MATERIALS AND METHODS

Molecular biology

Maintenance of cell lines

The human osteolytic breast cancer cell line MDA-MB-231 was obtained from ATCC (American Type Tissue Culture Collection, Manassas, VA, USA) and a bone metastatic variant generated in our lab was used for all *in vitro* and *in vivo* experiments, as previously published (28, 36). The human osteolytic squamous non-small cell lung carcinoma cell line RWGT2 was generated by the Mundy Laboratory (San Antonio, TX, USA), as previously published (149). MDA-MB-231 cells, RWGT2 cells, and human metastatic prostate cancer cell line PC-3 (ATCC), were maintained in DMEM (Cell-gro, Manassas, VA, USA) plus 10% Fetal Bovine Serum (FBS; Hyclone Laboratories, Logan, UT, USA) and 1% penicillin/streptomycin (P/S; Mediatech, Manassas, VA, USA). The murine chondrocyte cell line TMC23 and human non-osteolytic breast cancer cell line MCF-7 were obtained from ATCC and cultured in α-MEM (Invitrogen, Carlsbad, CA, USA) plus 10% FBS and 1% P/S. All cell lines are routinely tested for changes in cell growth and gene expression.

Reverse transcriptase-polymerase chain reaction (RT-PCR)

RNA was extracted from cells using RNeasy Mini Kit (QIAgen), per manufacturer's instructions. cDNA was synthesized using SuperScript III First-Strand Synthesis System for RT-PCR (Invitrogen) and random hexamers from 1-5µg of total RNA per manufacturer's instructions. cDNA (1.0µl) was used for RT-PCR using Platinum PCR SuperMix (Invitrogen). RT-PCR was conducted for the human homologues of the Hedgehog signaling receptors Patched (PTCH) and

Smoothened (SMO). Primers for amplifying hPTCH are as follows: F, 5'-CGCCTATGCCTGTCTAACCATGC-3'; R, 5'-TAAATCCATGCTGAGAATTGCA-3'. PCR was performed on the Bio-Rad iCycler with the following cycling conditions: 94°C for 2min, (94°C for 30sec, 66°C for 1min, 72°C for 30sec) x35 cycles, 72° for 2min. Primers for hSMO amplification are as follows: F, 5'-TTACCTTCAGCTGCCACTTCTACG-3'; R, 5'-GCCTTGGCAATCATCTTGCTCTTC-3'. PCR was performed with the following cycling conditions: 94°C for 4min, (94°C for 30sec, 56°C for 1min, 72°C for 45sec) x35 cycles, 72° for 2min.

Quantitative real-time RT-PCR (Q-PCR)

PTHrP, GLI2, and 18s mRNA expression were measured by Quantitative Real-Time RT-PCR (Q-PCR). After 48 hours' incubation, RNA was extracted from cells using RNeasy Mini Kit (QIAgen, Valencia, CA, USA), per manufacturer's instructions. Complementary DNA (cDNA) was synthesized from 1-5 µg of total RNA using SuperScript III First-Strand Synthesis System for RT-PCR (Invitrogen) and random hexamers, per manufacturer's instructions. cDNA was serially diluted to create a standard curve, and for TMC23 samples, was combined with SYBR Green PCR Master Mix (Applied Biosystems) and *GLI2*, *PTHrP*, or *GAPDH* primers, as previously published (225). A dissociation curve was created and a single peak was confirmed for each primer. MDA-MB-231 and RWGT2 cDNA was combined with *Taq*Man Universal PCR Master Mix (Applied Biosystems), and primer: *Taq*Man PTHLH (Hs00174969_m1), *Taq*Man GLI2 (Hs00257977_m1), or *Taq*Man Euk 18S rRNA (4352930-0910024; Applied Biosystems). Samples were loaded onto an optically clear 96-well plate (Applied Biosystems) and the Q-PCR reaction was performed under the following cycling conditions: 50^{o}C for 2min, 95^{o}C for 10min, (95^{o}C for 15sec, 60^{o}C for 1min) x40 cycles on the 7300 Real-Time PCR System (Applied Biosystems). Q-PCR reactions were quantified using the 7300 Real-Time PCR Systems software (Applied Biosystems).

Cell proliferation assay

In vitro cell proliferation was determined by 3-(4,5-dimethylthiazol-2-yl)-5-(3-carboxymethoxyphenyl)-2-(4-sulfophenyl)-2H-tetrazolium (MTS) assay using the CellTiter 96 Aqueous Non-Radioactive Cell Proliferation Assay Kit (Promega). Briefly, 2,000 cells/well were plated in 96-well plates in quadruplicate, and growth was measured at days indicated spectrophotometrically at 450nm on a Synergy2 plate reader, per manufacturer's instructions.

Western blot

Cells were harvested for protein into a 1X radio-immunoprecipitation assay (RIPA) lysis buffer (ThermoScientific) supplemented with a cocktail of protease inhibitors (Roche, Basel, Switzerland). Equal protein concentrations were prepared for loading with Laemmli sample buffer and electrophoresis was performed on sodium dodecyl sulfate polyacrylamide gel electrophoresis (SDS-PAGE) Mini-Protein II ready gels (Bio-Rad, Hercules, CA, USA). Separated proteins were then transferred to Polyvinylidene fluoride (PVDF) in transfer buffer [25 mmol/L Tris, 192 mmol/L glycine, 20% (v/v) methanol (pH 8.3)] at 200mA at room temperature for 90 minutes. Membranes were blocked with either 1X TBS buffer containing 1% Tween 20 (1XTBST) for 1 hour at room temperature and incubated with a 1:200 dilution of Omni-probe α-His antibody (Santa Cruz Biotechnology) in blocking buffer, or blocked with 1X TBS containing 1% BSA and 1% milk for 1 hour at room temperature and incubated with a 1:200 dilution of Gli2 antibody (Santa Cruz Biotechnology, Santa Cruz, CA, USA) in blocking buffer for 1 hour at room temperature. The membrane was washed with 1XTBST and signal was detected using an enhanced chemiluminescence system (Amersham, Piscataway, NJ, USA). Membrane was stripped using Restore Western Blot Stripping Buffer (Thermo Scientific), washed with 1XTBST, and re-probed with a 1:5000 dilution of β-actin antibody (Sigma-Aldrich) as a loading control.

Transfections

The CMV-GLI2-GFP construct was kindly provided by Dr. Rune Toftgard (226) (Karolinska Institute, Huddinge, Sweden). The GLI2 WT, mTCF, and mSmad promoter constructs were kindly provided by Dr. Sylvianne Dennler (60) (INSERM, Paris-Diderot University, Paris, France). The Gli2-Rep construct was kindly provided by Dr. Ilona Skerjanc (227) (University of Western Ontario). Cells were plated at a density of 5.0×10^4 per well in a 24-well plate (pGL3, GLI2 WT, mTCF, mSmad, and PTHrP promoter constructs) or 1.8×10^6 in a T25 flask (CMV-GLI2-GFP, GLI2-His, GFP, and pcDNA) 16-24 hours prior to transfection. Cells were transfected with 5 μg of construct. All transfections were performed using LipofectAMINE Plus (Invitrogen, Carlsbad, CA, USA) reagent per the manufacturer's instruction. MDA-CMV-GLI2-GFP, MDA-GFP, MDA-pcDNA, and MDA-Gli2-Rep stable cell lines were selected for antibiotic resistance into single cell clones by limiting dilutions or pooled colonies under 400μg/ml getecin (G418) selection medium 48 hours post-transfection and maintained in culture medium supplemented with 200μg/ml G418. For promoter studies, cells were harvested for luciferase assay 24 hours post-transfection, per manufacturer's instructions (see promoter luciferase assay).

mRNA stability

Confluent cells were treated with either 6-TG or purine as a control (see cell treatment, 6-TG), and actinomycin D [0.8 micromolar (μM)], a transcription inhibitor, was added 2 h after 6-TG treatment. Total RNA was extracted 24 hours after treatment and mRNA quantitative analyses were performed by Q-PCR as described above.

Promoter luciferase assay

Following successful transfection, cells were rinsed once with 1×PBS and directly lysed with 100 µl 1×Passive Lysis Buffer (Promega, Madison, WI, USA). Cells were subjected to at least one freeze-thaw cycle to complete lysis. Relative luminescence of cell lysate was determined using Luciferase Assay Reagent II (Promega) and Stop and Glo Buffer (Promega), per manufacturer's instructions, and performed on a Synergy 2 plate reader and luminometer (BioTek, Winooski, VT, USA).

Cell treatments

Cyclopamine. Cyclopamine (LC Labs) was re-constituted in (2-Hydroxypropyl)-beta-cyclodextrin solution 45% (w/v) in HOH (Sigma-Aldrich). For *in vitro* studies, 1-10µmol (with data from 3µmol shown) cyclopamine or tomatadine was added to cell culture medium and cells were harvested 24 hours later.

Tgf-β. Recombinant Tgf-β (R&D Systems, Inc, Minneapolis, MN, USA) was re-constituted in 4mM HCl and 1mg/ml bovine serum albumin (BSA). Prior to treatment, cells were washed once with serum-free medium, and Tgf-β added at 5-10ng/ml to serum-free cell culture medium.

2G7. Tgf-β neutralizing antibody 2G7 was obtained from the Vanderbilt Monoclonal Antibody Core. Prior to treatment, cells were washed once with serum-free medium, and 2G7 or control IgG 12CA5 was added at 50µg/ml to serum-free DMEM.

LiCl. Lithium Chloride solution (LiCl, 8M solution; Sigma-Aldrich) was added at 20mM (228, 229) or 40mM (228) to serum-free DMEM, as specified in text.

XAV939 and VU-WS113. Received 10mmol stock of XAV939 (Novartis, Basel, Switzerland) and VU-WS113 kindly provided by Dr. Ethan Lee and added drug or DMSO control at 100nmol, 1µmol, or 10µmol to DMEM supplemented with 5ng/ml recombinant Tgf-β to spike Gli2 levels prior to inhibition. MDA-MB-231 cells were also treated in serum-free conditions with similar results.

GANT58/GANT61. GANT58 and GANT61 were obtained from the NCI (Bethesda, MD, USA). GANT58 and GANT61 were re-suspended in methanol for *in vitro* studies and added at 10µmol to serum-free DMEM, unless otherwise specified in text.

6-TG. Cells were plated at a density of 5.0×10^4 per well in a 24-well plate, 7.2×10^5 per well in a 6-well plate, or 1.24×10^6 per well in a T25 flask 16-24 hours prior to treatment. Cells were washed once with serum-free DMEM, and 6-TG (Sigma-Aldrich, St. Louis, MO, USA) was added to cells at 100 µmol-1 mmol in DMEM supplemented with 10% FBS and 1% P/S and incubated for 2, 4, 8, or 24 hours.

PCR array

MDA-MB-231 cells were seeded onto soft Polyacrylamide (PA) gels or tissue culture polysterene (TCPS) coated in Fibronectin (Fbn) at 1.92 x 10^6 cells/well and harvested for RNA as described above after 24 hours incubation. cDNA was synthesized from 1µg RNA per manufacturer's instructions for the RT^{2}Profiler PCR Array System for Wnt Signaling (SABiosciences, Frederick, MD, USA). Samples were loaded onto pre-coated 96-well array plates and reverse transcription was performed on the 7300 Real-Time PCR System (Applied Biosystems) per manufacturer's instructions as follows: 95^{o}C for 10min, (95^{o}C for 15sec, 60^{o}C for 1min) x 40, (95^{o}C for 15sec, 60^{o}C for 1min, 95^{o}C for 15sec) Dissociation step. Reactions were

quantified using 7300 Real-Time PCR Systems software for CT value, per manufacturer's instructions.

β-catenin nuclear/cytoplasmic fractionation

MDA-MB-231 cells were seeded onto soft Polyacrylamide (PA) gels, tissue culture polysterene (TCPS), or tissue culture polysterene coated in Fibronectin (TCPS+Fbn) at 1.92 x 10^6 cells/well and harvested for cell pellets after 24 hours incubation. Pellets were washed twice with 1XPBS and fractionated into cytoplasmic and nuclear fractions using the NE-PER Nuclear and Cytoplasmic Extraction Reagents (Pierce/Thermo Scientific, Rockford, IL, USA), per manufacturer's instructions. Briefly, cellular membranes were disrupted using lytic buffer to expose cytoplasmic proteins, which were immediately harvested and stored at -80^{o}C. Remaining nucleus was recovered and lysed to yield nuclear fraction, which was immediately harvested and stored at -80^{o}C. According to the manufacturer, less than 10% contamination between cytoplasmic and nuclear fractions is anticipated (Pierce/Thermo Scientific).

β-catenin/Dkk1 shRNA

MDA-MB-231 cells were plated at a density of 1.92 x 10^6 cells/well and transfected with shRNA against CTNNB1 (β-catenin) or DKK1 (Open Biosystems/Thermo Scientific, Huntsville, AL, USA) 24 hours after plating. For transfection, 1.15µg of construct was diluted in 115µl Optim-MEM (CellGro), and 2.5µg Lipofectamine2000 was diluted in 115µl Opti-MEM. The Lipofectamine mixture was added to the construct, and incubated for 20 minutes at room temperature. Cells were washed once with Opti-MEM and left in 800µl Opti-MEM/well. Following incubation, construct and Lipofectamine solution was added to each well and incubated for 6 hours. Following incubation, 2mL of DMEM supplemented with 20% FBS was

added to each well. Tgf-β treatment was started 24 hours following transfection, and cells were harvested for RNA 24 hours later, as described above.

Stiffness studies

Tissue culture polystyrene (TCPS) and polyacrylamide (PA) hydrogels were employed to examine the effects of substrate rigidity on Wnt signaling in 2D *in vitro* culture. To facilitate cell adhesion and ensure that the surface chemistry was constant for all substrates tested, Fibronectin (Fbn) was adsorbed to the surface of the substrates by incubating them in a 4μg/ml solution of Fbn in PBS at 4°C overnight. PA hydrogels were synthesized by copolymerizing a 10% solution of acrylamide and bis-acrylamide in water via free-radical polymerization using a redox pair of initiators [tetramethyl ethylene diamine (TEMED) and 10% ammonium persulphate (APS) in water]. Additionally, acrylic acid N-hydrosuccinimide (NHS) ester was copolymerized to the surface of the gels. The NHS-acrylate layer was then allowed to react with a solution of Fbn in HEPES. To measure the surface concentration of Fbn, coated substrates were incubated in a solution of Fbn antibody (1:1000) followed by incubation with a secondary HRP-conjugated antibody. The relative amount of adsorbed antibody was then quantified by reaction with 2'-azino-bis(3-ethylbenzthiazoline-6-sulphonic acid) (ABTS) and subsequent optical density reading at 405nm. All PUR and PAA substrates were prepared at the same surface concentration of Fbn that yielded an optical density of 0.12 absorbance units cm^{-2}.

Animal studies

Animals

All animal protocols were approved by Vanderbilt University Institutional Animal Care and Use Committee and were conducted according to NIH guidelines. Female, 4-week old

athymic nude mice (at sacrifice, n=8, vehicle; n=13, cyclopamine and n=10, empty vector; n=7, Gli2-Rep and n=13, PEG; n=11 GANT58) were anesthetized by continuous isoflurane and inoculated with 100,000 MDA-MB-231-GFP, MDA-MB-231-cntrl, or MDA-MB-231-Gli2-Rep cells re-suspended in PBS via intracardiac injection into the left cardiac ventricle using a 27-gauge needle, as previously described (27, 36, 69). Mice were imaged weekly and sacrificed 4 weeks post-tumor cell inoculation. For mammary fat pad injections, female 4-week old athymic nude mice (at sacrifice, n=8/group for Gli2-Rep studies and n=8, PEG; n=6 GANT58) were anesthetized by continuous isoflurane and an incision was made on the ventral lower abdomen. The left inguinal mammary gland was inoculated with 1,000,000 MDA-231-Gli2-Rep or MDA-231-cntrl cells (for Gli2-Rep studies) or MDA-MB-231-GFP cells (for GANT58 studies) re-suspended in PBS. Tumor size was assessed by caliper measurements twice per week. Mice were sacrificed three weeks after tumor cell inoculation, and tumors excised, measured, and weighed. For cyclopamine studies, beginning two weeks post-tumor cell inoculation, mice were treated daily with either 10mg/kg cyclopamine or control tomatadine analog by i.p. injection, as previously published (230). For GANT58 studies, GANT58 powder was re-suspended in 25% polyethylene glycol (PEG)/75% sterile PBS, and mice were treated at 25mg/kg/day with either GANT58 or PEG/PBS vehicle by i.p.injection in tumor-bearing and normal mice. For non-tumor studies n=5, PEG; n=4, GANT58. For intratibial tumor-bearing studies, 4-week old athymice nude mice were inoculated with 2×10^5 MDA-MB-231-GFP cells directly into the tibia and treated at 25mg/kg/day with PEG (n=5) or GANT58 (n=7) by i.p. injection. Mice were sacrificed after 4 weeks after tumor cell inoculation.

Histology/histomorphometry

Hind-limb specimens (tibiae and femora) were removed during autopsy and fixed in 10% neutral buffered formalin (Fisher Scientific) for 48 hours at room temperature. Bone specimens were decalcified in 10% EDTA for 2 weeks at 4^{o}C and embedded in paraffin. 5µm-thick sections of bone were stained with hematoxylin & eosin (H+E), orange G, and phloxine. Tumor burden in the femora and tibiae was examined under a microscope and quantified using Metamorph software (Molecular Devices, Inc.) and region of interest (ROI) analysis.

Conventional imaging modalities

Radiographic imaging

Mice were radiographically imaged weekly beginning one week post-tumor cell inoculation using a Faxitron LX-60. Specifically, mice were anesthetized deeply with ketamine/xylazine and laid in a prone position on the imaging platform. Images were acquired at 35 kVp for 8 seconds. Lesion area and number were measured using quantitative image analysis software (Metamorph, Molecular Devices, Inc.) by ROI analysis. All data are represented as mean lesion area and number per mouse.

Ex vivo microCT

Tibiae were analyzed using the Scanco microCT 40. Specifically, 100 slices from the proximal tibiae were scanned at 12 µm resolution. Images were analyzed using the Scanco Medical Imaging software to determine the bone volume/total volume (BV/TV), trabecular number, spacing and thickness, and connectivity density.

Fluorescent imaging

GFP tagged tumor cell growth was measured and quantified using the CRi MAESTRO system. Mice were anesthetized using isoflurane and then placed in the MAESTRO imaging equipment. After the image was obtained, it was spectrally unmixed to remove the background fluorescence. Images were quantified using ROI software that is supplied with the MAESTRO system.

Evaluation of live animal microCT for quantitative analysis of tumor-induced osteolysis

Single-group longitudinal study

Preliminary studies were first performed on 16 mice to determine the effect of weekly irradiation on this cell line. Mice were broken down into four groups, and two different μCT protocols were performed using the Imtek MicroCAT II, one high resolution (Bin-2), and one lower resolution (Bin-4), with imaging being performed 1 (n=4), 2 (n=6), or 3 time(s) (n=3 Bin-2, n=3 Bin-4) during the four week study, with the group scanned one time receiving the CT scan only at sacrifice. The Bin-2 protocol used 80 kVp, 500 μA with 900 msec per projection and 600 projections over 360° for a total scan time of approximately 20 minutes, while the Bin-4 protocol was acquired with 80kVp, 500μA with 600msec per projection and 300 projections over 360° for a total scan time of approximately 10 minutes. All images were reconstructed to 512 × 512 × 512 voxels, with Bin-2 having 0.1 × 0.1 × 0.05 mm^3 voxel size and Bin-4 having 0.159 × 0.159 × 0.062 mm^3 voxel size. The radiation dose from Bin-2 and Bin-4 were estimated to be 148.3 mGy and 49.4 mGy respectively. Both protocols were reconstructed with the same conebeam filtered back projection algorithm with a Hamming filter.

Two-group longitudinal study

MDA-MB-231 tibia-injected mice were imaged using the Imtek MicroCAT II weekly for four weeks. Sixteen mice were divided into two groups, one treatment group (n=8) and one control group (n=8). All mice were injected in one tibia with tumor cells at week 0, and the treatment group received one tail-vein injection of 0.1mg/mouse of the bisphosphonate zoledronic acid on day 6 after injection. Images were acquired at weeks 1, 2, 3, and 4 post injection for all 16 mice, using the same Bin-2 protocol as was performed in the preliminary study, and were reconstructed to have 512 × 512 × 512 voxels, each 0.15 × 0.15 × 0.212 mm^3 in size.

Longitudinal CT quantification procedure

Image quantification of bone volume was performed using a threshold method based on Hounsfield Units (HU). Due to unstable detector performance and differences between intensity scales in each image, all images being quantified were first converted to Hounsfield Units (HU) to give them all the same intensity scale and to allow for reasonable week to week comparisons. In each image, the average value of ROIs drawn in air, bed (plastic), and bone were fitted to -1000, 0 and 1700 respectively; the resulting linear fit was used to convert all voxel values to HU. All image analysis was done using Amira 5.2 (Visage Imaging, Inc).

Following conversion to HU, each image was roughly cropped into two parts: the tibia region of the lesion limb, and the contra-lateral tibia region for use as a control limb. The lesion limb or control limb images were registered to the first time point using Amira's Affine Registration function using the Correlation metric with a Quasi Newton optimizer step. Each limb was then carefully cropped to extend from just below the patella, but above the growth plate, to the point where the tibia and fibula join, with the fibula being removed as well. It was

determined that a threshold of 1000 HU was most sensitive to changes in bone volume and subsequently applied to each image. The number of voxels that were above the threshold were then summed and converted to a volume measure of the tibia.

Tumor cell intratibial inoculation and histological processing

Confluent MDA-MB-231 human breast cancer cells were trypsinized, washed and re-suspended in PBS for injection into the right tibia of anesthetized 4-week-old female athymic nude mice (Harlan Sprague Dawley, Inc.) at 2.5 x 10^5 cells per mouse. Contralateral intratibial injections of PBS were used as an internal control for each mouse. Animals were sacrificed four weeks after injection. Hind limb specimens (tibia and femora) were removed during autopsy and fixed in 10% neutral buffered formalin (Fisher Scientific) for 48 hours at room temperature. Bone specimens were decalcified in 10% EDTA for 2 weeks and embedded in paraffin. Bone sections were stained with H+E, orange G and phloxine. Histomorphometry was used to analyze tumor burden in the tibiae and femora using Metamorph software (Molecular Devices, Inc.). Specifically, using the drawing tool in Metamorph the region between the cortices directly below the growth plate was selected and calculated by the software as the total area in centimeters^2. The tumor, as determined by H+E staining, was selected using the same approach. Tumor burden was calculated as a percentage of tumor area over total tissue area. Multiple levels of bone sections were stained and imaged, and all statistical analyses were quantified at the same histomorphometric level. All statistical analyses were performed using InStat version 3.03 software (GraphPad Software Inc.).

Statistical analyses for longitudinal studies

For statistical analysis of the two-group longitudinal microCT data, we fitted a linear mixed model to the data and included random subject effect to account for the correlation of

the longitudinal measurements from the same subject. Slope analysis for each group was performed and compared to zero. To adjust for multiple comparisons, we used 0.05/8=0.006 as the cut off point for p-values being statistically significant. The slope of the tibia volume as a function of time in the untreated control limb group was found to be significantly less than zero ($p<0.0001$) while the slope of the treated control limb was found to be significantly greater ($p<0.0001$). The statistical differences between the slopes of groups were determined. The treated and untreated lesion limb slopes were significantly different ($p<0.0001$), along with the untreated lesion limb and untreated control limb ($p<0.0001$). There was no statistical difference between the treated and untreated control limb slopes ($p=0.0132$) or between the treated lesion limb and treated control limb slopes ($p=0.0443$). Also for the untreated group, it was determined that week 3 and week 4 volumes had significant mean differences between the lesion and control limbs with $p=0.0031$ and $p<0.0001$ respectively.

Statistical analyses

All assays were performed in triplicate, and results were verified in subsequent experiments. All statistical analyses were performed using InStat version 3.03 software (GraphPad Software, Inc., La Jolla, CA, USA). Values are presented as mean ± standard error of the mean (SEM), and p-values determined using unpaired t-test, where *$p< 0.05$, **$p< 0.01$, ***$p<0.001$ unless otherwise stated.

CHAPTER III

RESULTS AND CONCLUSIONS

Live animal microCT allows for quantitative analysis of tumor-induced osteolysis

Introduction

Nearly 70% of breast cancer and 90% of prostate cancer patients with metastatic disease will develop bone metastases (231). In order to investigate breast and prostate tumor effects on bone, several small animal models have been developed that are capable of producing pathogenesis strikingly similar to the clinical condition in both tumor burden and bone disease (27, 69, 232-234). While these animal models accurately reflect the bone disease portion of the clinical disease, small animal imaging has lagged significantly behind clinical imaging. This has hindered pre-clinical rodent models in which drug treatments typically commence upon visual evidence of bone disease and is particularly limiting due to the difficulty of detecting tumors in animal bone as early as can be detected in human patients. In addition, the lack of precise small animal imaging has limited quantitative longitudinal analyses of animals in drug treatment studies. Therefore, significant improvements to small animal imaging modalities are needed.

Over the past 20 years the primary methods for monitoring cancer bone disease in small animal models have relied heavily upon radiography using Faxitron analyses (235). While this approach has been very successful, in our experience it is difficult to accurately view the entire skeleton and small, early stage lesions are undetectable by radiography. In recent years microCT analyses have gained popularity due to the ability to obtain high resolution 3-dimensional images and the degree of accuracy exhibited by this imaging modality. While the

highest resolution images can be obtained by *ex vivo* scanners, such as the Scanco microCT, the utility of these scanners is obviously limited to endpoint analyses. Recent reports combine microCT evaluation with other imaging techniques such as magnetic resonance imaging (MRI) and fluorescence stereomicroscopy to generate a more complete evaluation of the bone micro-environment in metastatic cancer (236), but the limitation of end-point analyses persists. Our group has previously used live animal microCT successfully for imaging bone, but found that high resolution scans killed the tumor cells (unpublished data), limiting its utility to endpoint analyses. In addition, it has been reported that certain doses of CT radiation may enhance metastasis to specific sites in bone (177).

Missbach-Guetner et al. addressed several of these issues utilizing a 3-dimensional flat-panel detector-based Volume Computed Tomography (fpVCT); however, the detector in use is fairly uncommon, and the majority of quantification performed was primarily 2-dimensional measurements. Quantitative analysis of 3-dimensional bone volume was only reported in one mouse, lacking statistical significance, and the method used for quantification was unclear (237).

In this study, we set out to determine if live animal microCT can be utilized to perform reproducible and quantitative longitudinal analyses of bone volume in tumor bearing mice, particularly in a drug treatment model of breast cancer metastasis to bone. To do this we utilized the MDA-MB-231 osteolytic breast cancer model in which the tumor cells are inoculated directly into the tibia of athymic nude mice and imaged mice weekly by Faxitron (radiography), Imtek microT (*in vivo*), and Maestro (GFP-imaging). Scanco microCT (*ex vivo*) and histology were performed at end-point for validation. After establishing a high resolution scanning protocol for the Imtek microCT, we determined whether clear, measurable differences in bone volume were detectable in mice undergoing bisphosphonate drug treatment. Bisphosphonates are clinically

utilized in breast and prostate cancer metastasis to bone in order to palliate tumor-associated bone pain and prevent the recurrence of skeletal related events by binding to the surface of bone and inducing osteoclast apoptosis (238). We found that *in vivo* microCT can be used to obtain quantifiable and longitudinal images of the progression of bone destruction over time without altering tumor cell growth. Additionally, we found that we could detect lesions as early as week one after tumor inoculation and that this approach could be used to monitor the effect of drug treatment on bone.

Longitudinal microCT does not alter tumor growth

In order to determine if microCT protocols could be developed that would allow for longitudinal microCT analyses of bone, we inoculated athymic nude mice with the osteolytic breast cancer cell line MDA-MB-231. We chose to use an intratibial model for this study, since there is less variability in this model than the intracardiac model, which allowed us to more easily validate the technology. After tumor cell inoculation we utilized two different imaging protocols, both with similar radiation doses to those previously reported (177, 237), but at different resolutions. Animals were either imaged three times (weeks 2, 3 and at sacrifice), twice (week 3 and at sacrifice), or once (only at sacrifice). We found by fluorescence imaging of the GFP tumor cells (Maestro) that while there was a slight reduction in the relative fluorescent units (RFU) at 4 weeks there were no significant changes in the overall RFUs between the groups (Figure 3A&B), suggesting no effect on the tumor cell growth over the course of the experiment. Although dead cells may still express GFP, we reasoned that the size of the tumors indicated considerable tumor growth over 4 weeks. These observations were verified by histology, which also showed no changes in tumor volume after 4 weeks (Figure 3C&D).

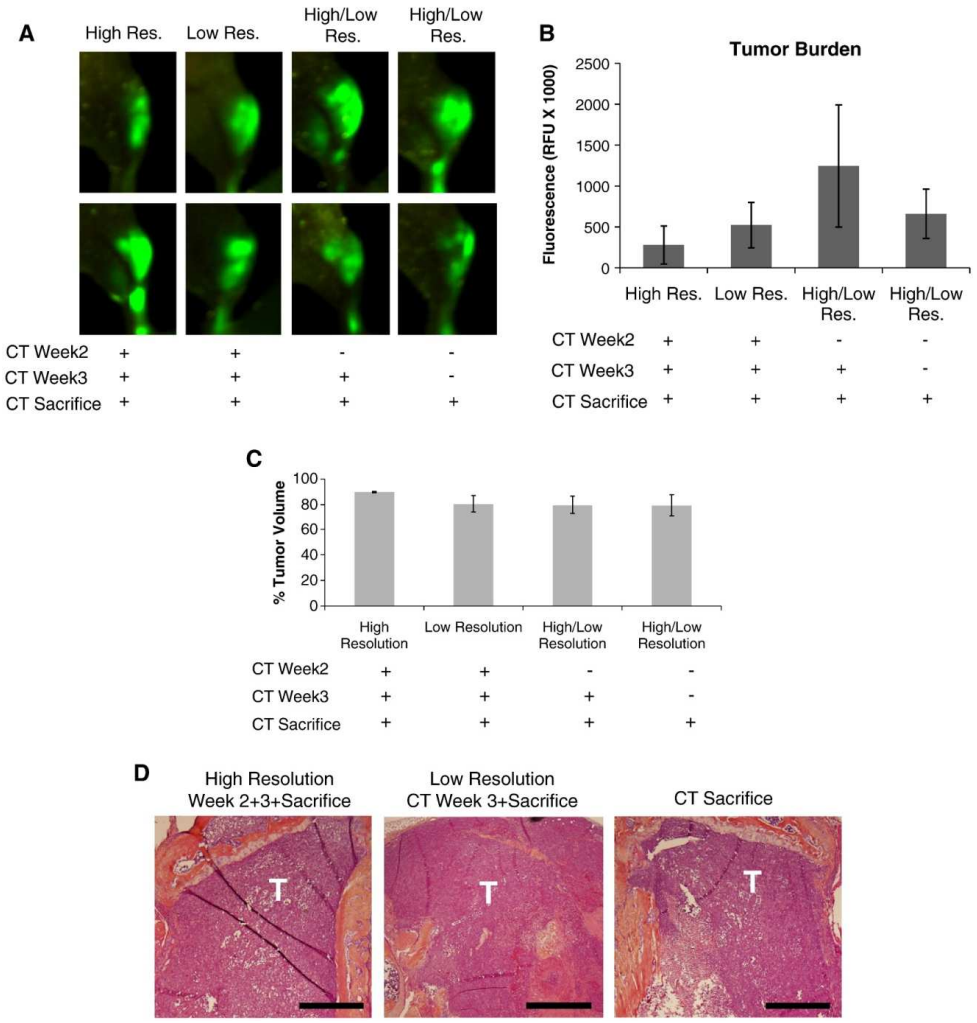

Figure 3. Longitudinal microCT does not affect tumor burden *in vivo*. Athymic nude mice were inoculated with MDA-MB-231 cells and imaged by microCT utilizing a Bin-2 (high resolution) or Bin-4 (low resolution) protocol. (A) Mice were monitored for tumor burden by tumor cell fluorescence utilizing CRi Maestro. Mice scanned at three time points by microCT at high (far left, $n = 3$) or low resolutions (middle left, $n = 3$) exhibited no change in tumor burden when compared to mice scanned twice ($n = 6$) or once ($n = 4$) by microCT at sacrifice. (B) Quantification of tumor burden by relative fluorescent units in mice scanned by microCT. (C and D) Histomorphometric analysis demonstrated no change in tumor volume in mice scanned at multiple time points by microCT when compared to mice scanned only upon sacrifice. Black bars represent a length of 500 µm. Columns indicate average group values, and error bars represent standard error (SE). Statistics demonstrated nonsignificance across all groups and are therefore not visually represented. Statistical significance is considered $p < 0.05$.

Longitudinal microCT illustrates bone loss over time

Weekly microCTs acquired during the course of the experiment were registered and over-laid into a single image so that we could visually see the loss in bone over time in tumor-bearing mice versus controls (Figure 4A&E). Individual scans were rendered at each week and can be visualized in Figure 4B-D and F-H. The representative image illustrates the loss in bone during the 3 weeks of image analysis, clearly showing a gradual loss of bone over time. Importantly, we were able to generate high resolution images and data such as these for each mouse. In addition, we quantified the changes in percent of bone volume/tissue volume (BV/TV) histologically in order to verify the observations found by our microCT data (Figure 4I). By histology, we found that although there were no significant differences between the tumor leg and control leg, there was a trend toward higher bone volume in the control limb. These data illustrate that longitudinal microCT may be a valid option for imaging tumor-induced bone disease over time, which we previously thought was not possible in animal models. We therefore pursued further studies to determine if this modality would be useful in a drug treatment model.

In vivo microCT renders quantifiable longitudinal images of tumor-induced bone destruction

The most useful application for this imaging tool is in drug treatment models in which investigators need to detect lesions at early stages to determine the best time-points for drug treatment. Therefore, we wanted to find methods to quantify the *in vivo* microCT data similar to quantification used in the *ex vivo* microCT system and histology. In order to do this we treated mice with zoledronic acid one week after tumor cell inoculation, when small osteolytic lesions were visible. We chose this model since it is well-established to reduce bone destruction

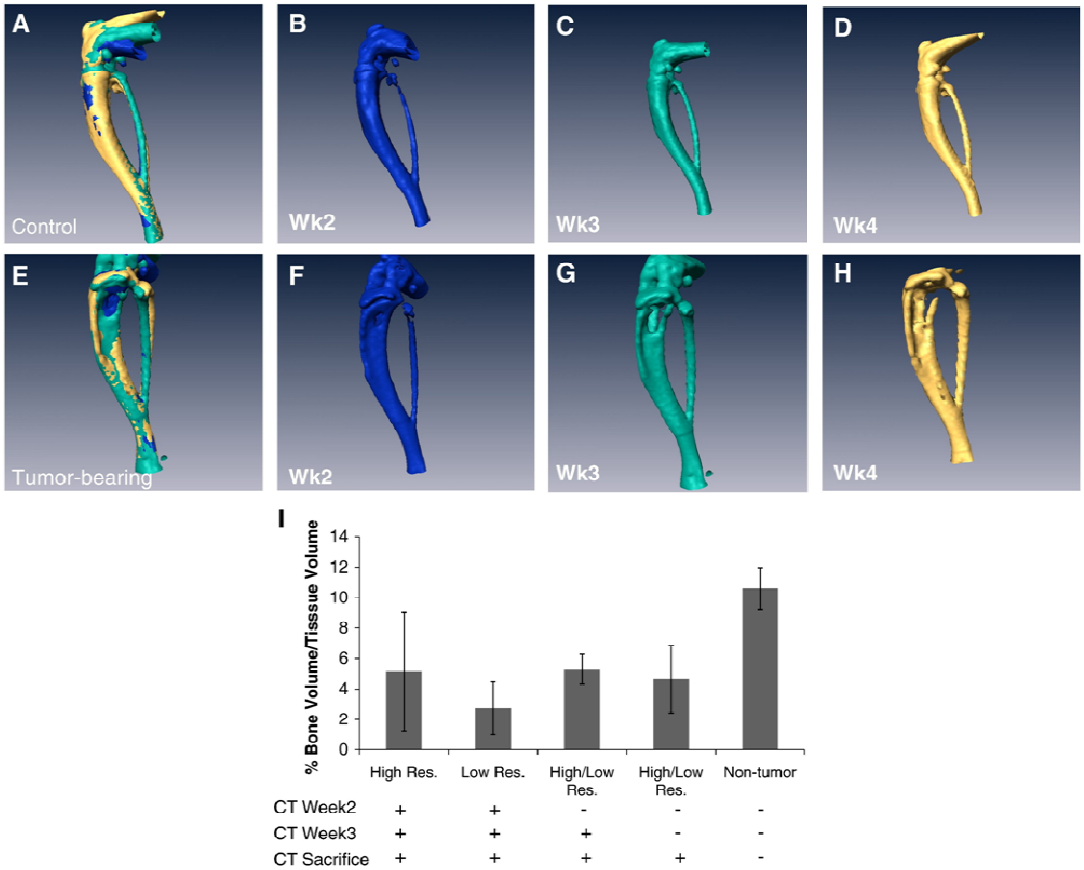

Figure 4. Longitudinal *in vivo* microCT demonstrates bone loss over time in individual mice. (A) Overlay of registered isosurface volume images from three individual time points of longitudinal in vivo microCT scans of control hind limb. (B–D) Weekly isosurface volume renderings of weeks 2, 3, and 4 (sacrifice) of the control hind limb of the same mouse using high-resolution microCT. (E) Overlay of registered isosurface volume images from three individual time points of longitudinal in vivo microCT scans of tumor-bearing hind limb. (F–H) Weekly isosurface volume renderings of weeks 2, 3, and 4 (sacrifice) of the tumor-bearing hind limb of the same mouse using high-resolution microCT. All rendering thresholds were set to 1000 HU. (I) Histomorphometric analyses indicate no significant difference in percent of bone volume/tissue volume, regardless of the number of microCT scans. Columns indicate average group values, and error bars represent standard error (SE). Statistics demonstrated nonsignificance across all groups and are therefore not visually represented.

in animal models and human patients (238), and would therefore provide clear differences in bone volume for quantification.

Initially, we examined the non-treated groups in this study and compared the control versus the tumor leg. Similar to the previous study we cropped and then registered the weekly acquired images (Figure 5A&B). We drew ROIs covering regions of empty space, bed (plastic) and bone and generated a calibration curve, which was used to convert each image's intensity values to HU. Using this approach we found that we could accurately measure the volume of bone destruction over time. These results are displayed per mouse in Figure 5C. In addition, the quantification results were able to statistically distinguish at a group level between the control limb and the lesion limb groups ($p<0.0001$).

In vivo microCT can be utilized to track changes in a drug treatment model

As described above, we treated mice with zoledronic acid starting at week 1 (when lesions were detectable) and imaged the mice weekly. With this approach we found that we could determine bone volumes for the treatment and control limbs in all mice, as well as quantify changes between the treated versus untreated groups by *in vivo* microCT (Figure 6A-D). Figure 4A and 4B demonstrate the ability to register weekly scans at end-point and determine average bone volume for treatment groups, as graphed per mouse and by groups in Figure 6C and 6D. There was no statistical significance ($p=0.0443$) between the mean bone volume of zoledronic acid treated tumor and non-tumor limbs, but there was a significant difference between the treated and untreated lesion limbs ($p<0.0001$). Interestingly, with this approach we could also see a statistical increase in the mean bone volume of the non-tumor limb when treated with zoledronic acid ($p<0.0001$).

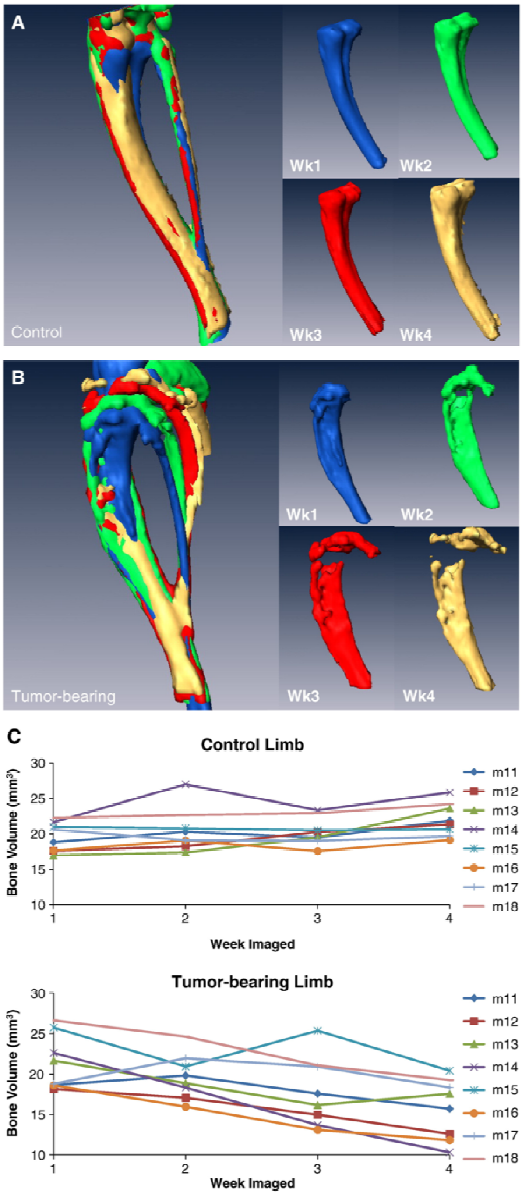

Figure 5. ***In vivo*** **microCT allows for quantifiable longitudinal images of tumor-induced bone destruction.** (A) Isosurface volume renderings of the control limb from a representative mouse at weeks 1 (blue), 2 (green), 3 (red), and 4 (tan), after intratibial sham PBS injection. (B) Isosurface volume renderings of the tumor-bearing limb from the same representative mouse at weeks 1, 2, 3, and 4 after intratibial inoculation of MDA-MB-231 cells. In addition, a registered rendering is shown for both the control (A, large panel) and tumor-bearing (B, large panel) limbs combining all four time points. All rendering thresholds were set to 1000 HU. (C) Bone volume was determined for each mouse at each time point (weeks 1, 2, 3, and 4) in both the control and tumor-bearing limbs.

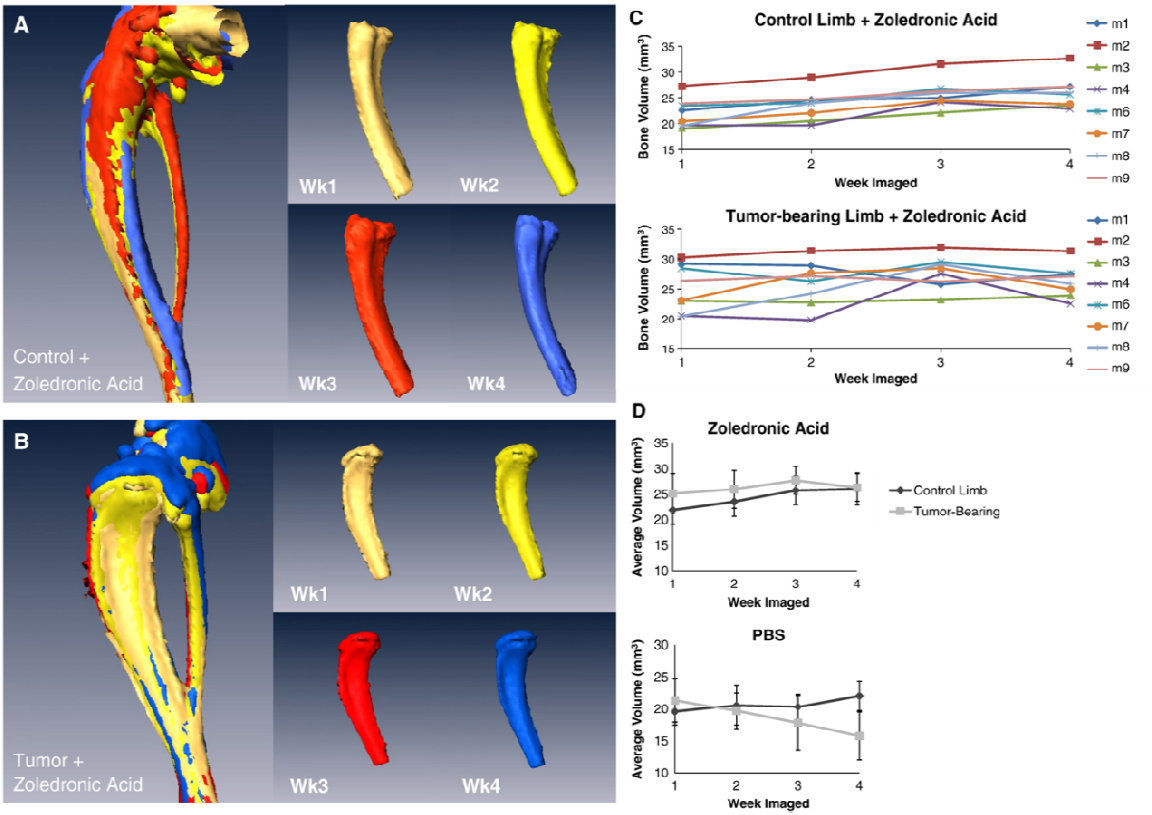

Figure 6. ***In vivo*** **microCT monitors changes in bone volume when mice are treated with zoledronic acid.** (A) Isosurface volume renderings of the zoledronic acid treatment group at weeks 1 (tan), 2 (yellow), 3 (red), and 4 (blue), after intratibial sham PBS injection. (B) Isosurface volume renderings of the zoledronic acid treatment group at weeks 1, 2, 3, and 4 after intratibial inoculation of MDA-MB-231 cells. In addition, a registered rendering is shown for both the control (A, large panel) and tumor-bearing (B, large panel) limbs at weeks 1, 2, 3, and 4. All rendering thresholds were set to 1000 HU. (C) Bone volume was determined for each mouse at each time point (weeks 1, 2, 3, and 4) in both the control and tumor-bearing limbs, as well as (D) the mean group volume and standard deviation over time for both the tumor-bearing and control limb of the zoledronic acid and control groups.

Conventional imaging methods demonstrate comparable bone volume to in vivo microCT

In order to validate the *in vivo* microCT quantification method we directly compared these results to *ex vivo* microCT (Figure 7A) and BV/TV results calculated from histological analyses (Figure 7B), and we found that the quantification of bone volume by *ex vivo* microCT and histomorphometry was comparable to *in vivo* microCT. We also found that while histological analyses were higher resolution than the longitudinal CT, we could obtain comparable results with lower resolution scans, and more importantly we could examine the progression of lesions in a single mouse over time with *in vivo* microCT. The tumor volume was found to be significantly decreased in bisphosphonate-treated mice by histology, which we believe is due to enhanced bone growth since it is not clear whether bisphosphonates can directly affect tumor cells. *In vivo* microCT bone volume computations were comparable to Faxitron data longitudinal analysis of lesion area and number (Figure 7C), and we confirmed that tumor cell fluorescence persisted throughout the duration of the study (Figure 7D).

Conclusions

In a model of breast cancer metastasis to bone, we found that *in vivo* microCT is a useful method for quantifying 3-dimensional longitudinal osteolysis without killing tumor cells, and is comparable to conventional methods of bone analysis such as *ex vivo* microCT, Faxitron analysis, and histomorphometry. In addition, we found that this method of *in vivo* microCT is reproducible and can detect significant changes in bone volume in a pre-clinical drug treatment model, suggesting its potential utility in blastic models of prostate cancer metastasis to bone. Further optimization of this protocol may also be useful in distinguishing changes in cortical and trabecular bone volume *in vivo*.

Taken together, these data indicate that *in vivo* microCT is an effective and reproducible method for longitudinal monitoring of tumor-associated bone destruction in mouse models of tumor-induced bone disease. However, due to its low throughput, its practicality in evaluating osteolytic bone disease in large-scale studies is not optimal, and therefore we utilized conventional imaging methods such as Faxitron and fluorescence to monitor tumor growth and bone destruction in our later studies, and *ex vivo* microCT to determine bone volume at end-point.

Acknowledgements

These data were published as a cover article in *Bone* as follows: Lindsay C. Johnson*, Rachelle W. Johnson*, Steve A. Munoz, Gregory R. Mundy, Todd E. Peterson, Julie A. Sterling. Longitudinal live animal microCT allows for quantitative analysis of tumor-induced bone destruction. Bone. 2011 Jan 1;48(1):141-51 (141). *These authors contributed equally.

This was published as a co-author publication owing to the significant amount of both animal work (completed by Rachelle Johnson and Julie Sterling) and computational methods devised for quantification (Lindsay Johnson and Todd Peterson). Steve Munoz assisted in *ex vivo* microCT analyses and the late Dr. Greg Mundy provided scientific critiques and guidance.

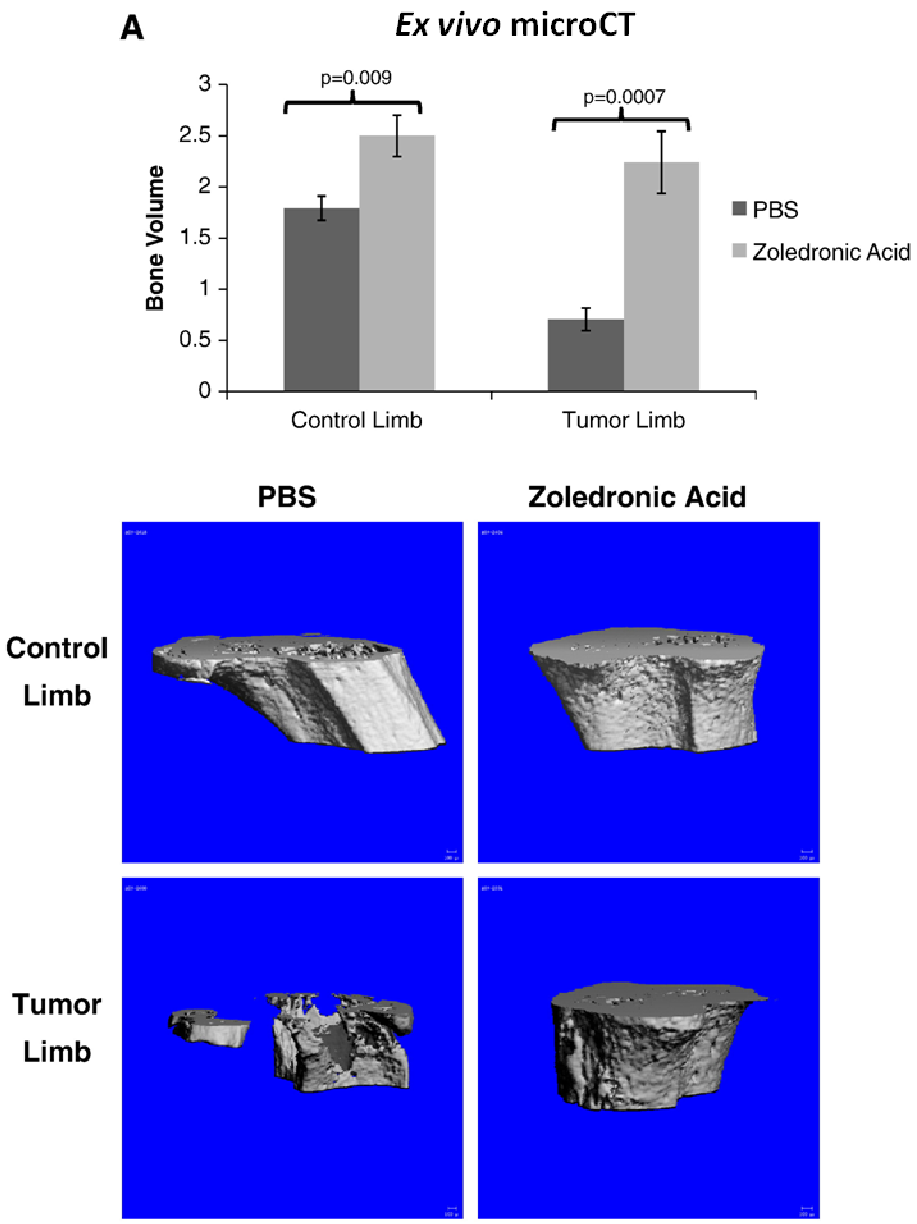
A
Ex vivo microCT
p=0.009
p=0.0007
Bone Volume
3
2.5
2
1.5
1
0.5
0
Control Limb
Tumor Limb
PBS
Zoledronic Acid
PBS
Zoledronic Acid
Control Limb
Tumor Limb

Figure 7.

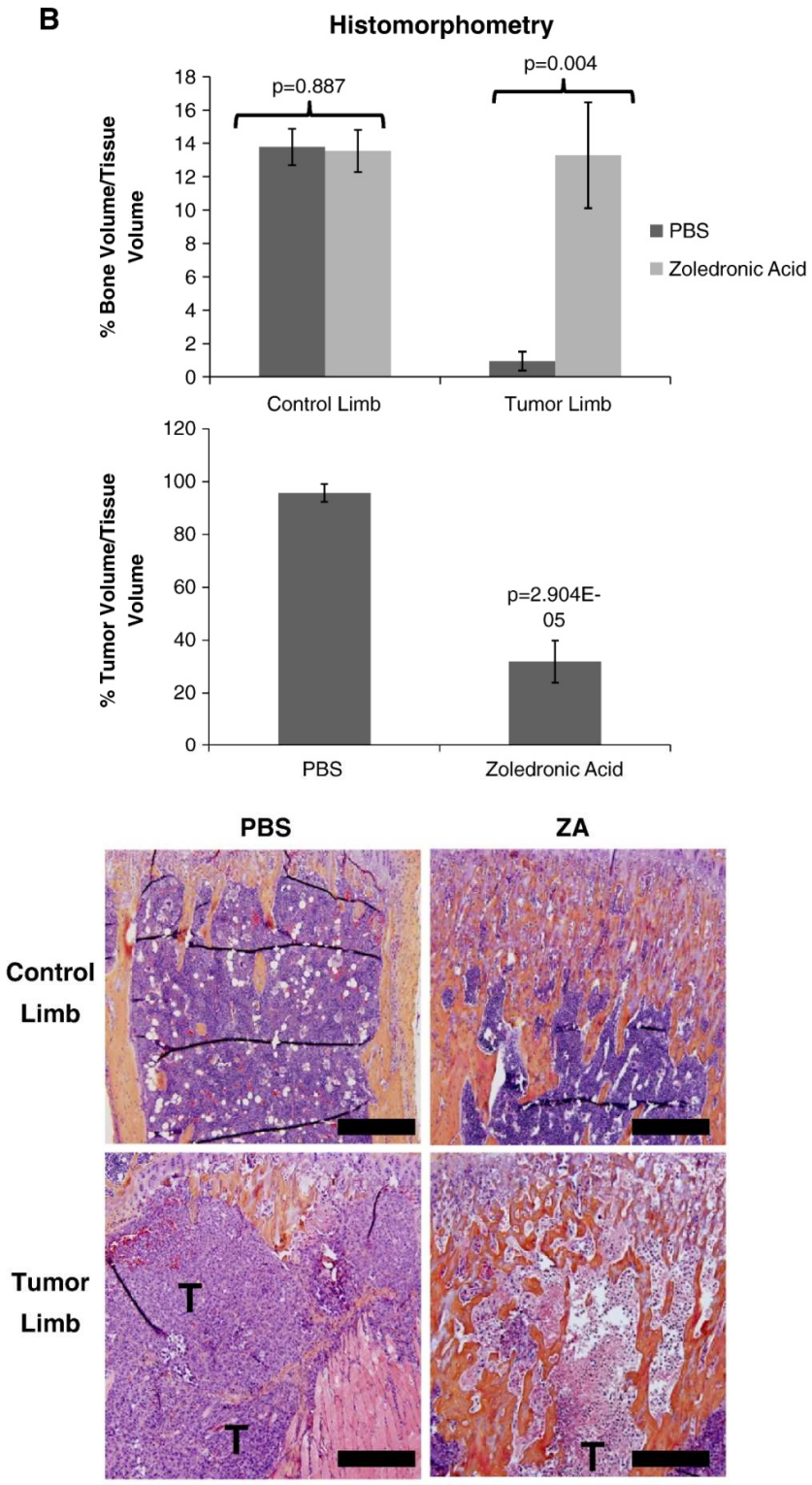
B
Histomorphometry
% Bone Volume/Tissue Volume
p=0.887
p=0.004
PBS
Zoledronic Acid
Control Limb
Tumor Limb
% Tumor Volume/Tissue Volume
p=2.904E-05
PBS
Zoledronic Acid
PBS
ZA
Control Limb
Tumor Limb
T
T
T

Figure 7.

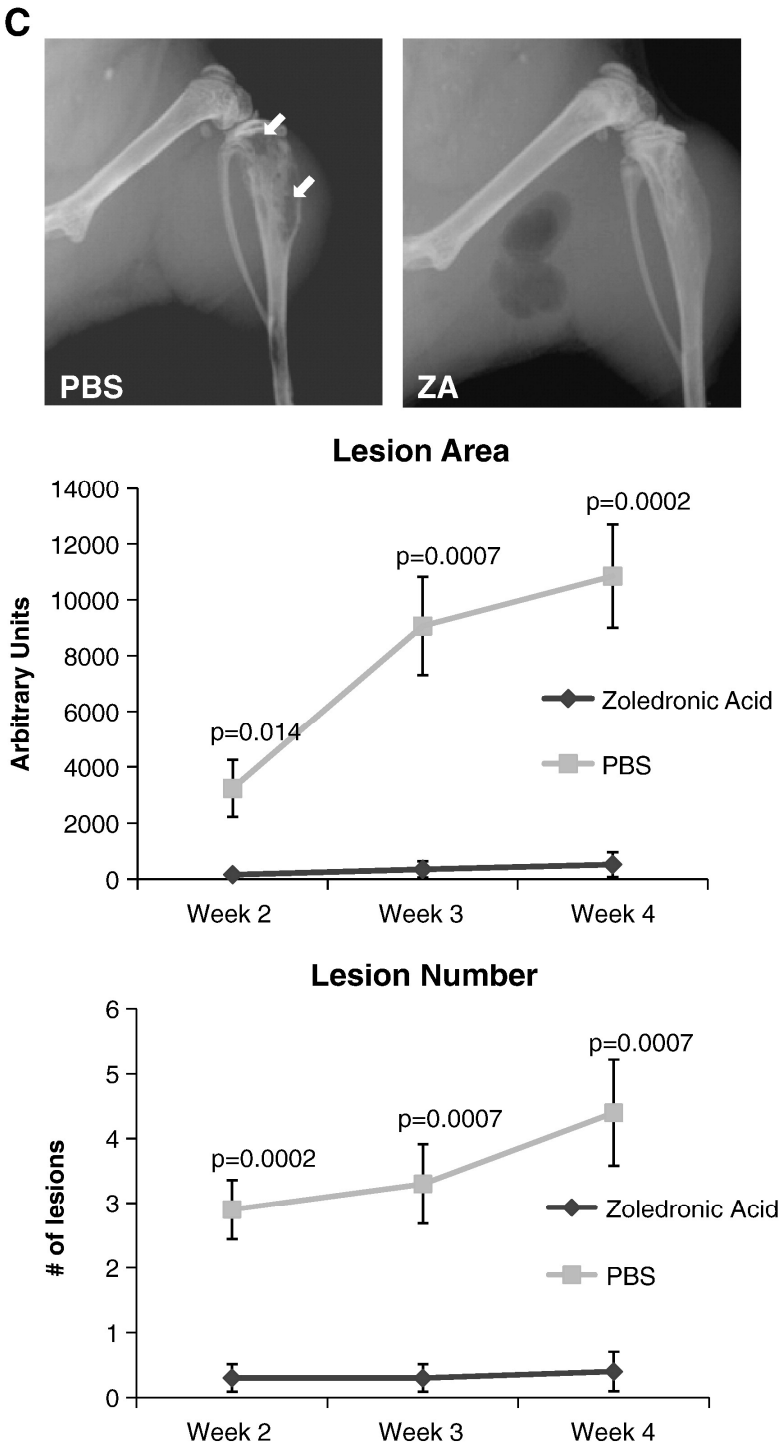
C
PBS
ZA
Lesion Area
Arbitrary Units
14000
12000
10000
8000
6000
4000
2000
0
p=0.014
p=0.0007
p=0.0002
Zoledronic Acid
PBS
Week 2
Week 3
Week 4
Lesion Number
# of lesions
6
5
4
3
2
1
0
p=0.0002
p=0.0007
p=0.0007
Zoledronic Acid
PBS
Week 2
Week 3
Week 4

Figure 7.

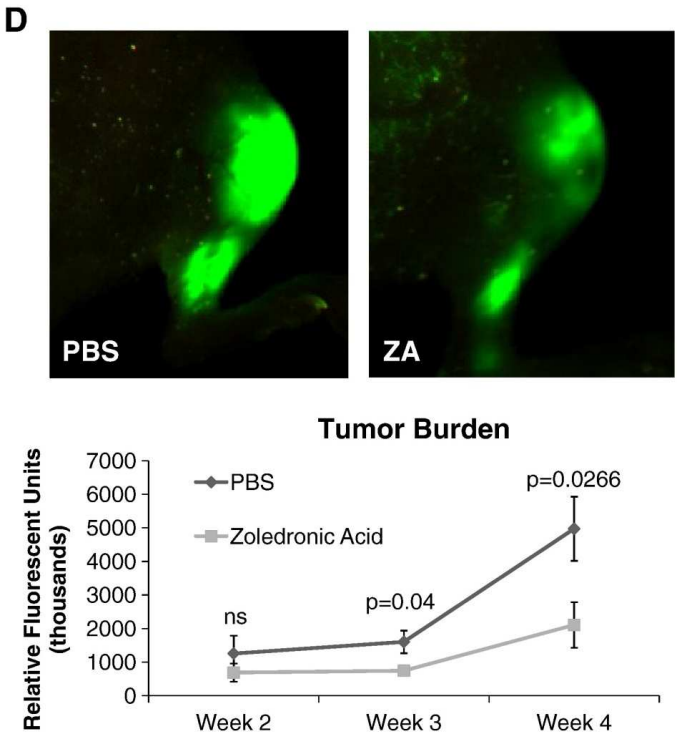

Figure 7. Conventional imaging methods are comparable to *in vivo* microCT bone volume analysis of zoledronic acid treatment mice. (A) *Ex vivo* microCT analysis demonstrates a significant difference in bone volume between the treated and untreated tumor-bearing limbs, similar to the group analysis by *in vivo* microCT in Fig. 4C. Representative images of control and tumor-inoculated hind limbs with and without zoledronic acid treatment demonstrate the rescue of bone volume in tumor-bearing limbs with bisphosphonate treatment. (B) Histological analyses indicate a significant increase in bone volume in tumor-bearing limbs of mice treated with zoledronic acid, further validating the data generated by *in vivo* microCT. Similar to the *in vivo* microCT, histomorphometry did not indicate any difference in bone volume in the control, nontumor limbs of mice treated with zoledronic acid or PBS. Black bars represent a length of 500 µM. (C) Faxitron images demonstrate tumor-associated osteolysis at week 4 in tumor-bearing mice treated with either PBS (left panel) or the zoledronic acid (right panel). White arrows indicate representative osteolytic lesions in bone. X-ray analyses indicate a decrease in lesion area in mice treated with zoledronic acid versus PBS, consistent with both *ex vivo* and *in vivo* microCT (bottom, left graph). Lesion number by Faxitron analyses is also decreased in mice treated with zoledronic acid versus PBS (bottom, right graph). (D) Tumor burden was monitored by tumor cell fluorescence utilizing Cri Maestro throughout the drug treatment study. Mice treated with zoledronic acid exhibited significantly smaller tumors at week 4 than control mice treated with PBS. Columns indicate average group values, and error bars represent standard error (SE). P values are represented respectively for each graph, and statistical significance is considered $p<0.05$.

Tgf-β promotion of Gli2-induced expression of PTHrP is independent of canonical Hh signaling

Introduction

Breast cancer metastasis to bone begins with initiation of the vicious cycle of bone destruction, commencing upon tumor cell establishment in the bone marrow and resulting in increased bone resorption, or osteolysis. Tumor cells receive signals from the bone marrow environment (e.g. Tgf-β), which up-regulates expression of the Hh signaling transcription factor, Gli2, and leads to increased production of osteolytic factors such as PTHrP (26). PTHrP propagates the vicious cycle via PTH-receptor binding on osteoblasts, leading to increased Rankl expression, which induces osteoclastogenesis. As the bone is resorbed, active Tgf-β is released from the bone matrix stimulating further tumor growth and PTHrP production (35).

Given the nature of the vicious cycle, inhibition at any point in this process should reduce bone destruction. For example, neutralizing antibodies against tumor production of PTHrP inhibits osteolytic bone destruction and tumor burden *in vivo* (28, 239). While a humanized anti-PTHrP antibody was developed in 2003, no official report has been made about the success of this antibody in patients (240, 241). Our laboratory has previously demonstrated that the Hh signaling transcription factor Gli2 positively regulates PTHrP expression and secretion in osteolytic breast tumor cells (36).

Gli protein activation has been demonstrated in numerous tumor types and results from a variety of mutations that occur throughout the Hh signaling pathway (66). In these tumor types, Hh receptor antagonists like cyclopamine have been used successfully to prevent Gli over-expression (230). While all Gli family members bind to the same binding sequence, they have separate and discrete functions in mammalian cells (242). Our group has shown that Gli2, but not the other Gli family members, enhances PTHrP expression. Furthermore, expression of Gli2

appears limited to tumor cells that have high metastatic potential, especially to bone resulting in osteolytic lesions (36).

Taken together, these data suggest that inhibition of Gli2 is a potential target for the development of therapeutics aimed at preventing and treating bone metastases. Therefore, we hypothesized that inhibition of Gli2 in bone metastatic lines would decrease PTHrP expression and cause a reduction in osteolytic lesions.

Cyclopamine treatment does not prevent tumor-induced bone destruction in vivo

Cyclopamine treatment has previously been reported to block Hh signaling and inhibit tumor growth in some *in vivo* models (67) through its action as a Smo antagonist (68). Therefore, we first proposed to determine the effects of cyclopamine treatment on osteolytic bone metastases. Mice inoculated with MDA-MB-231 human breast cancer cells were treated with 10mg/kg cyclopamine or control tomatadine analog daily, beginning two weeks post-inoculation and after tumor cells had seeded to bone, similar to previously published treatment regimens which successfully inhibited tumor growth (243). Surprisingly, cyclopamine inhibited neither tumor growth nor cancer-induced bone disease in the bone metastasis model. Indeed, examination by radiography (Figure 8A) indicated that there was a slight increase in osteolytic lesion number in mice treated with cyclopamine when compared to tomatadine-treated mice. After sacrifice, bones were collected from tumor bearing mice from both treatment and control groups for histology and histomorphometry. Histologically, cyclopamine treatment had little or no effect on tumor burden in bone (Figure 8B) or trabecular bone volume at multiple sites commonly examined by histology (Figure 8C). It was concluded that the Hh receptor antagonist cyclopamine is ineffective treatment for osteolytic bone metastases in this experimental model of breast cancer-induced bone destruction.

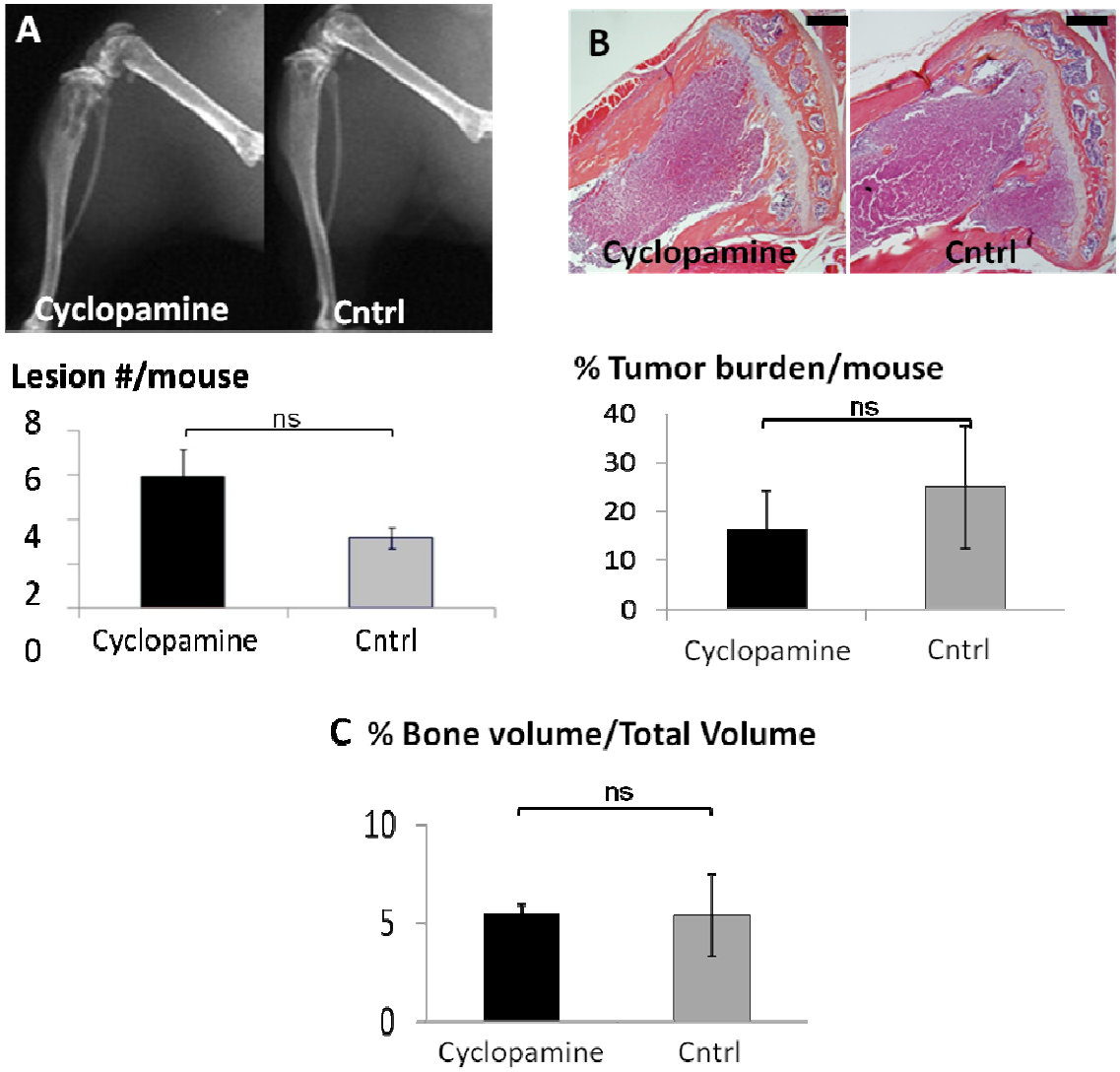

Figure 8. Cyclopamine does not reduce osteolysis or tumor burden. Mice were treated daily with 10 mg/kg of cyclopamine (*n* = 13) or control tomatadine analogue (*n* = 8) and imaged radiographically weekly. (A) Faxitron analyses indicate no significant difference (ns) in lesion number in cyclopamine-treated versus nontreated mice. There was no significant (ns) change in (B) tumor burden detected by % tumor area, or (C) bone volume measured as trabecular BV/TV, on histomorphometric analyses of H&E-stained sections. The black bar on the histologic sections represents a length of 500 µm. Values = mean ± SE, and p values were determined using unpaired *t* test. *p < 0.05; **p < 0.01, ***p<0.001.

Many tumor types have mutations that lead to a constitutive activation of Gli proteins, demonstrating a clinical need for identifying targets to inhibit this pathway. Current therapeutic approaches focus primarily on the development of Smo antagonists, such as cyclopamine analogs. However, our data suggest that at least in some cancers, cyclopamine analogs are unlikely to be effective in blocking tumor-induced osteolysis.

Canonical Hh signaling does not regulate GLI2 in MDA-MB-231 cells

To determine why MDA-MB-231 breast cancer cells are not inhibited by cyclopamine, we next examined the expression of Hh signaling receptors. MDA-MB-231 cells, which express both GLI2 and PTHrP and are known to cause osteolysis, did not express SMO mRNA, and MCF-7 breast cancer cells (non-osteolytic) and RWGT2, a squamous non small cell lung carcinoma cell line, expressed low levels of SMO mRNA (Figure 9A). In contrast, PC-3 prostate cancer cells were found to express SMO mRNA, consistent with findings by another group that showed these cells are inhibited by cyclopamine (Figure 9A) (230).

Treatment of MDA-MB-231 cells with cyclopamine *in vitro* did not alter tumor cell growth over a 7-day treatment period (Figure 9B), indicating that Hh signaling does not play a significant role in the growth of these cancer cells. We next examined cyclopamine-treated MDA-MB-231 and RWGT2 cells for PTHrP and Gli2 expression by Q-PCR. As a positive control, we also tested the cyclopamine-treated chondrocyte cell line, TMC-23, which expresses SMO and is responsive to cyclopamine. Blocking Hh signaling had no effect on PTHrP mRNA expression in either of the tumor cell lines, and cyclopamine treatment did not inhibit and in fact increased GLI2 mRNA in both the MDA-MB-231 and RWGT2 cells (Figure 9D&E). Since Hh signaling is known to regulate PTHrP expression in proliferating chondrocytes (244), we reasoned that TMC-23 cells would be inhibited by cyclopamine, and as expected, PTHrP

expression was indeed inhibited by cyclopamine treatment in TMC-23 cells (Figure 9C). Together, these data confirm that the compound was active and suggests that osteolytic tumor cells rely on an alternative mechanism for PTHrP expression. Thus, Hh signaling inhibition by cyclopamine appears ineffective towards breast tumor cell growth or expression of osteolytic factors by tumor cells, and we concluded that elevated GLI2 expression levels in MDA-MB-231 cells is not due to enhanced Hh signaling through the canonical pathway.

Our data indicate that several osteolytic tumor cell lines, including human breast cancer MDA-MB-231 cells, either do not express SMO or express it at very low levels, providing an explanation for the observed failure of cyclopamine to inhibit PTHrP expression or tumor-induced bone disease. In light of this data, the expression levels of Hh receptors SMO and PTCH would have been useful prior to *in vivo* studies. However, it is generally assumed that elevated Gli expression is mediated primarily via upstream Hh receptor activation. Although Smo-independent mechanisms have been described in prostate cancer (24), this is the first report with regards to bone metastases of Gli over-expression mediated via a Smo-independent mechanism. Surprisingly, we found that cyclopamine treatment actually increased GLI2 expression, though these results were not significant in some osteolytic tumor cells. While the mechanism of this increase remains unclear, Zhang et al reported that cyclopamine has 'off-target' effects on other signaling pathways (245). In addition, other groups have reported that cyclopamine impacts normal bone marrow cell compartments (246-250). Since cyclopamine had no significant effect on overall bone disease in our model, it is unlikely that the compound had any effect on other cells in the bone-tumor micro-environment. However, since duration of treatment in our experiments was relatively short, we cannot rule out that longer-term treatments may alter cells within the bone marrow.

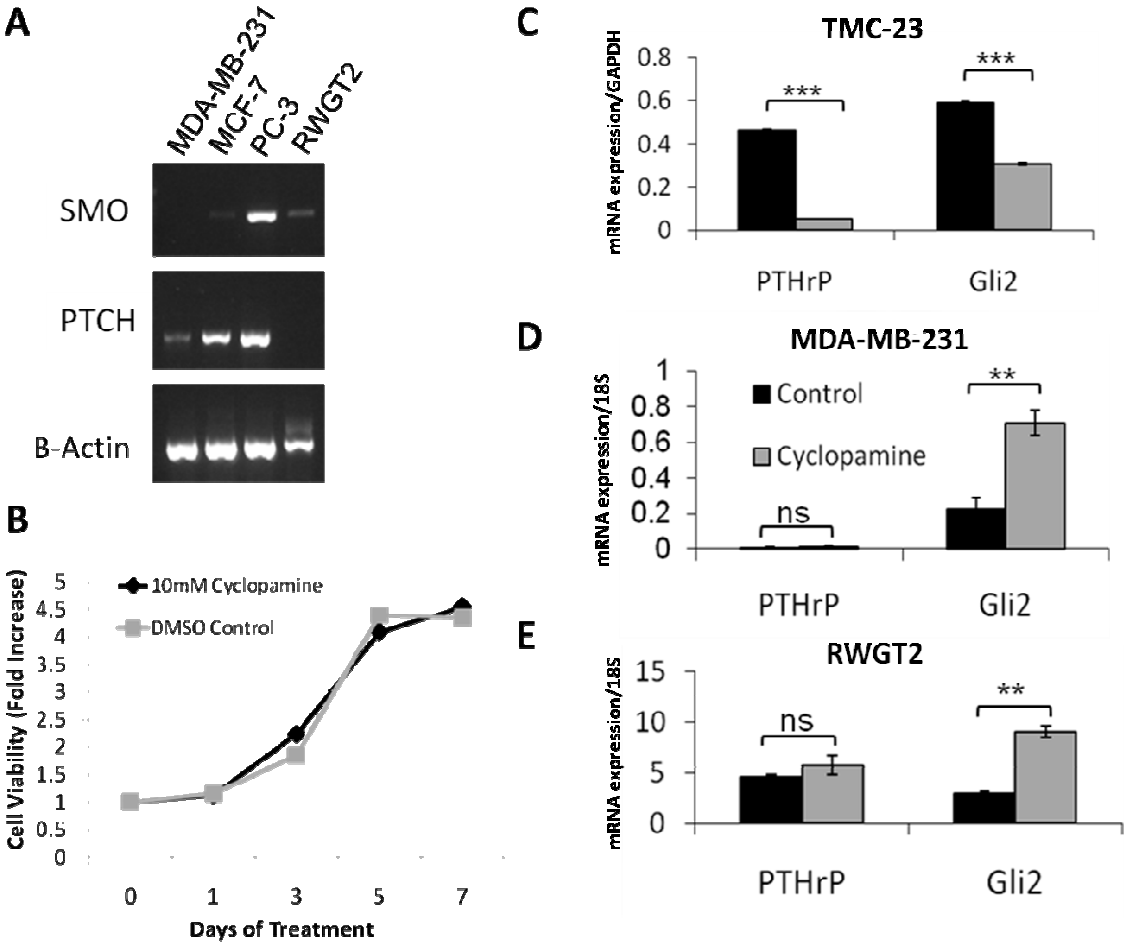

Figure 9. Gli2 is regulated by a Hedgehog independent mechanism. (A) PCR analyses for Ptch and Smo receptor expression in osteolytic and nonosteolytic cell lines show MDA-MB-231 cells do not express Smo. (B) MDA-MB-231 cells treated with 3 µmol/L of cyclopamine exhibit no significant (ns) difference in tumor cell growth by MTS assay. Tumor cells treated with 3 µmol/L of cyclopamine (gray bars) were compared with control tomatadine treatment (black bars) and examined after 24 hours for GLI2 and PTHrP mRNA expression by Q-PCR. (C) Chondrocyte cell line TMC-23; (D) MDA-MB-231; and (E) RWGT2 cells. Values = mean ± SE, and p values were determined using unpaired *t* test. *$p < 0.05$; **$p < 0.01$, ***$p<0.001$.

These data suggest that Smo antagonists are unlikely to be effective and may even have detrimental effects in some cases of tumor metastasis to bone. It will be necessary to establish how commonly breast and other bone-metastasizing cancers are deficient in Smo expression. Our data indicate that Gli2 is regulated independent of Hh signaling in osteolytic tumor cells, allowing us to bypass the Hh signaling pathway altogether, and we therefore looked to alternative signaling pathways known to regulate GLI2 transcription and its downstream targets.

Tgf-β regulation of Gli2 signaling in human osteolytic breast cancer cells

Since Tgf-β is known to regulate PTHrP, and other groups have shown that Tgf-β regulates GLI2 expression in hepatocarcinoma cells (60), we set out to determine if Tgf-β stimulates GLI2 expression in osteolytic tumor cells. MDA-MB-231 cells were tested to determine if Tgf-β enhances GLI2 mRNA expression following treatment with 5ng/mL recombinant human Tgf-β for 48 hours. Consistent with previous studies in other cell types, Tgf-β significantly enhanced GLI2 and PTHrP mRNA expression (Figure 10A) in MDA-MB-231 cells by Q-PCR. As expected, Tgf-β also increased PTHrP protein secretion (Figure 10B). We have found similar results when cells were treated with Tgf-β up to 24 hours (data not shown). These data indicate that Tgf-β, in addition to regulating PTHrP production, may also regulate Gli2 in osteolytic tumor cells; however, the necessity of Gli2 for TGF-β effects on PTHrP remains unclear.

In order to determine if Gli2 is required for Tgf-β to stimulate PTHrP, MDA-MB-231 cells were stably transfected with an empty vector control or Gli2-Repressor construct (Gli2-Rep) in which the activation domain of the GLI2 promoter has been replaced with the engrailed repressor domain as previously described (227), resulting in effective blockade of GLI2 transcription. We have found that this construct efficiently knocks down Gli2 activity in vitro

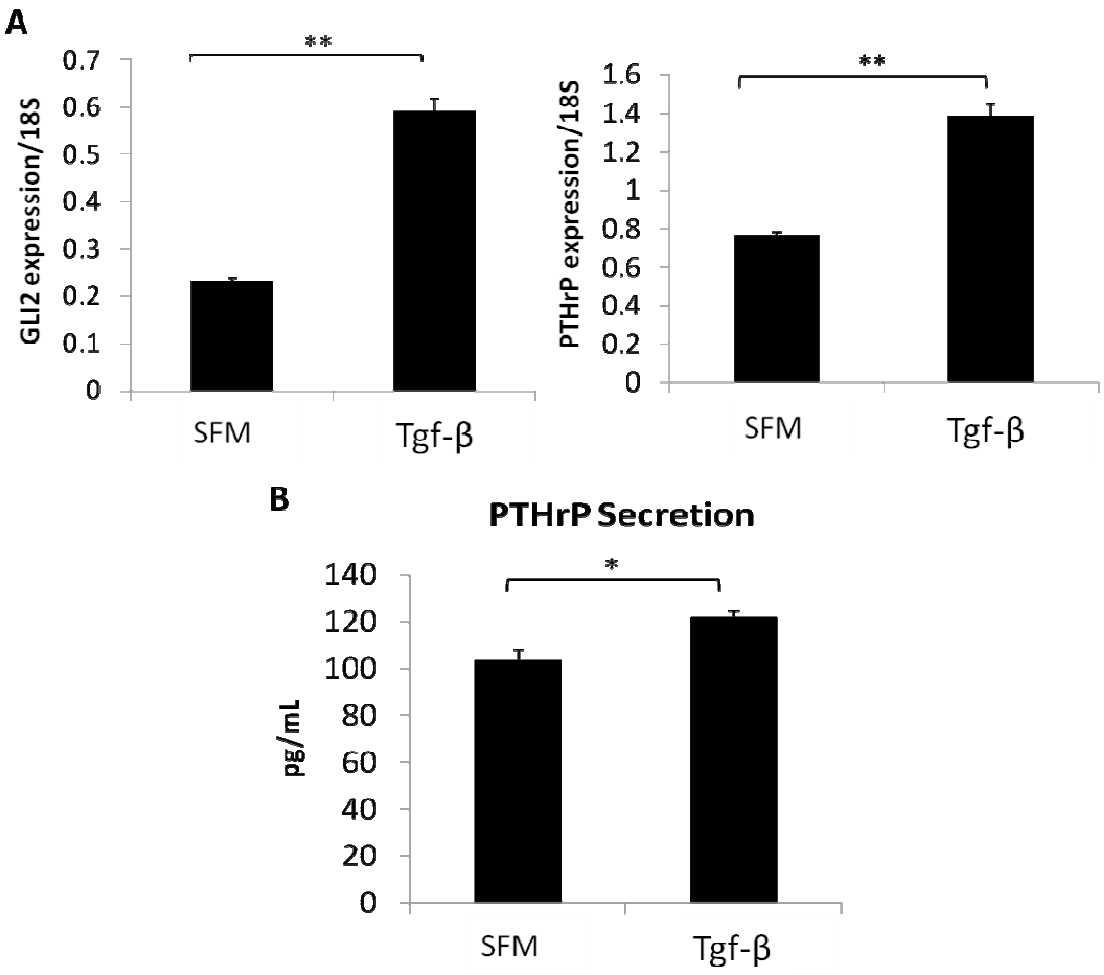

Figure 10. Tgf-β stimulates GLI2 and PTHrP production. (A) GLI2 mRNA expression (left) increases significantly in MDA-MB-231 cells cultured in serum-free medium (SFM) supplemented with 5 ng/mL recombinant Tgf-β. As previously published, PTHrP mRNA expression (right) increases in MDA-MB-231 cells following 5 ng/mL Tgf-β treatment. (B) stimulation with 5 ng/mL Tgf-β modestly enhances PTHrP protein secretion in MDA-MB-231 cells. Values = mean ± SE, and p values were determined using unpaired *t* test. *p < 0.05; **p < 0.01, ***p<0.001.

(36). After generating stable cell lines, positive cells were selected based on neomycin resistance, with both single cell clones and pools of transfectants generated. Because of concerns that single cell clones may result in a selection of a population with a constitutive decrease in PTHrP or a decrease or increase in aggressiveness, we focused on the pooled populations for these studies. However, similar results were obtained for all populations tested. Positive cells were screened for the expression of Gli2-Rep with an anti-His-tag antibody by Western blot (Figure 11A). Consistent with our previous observation that Gli2 stimulates PTHrP expression, the expression of Gli2-Rep caused a reduction in endogenous PTHrP mRNA expression in MDA-MB-231 cells (Figure 11B). Interestingly, expression of Gli2-Rep had no effect on tumor cell growth *in vivo* when cells were injected orthotopically into the mammary fat pad of athymic nude mice (Figure 11C).

Following successful transfection, stable pooled MDA-231-Gli2-Rep cells were treated with 5ng/ml recombinant human Tgf-β1 in serum-free medium and evaluated for PTHrP mRNA expression. We found that the Gli2-Rep construct significantly blocked the ability of Tgf-β to induce PTHrP mRNA expression (Figure 12A), indicating that Gli2 is necessary for TGF-β stimulation of PTHrP. Importantly, basal PTHrP mRNA expression in MDA-MB-231 cells was not affected by Gli2 inhibition when cells were grown in serum free medium in Figure 12A, as compared to its effect on cells grown in 10% fetal bovine serum containing biologically active Tgf-β in Figure 11B. Our data suggest that directly targeting Gli2 may attenuate TGF-β induction of PTHrP, and thereby abrogate subsequent PTHrP-mediated bone destruction.

To further clarify the role of Gli2 in the Tgf-β-PTHrP signaling axis, and to determine whether Gli2 acts downstream of Tgf-β signaling to regulate PTHrP in MDA-MB-231 cells, we disrupted the Tgf-β signaling pathway by stable expression of a dominant negative TGF-β

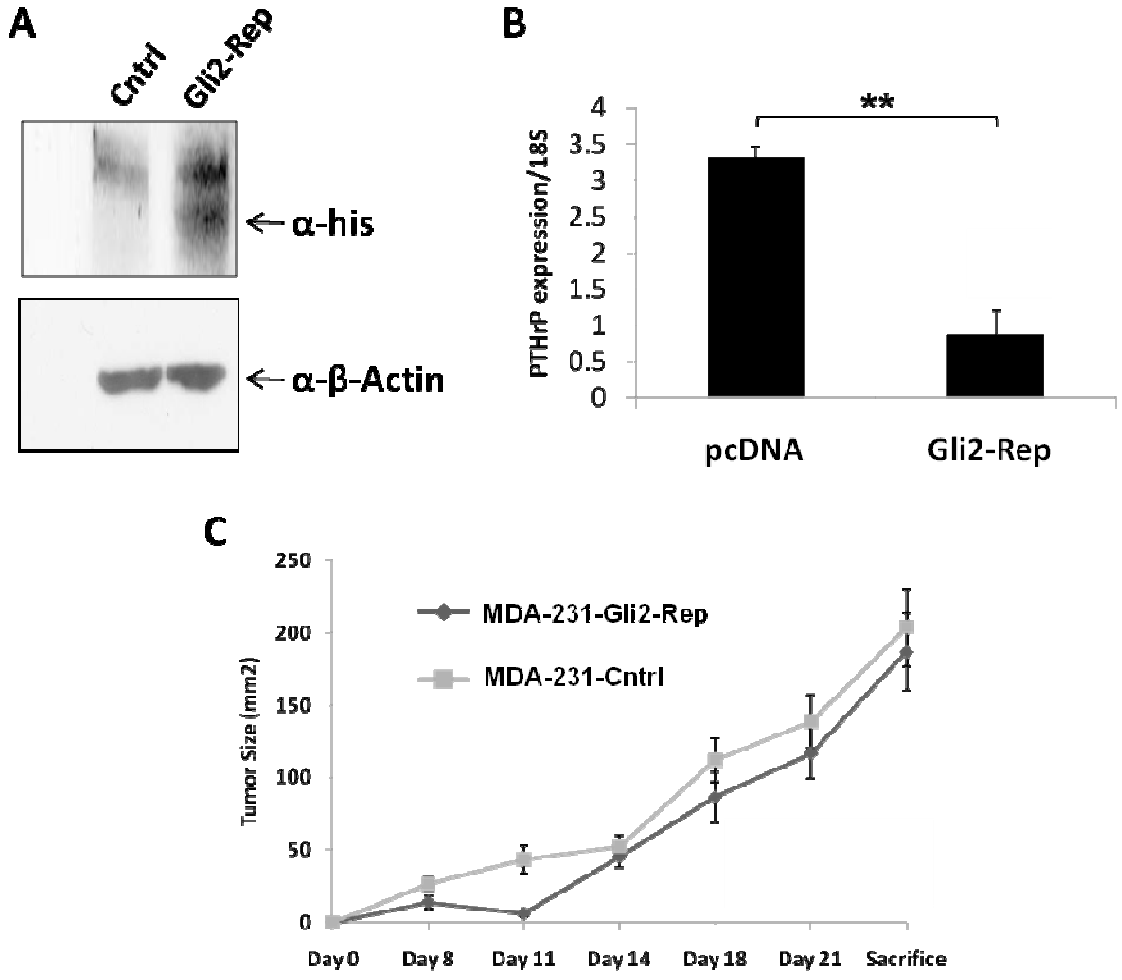

Figure 11. Gli2-Rep inhibits PTHrP production, but not tumor growth. Pooled populations of MDA-MB-231 cells transfected with the Gli2-Rep construct and selected for antibiotic resistance were examined by (A) Western blot to verify efficient expression of Gli2-Rep. (B) MDA-MB-231-Gli2-Rep cells grown in culture medium supplemented with 10% FBS and examined for PTHrP mRNA expression by Q-PCR have reduced PTHrP mRNA expression. (C) MDA-MB-231-Gli2-Rep (*n* = 8) or MDA-MB-231-cntrl (*n* = 8) cells injected into the mammary fat pad of mice and sacrificed after 3 weeks to determine tumor cell growth *in vivo*. Values = mean ± SE, and p values were determined using unpaired *t* test. *p < 0.05; **p < 0.01, ***p<0.001.

receptor type II (DNRII) construct in the MDA-MB-231 cells, as previously published (69). When Tgf-β signaling was abolished in this way, both GLI2 (Figure 12B) and PTHrP mRNA expression (Figure 12C, right panel) were significantly decreased. These data suggest that GLI2 inhibition impairs the ability of Tgf-β to stimulate PTHrP production, resulting in abrogation of tumor-induced bone destruction. Additionally, over-expression of Gli2 protein in the MDA-231-DNRII cells resulted in a dramatic increase in PTHrP promoter activation (Figure 12C, left panel), and a partial rescue of PTHrP mRNA expression (Figure 12C, right panel), further suggesting that Gli2 expression is downstream of Tgf-β signaling. We therefore conclude that the stimulatory effect of Tgf-β on PTHrP expression is likely to be mediated through Gli2.

Tgf-β inhibition decreases PTHrP activity

Since our data strongly indicate that Tgf-β stimulates Gli2 and PTHrP production, and previous data has shown that Tgf-β inhibition *in vivo* provides bone anabolic effects (12, 13), we reasoned that Tgf-β inhibition would likely inhibit PTHrP *in vitro*. Accordingly, when we treated MDA-MB-231 cells with the Tgf-β neutralizing antibody, 2G7, we found that PTHrP promoter activity was significantly decreased (Figure 13). Our group has since moved *in vivo* with Tgf-β neutralizing antibodies in mouse models of breast cancer metastasis to bone, where mixed results were observed. It appears that Tgf-β inhibition blocks tumor-induced bone disease when given at the time of tumor cell inoculation, but is less effective at blocking bone disease in more established tumors (*Biswas et al.*, unpublished data). These studies are on-going, but even if successful in blocking tumor burden, the use of Tgf-β inhibitors to block bone disease clinically could have detrimental effects on patients with residual primary tumor (216). Genetic mouse models have shown that when TGF-β is activated, it is protective against tumor growth at the primary site, but at later stages of disease it can promote metastasis (216).

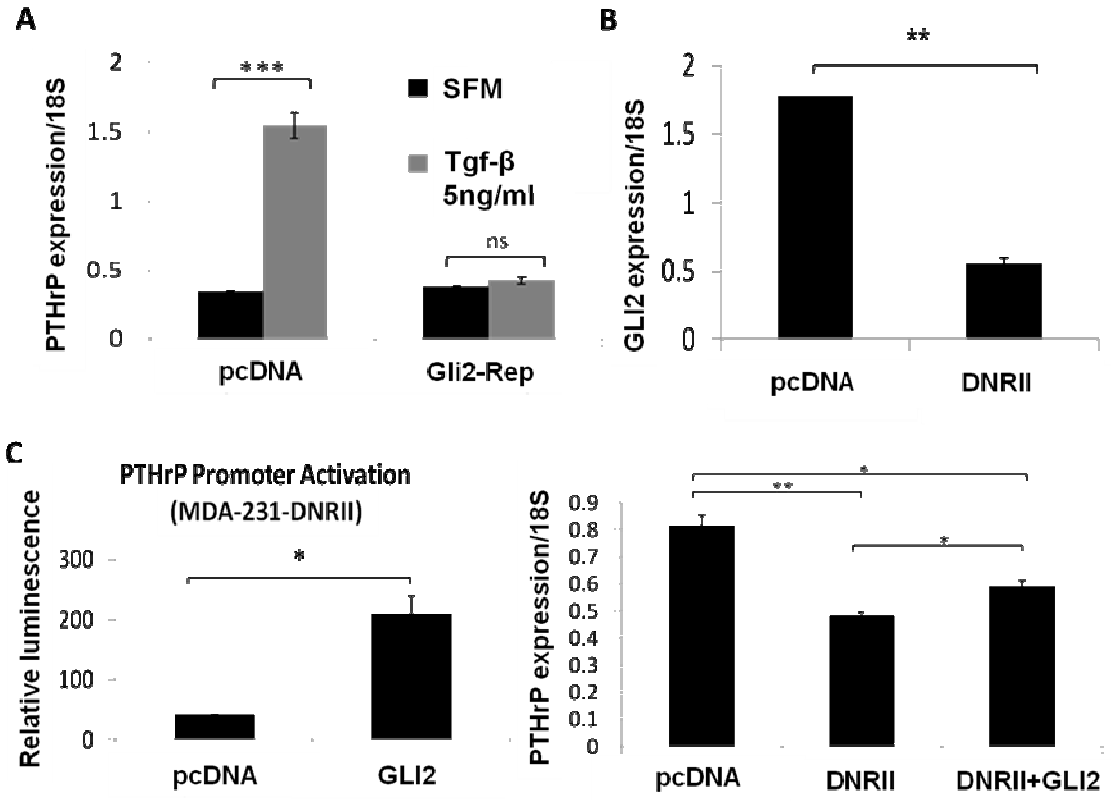

Figure 12. Tgf-β regulates GLI2 expression, which is required for PTHrP stimulation. (A) MDA-231-cntrl or MDA-231-Gli2-Rep cells were grown in serum-free medium and treated with 5 ng/mL exogenous Tgf-β. (B) MDA-MB-231 cells stably transfected with the dominant-negative TGF-β receptor type II (DNRII) construct, which abrogates Tgf-β signaling, have reduced GLI2 mRNA when compared with empty vector control pcDNA-expressing MDA-MB-231. (C) MDA-MB-231-DNRII cells exhibit low levels of PTHrP promoter activity, but when GLI2 is overexpressed by transfection with a GLI2 expression vector, PTHrP promoter activation is significantly enhanced (left) and PTHrP mRNA expression (right) is partially restored. Values = mean ± SE, and p values were determined using unpaired *t* test. *p < 0.05; **p < 0.01, ***p<0.001.

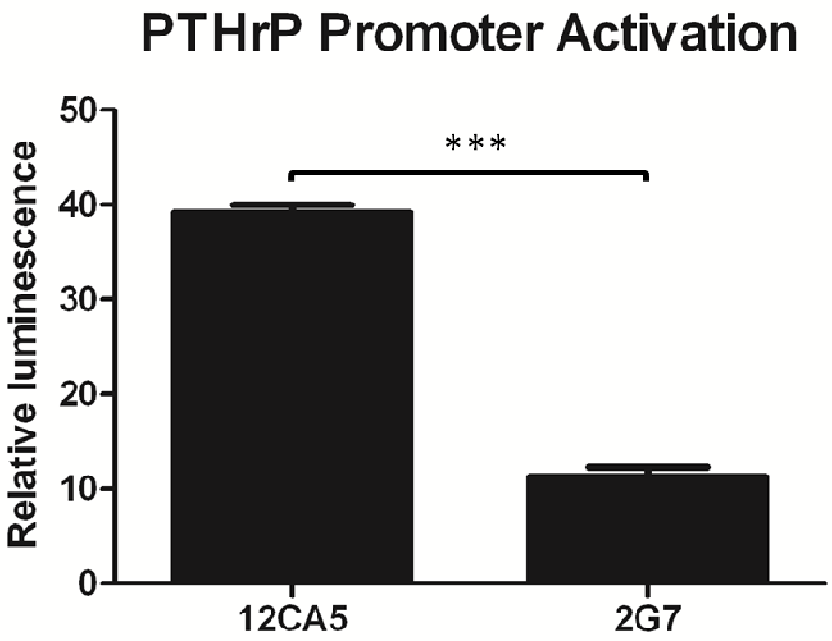

Figure 13. Tgf-β inhibition reduces PTHrP promoter activation. MDA-MB-231 cells were transfected with PTHrP promoter construct, treated with 50μg/ml Tgf-β neutralizing antibody, 2G7, or control antibody, 12CA5, for 24 hours and harvested for luciferase assay. Values = mean ± SE, and p values were determined using unpaired *t* test. *$p < 0.05$; **$p < 0.01$, ***$p<0.001$.

Conclusions

These studies indicate that Gli2 is regulated independent of Hh signaling in some osteolytic tumor cells, specifically human MDA-MB-231 breast and RWGT2 non-small cell lung carcinoma cells. These data are important considering the current clinical emphasis on pursuing Smo antagonists for the treatment of primary cancer. We also show that although Gli2 lacks regulation through the Hh signaling pathway, Tgf-β signaling, which is known to regulate PTHP production, stimulates GLI2 mRNA expression and requires Gli2 for its stimulatory effects on PTHrP. In combination, these data indicate that Tgf-β inhibition would likely be beneficial in blocking Gli2 and PTHrP-induced bone destruction. Although *in vitro* studies confirm decreased PTHrP promoter activity, the *in vivo* studies are in progress and require further analysis in multiple tumor types. However, the biphasic role of Tgf-β in primary and metastatic breast cancer suggests that alternative pathways regulating Gli2 should be explored.

Acknowledgements

A portion of these data were published in *Cancer Research* as follows: Rachelle W. Johnson, Mai P. Nguyen, Susan S. Padalecki, Barry G. Grubbs, Alyssa R. Merkel, Babatunde O. Oyajobi, Lynn M. Matrisian, Gregory R. Mundy, Julie A. Sterling. TGF-beta promotion of Gli2-induced expression of parathyroid hormone-related protein, an important osteolytic factor in bone metastasis, is independent of canonical Hedgehog signaling. Cancer Res. 2011 Feb 1;71(3):822-31. Epub 2010 Dec 28 (61).

Dr. Mai Nguyen completed a portion of the *in vitro* preliminary data for the cyclopamine study at Vanderbilt University, and Dr. Julie Sterling, Dr. Susan Padalecki , Mr. Barry Grubbs, and Dr. Babatunde (Kay) Oyajobi completed a portion of the cyclopamine studies in San Antonio, Texas. Ms. Alyssa Merkel contributed technical expertise in both the cyclopamine and TGF-β

signaling studies at Vanderbilt University. Dr. Julie Sterling, Dr. Lynn Matrisian, Dr. T. John Martin and the late Dr. Greg Mundy provided scientific critiques and guidance.

Bone stiffness drives Wnt signaling regulation of Gli2 in osteolysis

Introduction

Upon metastasis to bone, breast tumor cells up-regulate the expression of the transcription factor GLI2, which directly stimulates the expression and secretion of PTHrP into the tumor-bone micro-environment (251). The release of PTHrP and other osteolytic factors activates osteoclasts and stimulates bone resorption, enabling the release of active Tgf-β from the mineralized bone matrix (26, 251). Previous reports have indicated that Tgf-β positively regulates tumor-derived Gli2 and PTHrP expression (61, 69, 76), and stimulates tumor cell proliferation in bone (26).

In addition to Tgf-β, it is well established that matrix stiffness impacts tumor cell evolution at the primary site of disease (252-254), and there is increasing evidence that matrix rigidity has a significant impact on tumor cell behavior in the mineralized bone micro-environment (95, 251). Indeed, our group has reported that the structural components of bone enhance tumor cell gene expression of GLI2, PTHrP, and TGF-β1 ligand (97) through mechanotransduction, suggesting that bone stiffness and the Tgf-β signaling pathway are significantly linked and may play an important role in the establishment and initiation of tumor-induced osteolysis.

Published reports of the GLI2 promoter identified a SMAD-binding element (SBE) and TCF-binding element (TBE) in a regulatory region upstream of the transcription initiation site in keratinocytes (60), suggestive of both Tgf-β and Wnt regulation of Gli2 signaling. Recent data has also linked the Wnt signaling pathway with mechanotransduction and the Src family kinases. For example, Previdi et al showed that phospho-Src and β-catenin co-localize in the nuclei of bone-metastatic breast tumor cells (255), and other groups have indicated that c-Src may

phosphorylate β-catenin (256, 257). Additional work has shown that Wnt inhibition blocks phospho-wbp2-mediated breast tumor cell growth, which is a phosphorylation target of c-Src (258). Furthermore, a lack of β-catenin nuclear accumulation in association with E-cadherin down-regulation in breast and colon cancer has been demonstrated in a subset of brain metastases (259), and non-canonical Wnt signaling has been identified as a key regulator of brain metastatic breast cancer cells (260).

Since we have previously shown that Tgf-β signaling is an upstream regulator of Gli2 in osteolytic breast cancer cells (61), we hypothesized that Wnt signaling may also regulate Gli2 in bone metastatic breast cancer cells, and furthermore, that this effect is influenced by the rigidity of bone. Our data presented here indicate that downstream Wnt signaling molecules facilitate GLI2 and PTHrP up-regulation, and that downstream Wnt signaling is activated when tumor cells are exposed to stiff substrates similar to the rigidity of bone.

Stiffness causes alterations in Wnt signaling which lead to GLI2 and PTHrP activation

Previous studies have shown that Wnt signaling and mechanotransduction are linked at the nuclear level (255, 258) through Src kinase activity, and our group has previously published that the rigidity of bone enhances Gli2 and PTHrP expression through alterations in Tgf-β signaling (95, 97). We therefore reasoned that stiffness may also influence Wnt signaling upstream of Gli2 and PTHrP. To test this, MDA-MB-231 cells were seeded onto substrates representative of soft breast tissue [polyacrylamide (PA) gel containing fibronectin (Fbn) to facilitate cell attachment] or stiff trabecular bone [tissue culture polysterene (TCPS) + Fbn], as previously published (97), and Wnt signaling activation was examined by transfecting MDA-MB-231 cells with a TOPFlash reporter for TCF activity. We found that MDA-MB-231 cells plated on the stiff TCPS or TCPS+Fbn exhibited a 7-fold increase in TOPFlash activity when compared to

cells plated on PA gels (Figure 14A), indicating enhanced β-catenin signaling through T-cell factor (TCF). In addition, MDA-MB-231 cells seeded onto TCPS exhibited overall greater Wnt signaling activity in a Wnt Signaling PCR-based microarray (SABiosciences) through enhanced expression of numerous Wnt signaling molecules (Table 1), primarily downstream of the Wnt ligands.

To verify that the enhancement of downstream Wnt signaling on TCPS resulted in functional translocation of β-catenin to the nucleus of MDA-MB-231 cells, we examined β-catenin expression by Western blot in nuclear and cellular fractions of cells plated on TCPS, TCPS + Fbn and PA gels. Cells seeded onto TCPS or TCPS + Fbn showed abundant β-catenin expression in both cytosolic and nuclear fractions, while cells seeded onto PA gels exhibited approximately 57% less nuclear β-catenin as calculated by region of interest (ROI) analysis and when compared to the cytosolic fraction (Figure 14B, results representative of n=3).

Based on previous data implicating Wnt signaling in bone mechanotransduction and crosstalk with Src kinase (255-258), its role in mechanical bone loading (261, 262), and our observation that TCF activity downstream of Wnt signaling was enhanced on stiff substrates, we wanted to determine if this was due to an accumulation of nuclear β-catenin, or through some other mechanism. Our Western analyses in Figure 14B indicated that cells seeded onto soft substrates contain less nuclear β-catenin, which correlates nicely with previously published data showing that β-catenin is localized to the nucleus of bone metastatic MDA-MB-231 cells plated on standard TCPS by immunofluorescence (255). Unfortunately, direct confirmation of these data are not possible; the nature of the PA gels prevents accurate visualization of the cytoplasm and nucleus, the process of fixation alters the structure of the PA gel, and the gel itself auto-fluoresces. It should also be noted that although MDA-MB-231 cells normally express relatively

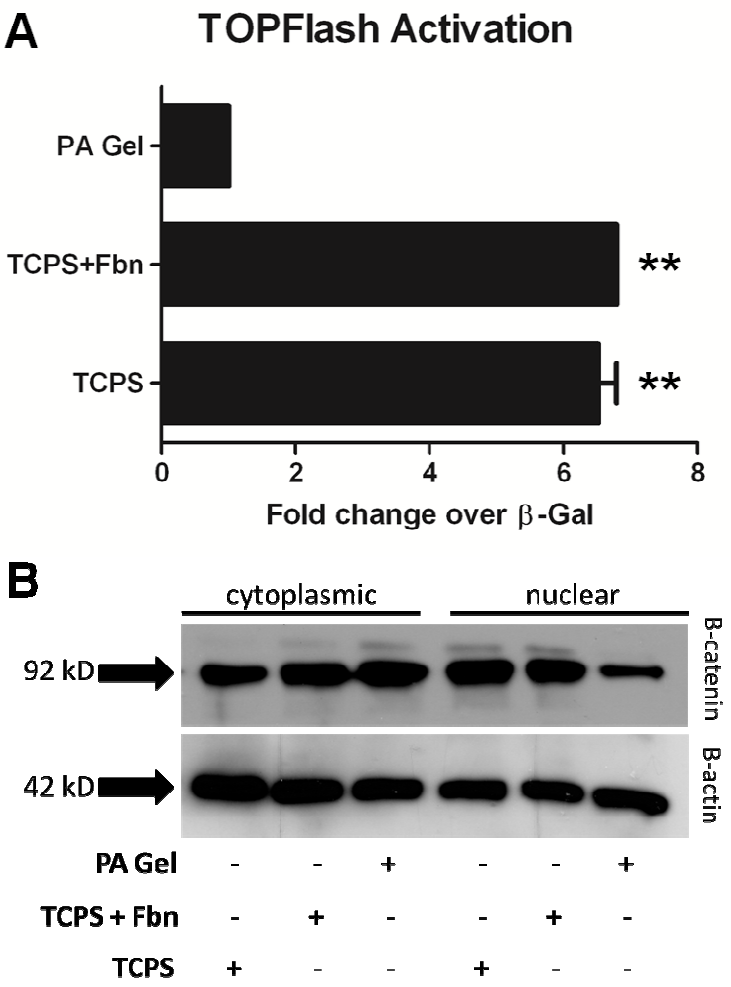

Figure 14. Stiffness activates Wnt signaling and induces nuclear β-catenin accumulation. (A) MDA-MB-231 cells were transfected with TOPFlash reporter construct and evaluated for TCF activation by dual-luciferase reporter assay system (n=3/column). (B) MDA-MB-231 cells seeded onto stiff substrate (TCPS), stiff substrate coated in fibronectin (TCPS+Fbn), and soft substrate containing Fbn to facilitate cell attachment (PA gel) were harvested for cytoplasmic and nuclear protein fractions and examined for β-catenin accumulation by Western blot (representative of n=3). Values = mean ± standard error, and p-values were determined using unpaired t-test. *p< 0.05, **p< 0.01, ***p<0.001.

Table 1. Wnt signaling PCR-based microarray.

MDA-MB-231 cells were seeded onto stiff substrate (TCPS+Fbn) or soft substrate (PA Gel) and harvested for use in a Wnt signaling PCR-based microarray. Genes which were increased or decreased more than 1-fold on TCPS+Fbn compared to PA Gel are presented, and genes demonstrating a greater than 4-fold increase are bolded to indicate significance. Italics indicate a fold increase, and un-italicized numbers indicate a fold decrease. Gene names are clustered into families for easier navigation.

Gene Family	**Gene Name**	**Fold *increase* or decrease**
Canonical Wnt Signaling	**DIXDC1**	***5.3***
	FZD8	***4.3***
	DVL1	*3.0*
	FZD3	*2.8*
	FZD4	*2.7*
	FZD6	*1.9*
	FZD7	2.3
	AXIN1	1.2
	DVL2	1.2
Protein Ubiquitination	**BTRC (b-TrCP)**	***11.1***
	FBXW2	***8.9***
	FBXW11	*3.3*
	FBXW4	*1.5*
Non-canonical Wnt Signaling	**WNT5B**	***8.9***
	WNT5A	*2.4*
	WNT16	*2.2*
	WNT4	2.5
	WNT10A	1.6
	WNT3	1.4

low levels of β-catenin (260), the process of nuclear fractionation causes protein enrichment, making it appear in Figure 14B that endogenous β-catenin is abundant.

Interestingly, β-catenin accumulation in the nucleus and enhanced Wnt signaling activity on stiff substrates hold implications for the way we currently study osteolytic tumor cells and changes in mRNA gene expression. Indeed, the stiff substrate we utilize to represent trabecular bone in these experiments is tissue culture polysterene (TCPS), which is the standard material used for plating cell culture-based assays. This suggests that our bone-seeking strain of osteolytic tumor cells is already in its "active" or bone-altered state in normal assays. Accordingly, culturing parental MDA-MB-231 cells onto TCPS does not make them as aggressive as a bone seeking clone, which suggests that the rigidity of bone may only affect tumor cell behavior once it has metastasized to bone and may not affect tumor cell expression prior to metastasis.

GLI2 and PTHrP expression and activity are responsive to downstream Wnt signaling

Recent publication of the GLI2 promoter in keratinocytes and hepatocarcinoma cells revealed that in addition to Hh signaling, the GLI2 transcription factor can be regulated through a combination of downstream Tgf-β and Wnt signaling molecules, namely Smad2/3 and the co-factor for β-catenin, T-cell factor (TCF) (60). These molecules bind a SMAD-binding element (SBE) and TCF-binding element (TBE) located within the regulatory region of the GLI2 promoter (60). Given the location of these binding elements, we proposed that Gli2, which is up-regulated in osteolytic breast tumor cells (36), may also be regulated via the Tgf-β and Wnt signaling pathways. Wnt signaling alterations have been implicated in a number of different cancers (263-268), and we have previously shown that Tgf-β signaling does in fact regulate Gli2

expression in osteolytic tumor cells (61). In combination, these data suggest that Wnt signaling may also influence Gli2 expression in osteolysis.

To determine the effect of enhanced Wnt signaling in osteolytic tumor cells on Gli2 expression, MDA-MB-231 cells, which normally express low levels of β-catenin even when plated on TCPS (260), were transiently co-transfected with a non-degradable form of β-catenin and its co-factor TCF4. We found that over-expression of β-catenin/TCF4 resulted in an up-regulation of GLI2 mRNA expression by Q-PCR, and significantly activated the Wild-type (WT) GLI2 promoter (Figure 15A&B). When we looked at factors downstream of Gli2, we found that PTHrP promoter activity was enhanced when β-catenin was over-expressed (Figure 15C). Since β-catenin functions downstream of Wnt signaling, we also stimulated upstream Wnt signaling by LiCl treatment, which has been previously reported to up-regulate the Wnt signaling pathway by inhibiting GSK3-β phosphorylation of β-catenin (229). LiCl treatment was added at a dosage of 20mmol (228, 229)and 40mmol (228) as previously published, where we observed a significant increase in both GLI2 (approx. 295-fold) and PTHrP (approx. 2,000-fold) mRNA expression (Figure 16A&B) at 40mM only (20mmol not shown) and a trend toward promoter activation (results not significant) (Figure 16C&D).

Given the extent of GLI2 and PTHrP up-regulation following LiCL treatment, it is possible that other molecules stimulated by LiCl treatment may also affect GLI2 and PTHrP mRNA transcription or stability. Interestingly, we were unable to inhibit GLI2 or PTHrP mRNA expression or activity by blocking Wnt signaling with small molecule inhibitors XAV939 or VU-WS113, even if we first stimulated their expression with recombinant TGF-β treatment (Figure 17B). MDA-MB-231 cells were also tested in serum-free conditions with similar results (Figure 17A). XAV939 abrogates Wnt signaling by stabilizing axin and promoting β-catenin degradation

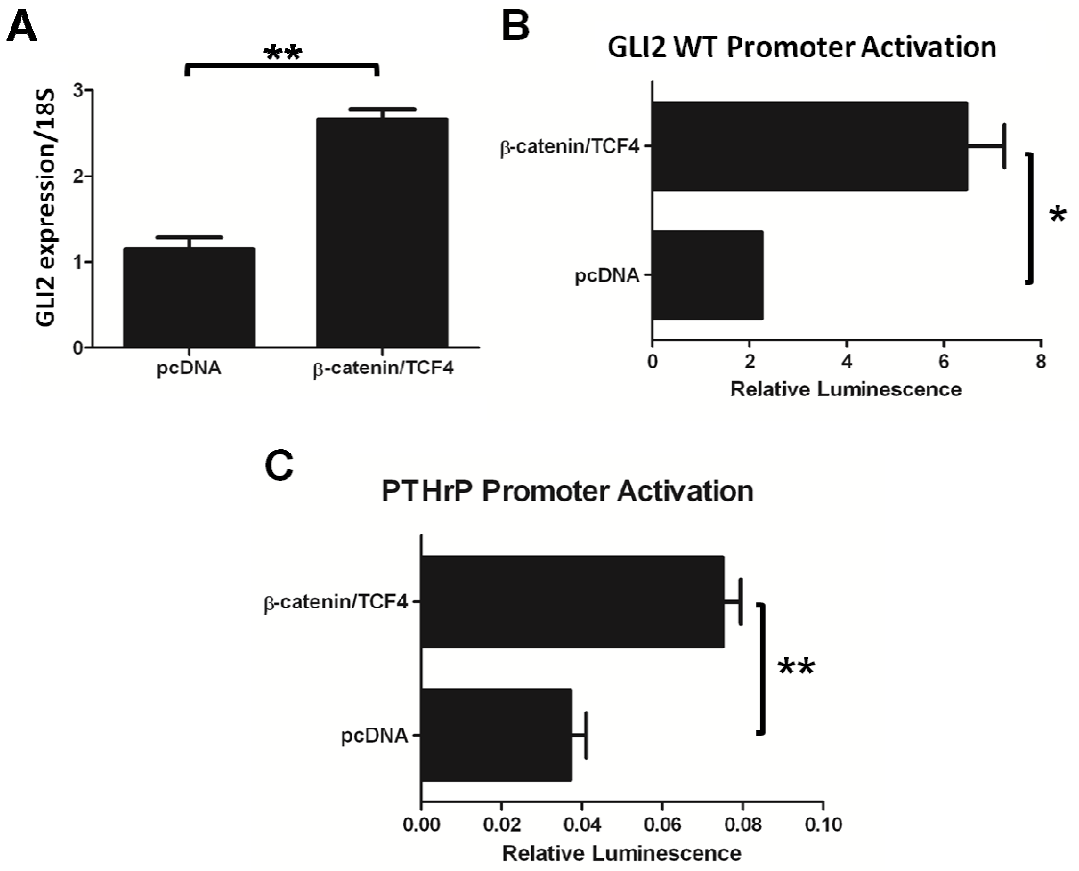

Figure 15. Effects of constitutive β-catenin expression on GLI2 and PTHrP transcription. (A) MDA-MB-231 cells co-transfected with constitutively expressed β-catenin construct S33Y and its co-factor TCF4 were evaluated for GLI2 mRNA expression (n=3/column). Data is normalized to 18S eukaryotic rRNA. MDA-MB-231 cells were co-transfected with S33Y/TCF4 construct and the wild-type (WT) GLI2 promoter (B), or PTHrP promoter (C) (n=3/column). Values = mean ± standard error, and p-values were determined using unpaired t-test. *p< 0.05, **p< 0.01, ***p<0.001.

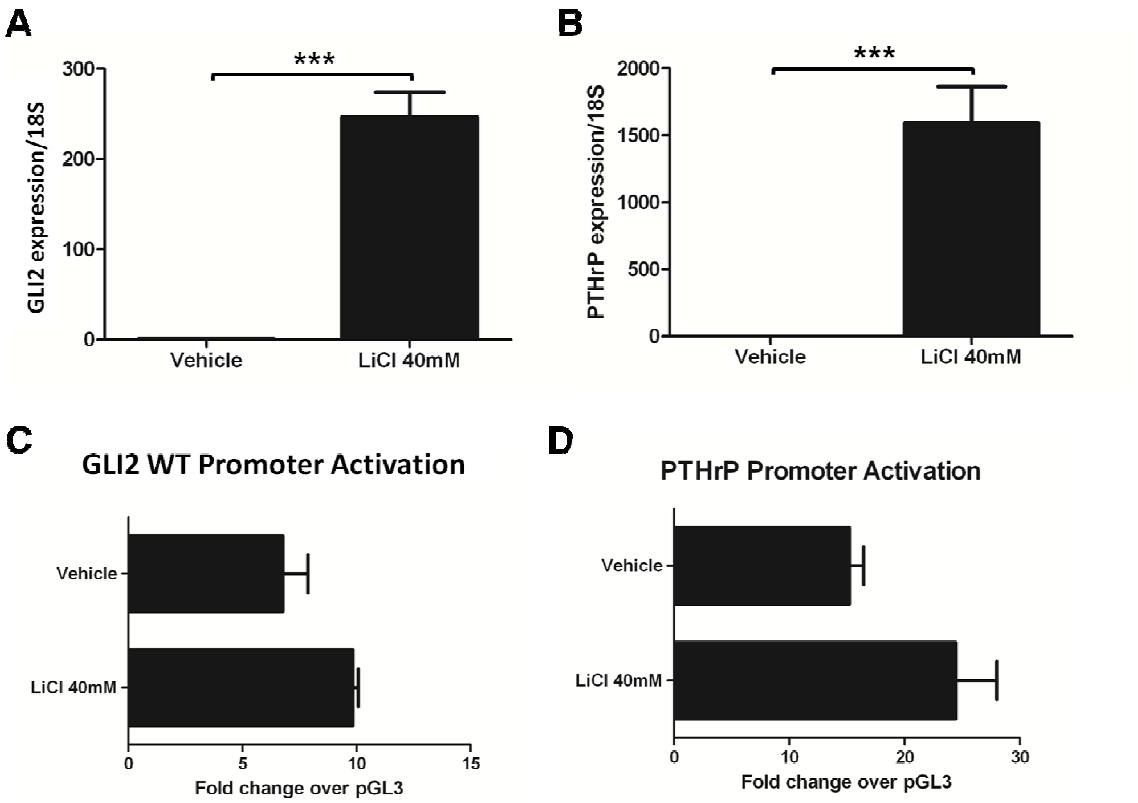

Figure 16. LiCl treatment stimulates GLI2 and PTHrP mRNA expression and promoter activation. MDA-MB-231 cells were treated for 24 hours with vehicle (water), 20mM, or 40mM LiCl solution to stimulate Wnt signaling through GSK3-β inhibition. RNA was evaluated for (A) GLI2 mRNA expression and (B) PTHrP mRNA expression (n=3/column). Both sets of data are normalized to 18s eukaryotic rRNA. MDA-MB-231 cells transfected with GLI2 WT (C) or PTHrP promoter (D) were harvested for luciferase assay following 24 hour LiCl treatment (n=3/column). Values = mean ± standard error, and p-values were determined using unpaired t-test. *p< 0.05, **p< 0.01, ***p<0.001.

through tankyrase inhibition (269), and VU-WS113 is a pyrvinium analogue developed by Ethan Lee's lab at Vanderbilt, which antagonizes Wnt signaling by enhancing CK1 activity, an enzyme partly responsible for β-catenin phosphorylation and its subsequent degradation (270). Although initially surprised by these data, we believe that the lack of inhibition of GLI2 and PTHrP mRNA expression may be contributed to up-regulated proteasome activity in our tumor cells, which is apparent in our Wnt signaling PCR microarray data in Table 1, or an indication of alternative regulators of β-catenin.

Since we observed elevated Gli2 and PTHrP expression when Wnt signaling was enhanced, and direct inhibition of Wnt signaling was ineffective in blocking GLI2 or PTHrP mRNA expression, we explored an alternative method of Wnt signaling inhibition and the effect on gene expression. Since MDA-MB-231 cells express relatively low levels of β-catenin (260), as well as low levels of Gli2 and PTHrP in the absence of Tgf-β (36), we reasoned that it may be difficult to block endogenous Gli2 and PTHrP through knockdown of β-catenin. However, MDA-MB-231 cells express high levels of the Wnt signaling antagonist, Dkk1 (271), which is also a downstream target of Wnt signaling. Therefore, we proposed that knockdown of DKK1 would result in elevated GLI2 and PTHrP mRNA expression. To test this, MDA-MB-231 cells were transiently transfected with shRNA against β-catenin (CTNNB1) or DKK1 and examined for GLI2 and PTHrP expression in the presence or absence of recombinant human TGF-β. As anticipated, we found that CTNNB1 knock-down was not sufficient to inhibit endogenous levels of GLI2 even in the presence of excess Tgf-β, but when we knocked down DKK1 in MDA-MB-231 cells, GLI2 and PTHrP mRNA expression were significantly enhanced (Figure 18A&B).

The basal expression of Gli2 and PTHrP in MDA-MB-231 cells, although higher than in tumor cells which do not cause osteolytic bone destruction *in vivo* (36), is relatively low in the

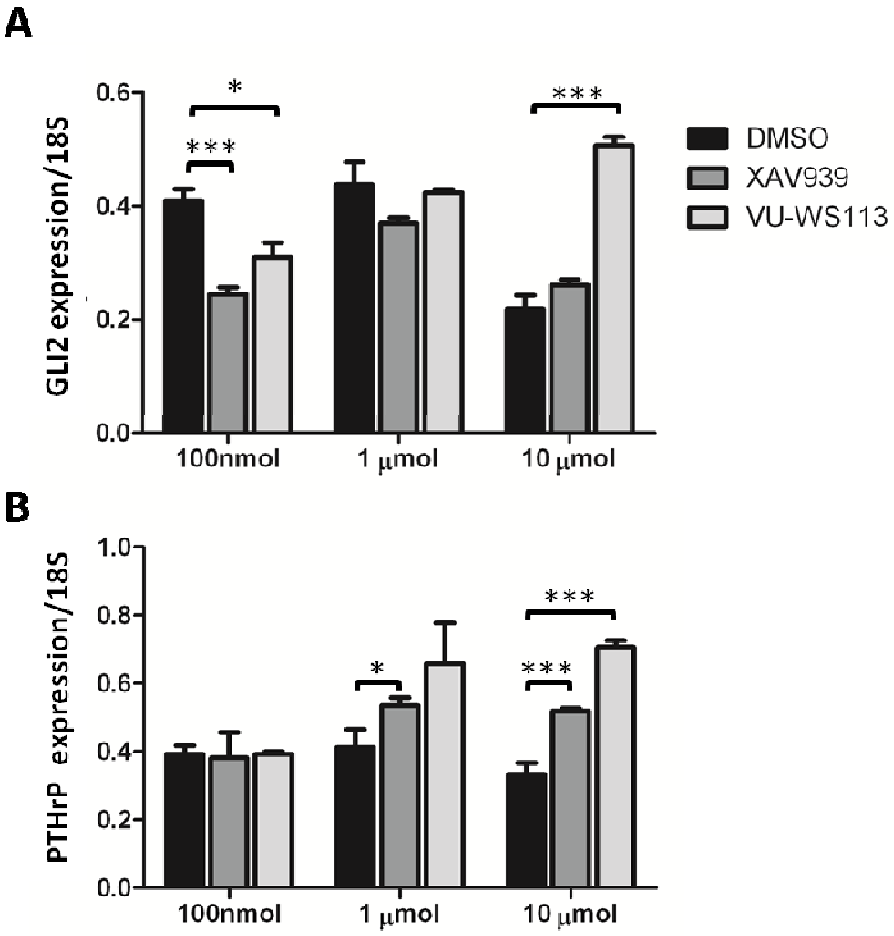

Figure 17. Wnt small molecule antagonists do not consistently inhibit GLI2 or PTHrP expression. MDA-MB-231 cells were treated for 24 hours with 100nmol-10μmol DMSO (control), XAV939, or VU-WS113 to block Wnt signaling and harvested for RNA. (A) GLI2 and (B) PTHrP mRNA expression were evaluated by Q-PCR. Values = mean ± standard error, and p-values were determined using unpaired t-test. *p< 0.05, **p< 0.01, ***p<0.001.

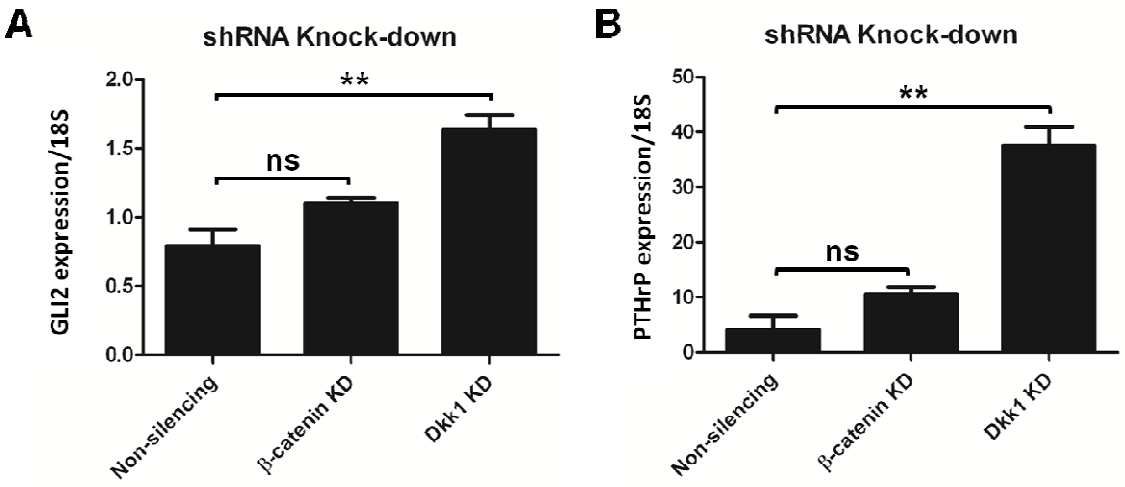

Figure 18. DKK1 knockdown up-regulates GLI2 and PTHrP mRNA expression. MDA-MB-231 cells transfected with shRNA against β-catenin (CTNNB1) or DKK1. Non-silencing vector serves as a control. Recombinant human Tgf-β1 was added at 10ng/mL in serum-free DMEM 24h following transfection. (A) GLI2 mRNA expression and (B) PTHrP mRNA expression are normalized to 18S eukaryotic rRNA (n=3/column). Values = mean ± standard error, and p-values were determined using unpaired t-test. *p< 0.05, **p< 0.01, ***p<0.001.

absence of Tgf-β. Therefore, inhibitors of their endogenous expression are difficult to find, and we are generally able to enhance Gli2 and PTHrP production more efficiently than inhibiting their expression. Since MDA-MB-231 cells have previously been shown to express low levels of β-catenin (260) and elevated levels of Dkk1 (271), we reasoned that knockdown of CTNNB1 would likely not affect Gli2 and PTHrP, while knockdown of DKK1 would enhance Gli2 and PTHrP. As anticipated, CTNNB1 knockdown did not affect GLI2 or PTHrP mRNA expression, despite our data showing that β-catenin over-expression significantly enhanced Gli2 transcription. Accordingly, knocking down DKK1 enhanced GLI2 and PTHrP expression. It is important to note that the publication citing Dkk1 levels in MDA-MB-231 cells to be >78-fold higher than in MCF-10A cells (271) conducted these experiments when MDA-MB-231 cells were cultured on TCPS, making it difficult to determine the contribution of matrix stiffness to the endogenous levels of Dkk1.

Effects of Wnt and Tgf-β signaling on mRNA stability

Since our group has demonstrated that Tgf-β signaling regulates GLI2 mRNA expression in osteolytic tumor cells (61) and since the knockdown of DKK1 enhanced GLI2 expression only when Tgf-β was in excess, we examined whether Tgf-β or β-catenin affects GLI2 mRNA stability. MDA-MB-231 cells were either transfected with non-degradable β-catenin or treated with 5ng/ml human recombinant Tgf-β1 and incubated with 0.8μM actinomycin D to block transcription over a period of 10 hours. The cells were harvested for RNA at multiple time points and examined for GLI2 mRNA expression by Q-PCR. Using Linear Regression analysis and slope comparison, we found that neither Tgf-β alone, nor Tgf-β in combination with β-catenin over-expression, significantly altered GLI2 mRNA stability (Figure 19A).

Recombinant human Tgf-β1 was added to the culture medium in these experiments, as indicated, to more accurately reflect the physiological environment of the tumor cells within rapidly resorbing bone matrix, which is an abundant source of Tgf-β (26). Since the up-regulation of GLI2 following DKK1 knockdown was achieved in conditions with excess Tgf-β, we thought it likely that Tgf-β was stabilizing the GLI2 transcript; however, when we attempted to rescue GLI2 transcription with Tgf-β, it was unable to stabilize GLI2 mRNA, suggesting that in addition to β-catenin regulation of Gli2, Wnt signaling may crosstalk with other signaling pathways in MDA-MB-231 cells, such as Src kinase. Our group is currently investigating the effects of Src kinase as a function of mechanotransduction on Gli2 and PTHrP regulation (*Ruppender et al*.; submitted). It is possible that a combination of lifting the "brakes" on the Wnt signaling pathway through Dkk1 inhibition and adding excess Tgf-β results in optimal GLI2 transcription conditions in MDA-MB-231 cells, but it is unlikely that this is due to mRNA stabilization. These data correlate nicely with the results published by Dennler and colleagues on Tgf-β activation of the GLI2 promoter in keratinocytes (60).

Previous reports have suggested that Tgf-β signaling plays a crucial role in regulating PTHrP mRNA stability (75-77); however, there are conflicting published data concerning Tgf-β regulation of PTHrP mRNA stability (78), and these data remain controversial to some extent. To determine the dual effect of Tgf-β and Wnt signaling on PTHrP mRNA stability, we again transfected MDA-MB-231 cells with non-degradable β-catenin or treated with 5ng/ml human recombinant Tgf-β1 and incubated with 0.8μM actinomycin D to halt transcription. Following actinomycin D treatment, we found that neither Tgf-β nor β-catenin alone or in combination rescued PTHrP mRNA expression over the course of the experiment (Figure 19B). When we looked at select individual time-points, we found that a combination of recombinant Tgf-β and β-catenin over-expression significantly stabilized PTHrP mRNA, but when we conducted the

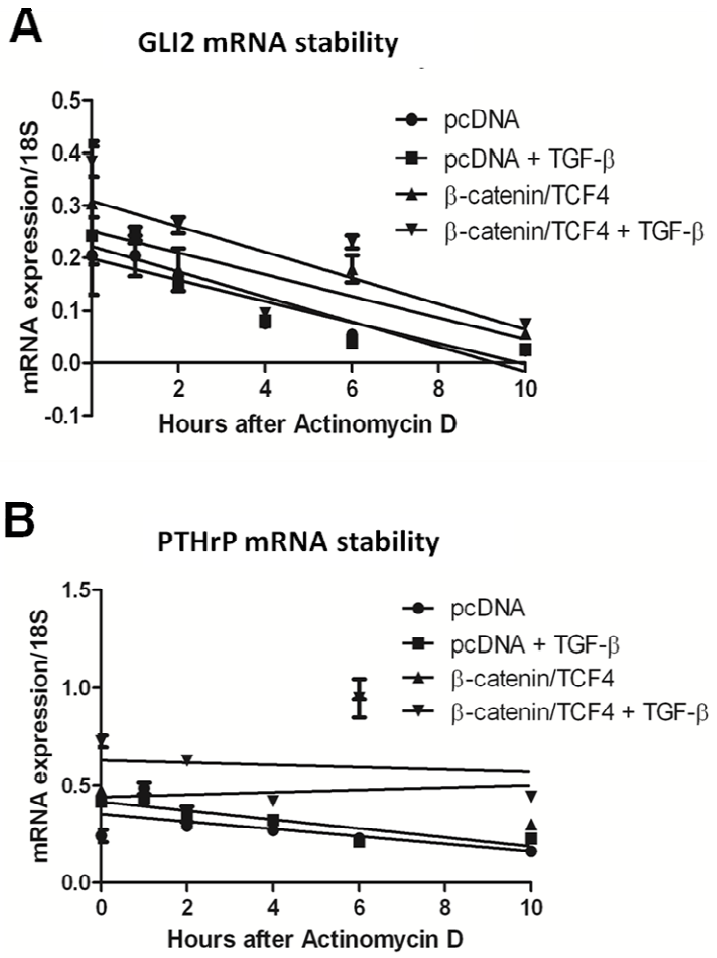

Figure 19. Wnt signaling and Tgf-β effects on mRNA stability. (A) Linear regression analysis on MDA-MB-231 cells transfected with non-degradable β-catenin or recombinant Tgf-β and harvested for Q-PCR. Plot points indicate average GLI2 or (B) PTHrP mRNA expression normalized to 18S as a percentage of zero hour mean value, and regression lines indicate overall trend of mRNA expression (n=3/plot point). Values = mean ± standard error, and p-values were determined using unpaired t-test. *p< 0.05, **p< 0.01, ***p<0.001.

linear regression analyses, these data were no longer significant. Therefore, the up-regulation of PTHrP mRNA expression that we observe downstream of enhanced Tgf-β and Wnt signaling is likely due primarily to an alteration in Gli2 and PTHrP transcription.

Our data further supports the idea that Tgf-β signaling is important at the transcription level, and to that end, also introduces the idea that β-catenin is a PTHrP transcription regulator. Whether these effects are strictly through GLI2 mRNA expression, or rely on another mechanism, is unclear. Recent data has suggested that PTHrP peptides may in fact stimulate β-catenin in osteocytes (terminally differentiated osteoblasts) (272), and our data does not rule out the possibility that an autocrine signaling loop exists in osteolytic breast tumor cells. In an effort to address previously published data, we did in fact examine Wnt signaling ligand expression by RT-PCR analysis. MDA-MB-231 cells do not express most of the Wnt ligands, but surprisingly, none of the Wnt ligands we examined were elevated on the stiffer substrate, and several actually appeared to decrease slightly on TCPS (data not shown). Indeed, it is quite conceivable that bone stiffness may be the ultimate regulator which initiates and activates Gli2 and PTHrP through mechanotransduction (97), and that β-catenin is turned on secondary to these events, perhaps through its well-established association with E-cadherin (273) or interactions with the Src family kinases. Unfortunately, studies examining the timing of these mechanisms in establishing and maintaining tumor-induced bone disease remain limited by both imaging techniques and molecular models of breast cancer metastasis to bone.

Wnt and Tgf-β co-regulation of the GLI2 promoter

There is ample evidence that the Tgf-β and Wnt signaling pathways crosstalk, both during development (274) and in cancer cells (275). To this end, we examined the inter-dependence of Wnt and Tgf-β signaling on GLI2 promoter activity using a construct in which the

TBE (mTCF) or SBE (mSmad) located within the GLI2 promoter has been mutated (60). MDA-MB-231 cells were transiently co-transfected with a GLI2 WT, mSmad, or mTCF promoter construct and Smad3 or β-catenin and harvested for luciferase assay analyses. We found that β-catenin stimulated GLI2 promoter activity when the SBE was mutated (Figure 20A), but Smad3 activated the GLI2 promoter to a much lesser extent when the TBE was mutated (Figure 20B). These data indicate that Tgf-β signaling has some dependence on Wnt signaling for full Gli2 regulation, but that Wnt signaling may not require active Tgf-β signaling to stimulate Gli2 activity.

Conclusions

Our data indicate that there is a strong role for β-catenin regulation of GLI2 gene expression downstream of Wnt signaling in osteolytic tumor cells, and furthermore, that Wnt signaling is influenced by the rigidity of bone. It is that stiffness plays a critical role in the early stages of tumor-induced bone disease through mechanotransduction and downstream Wnt and TGF-β signaling regulation, but does not affect tumor cell homing to bone, since the physical microenvironment is required for activation of mechanostransduction pathways. These data provide further insight into the regulation of key players in osteolytic bone destruction, and may be important when considering novel therapeutic targets for use in breast tumor-induced bone disease.

Importantly, we are hesitant to support the Wnt signaling pathway as a clinical target in blocking tumor-induced bone disease due to its critical role in osteoblast differentiation and protective effects in bone (126). However, most pharmacological interventions for blocking breast tumor metastases and growth in bone are limited by their catabolic effects on bone, and are therefore coupled with adjuvant bisphosphonates (276), which inhibit osteoclast resorption,

or more recently denosumab (277), which targets RANKL in bone. Despite its potential negative effects on bone, targeting the Wnt signaling pathway in bone metastases may be beneficial when combined with a bone protective adjuvant therapy.

Acknowledgements

These data have been compiled into the manuscript entitled "Bone stiffness drives Wnt signaling regulation of Gli2 in osteolytic breast cancer cells," authored by Rachelle W. Johnson, Alyssa R. Merkel, Nazanin S. Ruppender, Scott A. Guelcher, Lynn M. Matrisian, Gregory R. Mundy, and Julie A. Sterling, with intentions to submit these data for publication in the near future.

Ms. Alyssa Merkel contributed technical expertise in the stiffness studies, and Dr. Nazanin Ruppender and Mr. Jonathan Page created substrates for the completion of these studies. Dr. Julie Sterling, Dr. Scott Guelcher, Dr. Lynn Matrisian, Dr. T. John Martin, and the late Dr. Greg Mundy all provided scientific expertise and guidance.

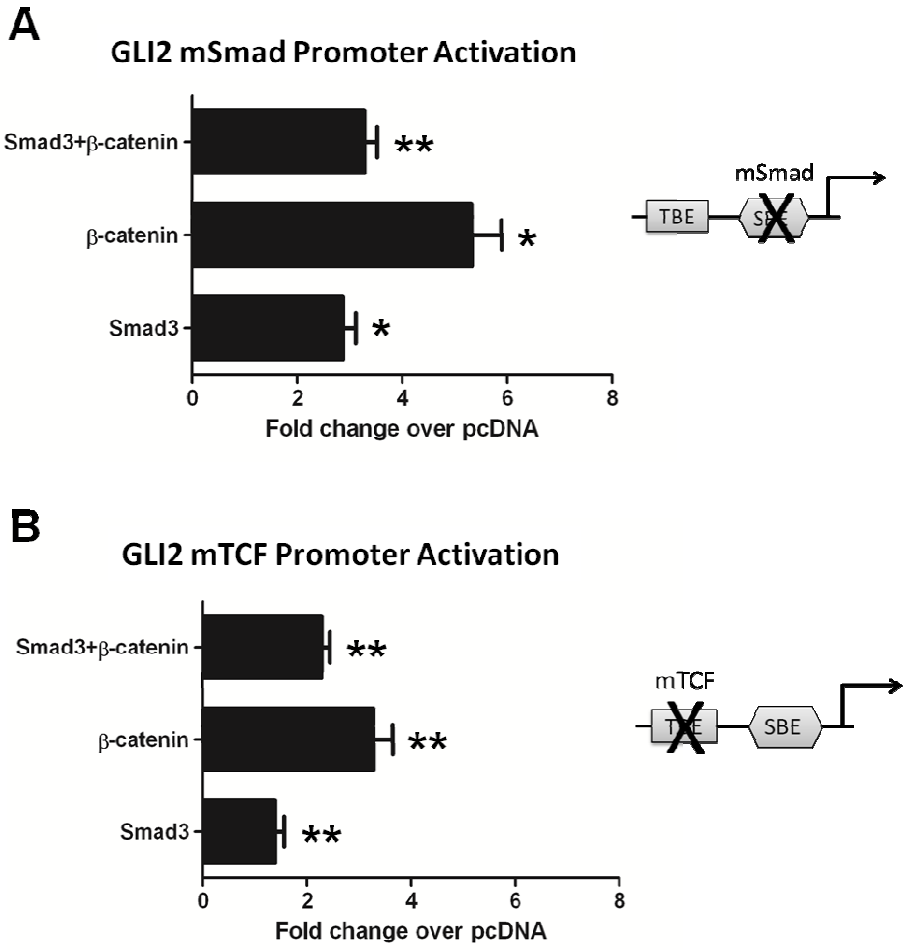

Figure 20. Wnt/Tgf-β signaling effects on mutated GLI2 promoter. MDA-MB-231 cells were co-transfected with either S33Y/TCF4 (constitutive β-catenin construct), Smad3, or S33Y/TCF4+Smad3 and the GLI2 mSmad (A) or mTCF (B) constructs and evaluated for promoter activation by dual-luciferase reporter assay system (n=3/column). Values = mean ± standard error, and p-values were determined using unpaired t-test. *p< 0.05, **p< 0.01, ***p<0.001.

Gli2 inhibition blocks tumor-induced bone disease

Introduction

Gli2 up-regulation is a significant component of PTHrP-mediated bone destruction in breast tumor metastasis to bone (36), and our data presented here indicate that the Tgf-β and Wnt signaling pathways are potential targets in blocking Gli2 and PTHrP-induced osteolysis; however, both of these pathways impart a significant contribution to tumorigenesis at the primary tumor site, which may compromise their effectiveness in patients with metastatic disease. Although Gli2 is expressed ubiquitously throughout development and participates in patterning, etc., it is effectively shut off after puberty. Thus targeting Gli2 directly may be a more promising approach to block osteolysis with minimal toxicity in humans.

We therefore hypothesized that inhibiting Gli2 through genetic or pharmacological approaches in a mouse model of breast cancer metastasis to bone would result in decreased osteolysis. For the genetic studies, MDA-MB-231 cells stably transfected with the Gli2-Rep construct, as described in an earlier section, were used in a mouse model of breast cancer metastasis to bone. The Gli-Antagonist (GANT) compounds, which inhibit Gli function irrespective of the mutation leading to the activation of Gli (24), were used to pharmacologically inhibit Gli2 signaling. These compounds were identified in a cell-cased screen for inhibitors of Gli1, so they lack some specificity for Gli2. Perhaps due to limited availability as a result of lack of large-scale synthesis of these compounds, they have been tested in relatively few models (62, 278).

Gli2 repression inhibits tumor-mediated osteolytic bone destruction

In order to determine if blocking Gli2 activity could indeed inhibit tumor-induced osteolysis, we inoculated pooled MDA-MB-231-Gli2-Rep and MDA-MB-231-cntrl cells into 4-

week old athymic female nude mice via the left cardiac ventricle. After 4 weeks, extensive osteolytic lesions were visible by radiography in the femora/tibiae of the control mice. In contrast, the Gli2-Rep mice had either small or undetectable lesions (Figure 21A). Quantification of lesion number and size on radiographs indicated that mice bearing MDA-MB-231-Gli2-Rep tumor cells had significantly fewer and smaller lytic lesions than the mice bearing control cells (Figure 21B&C). Similar results were obtained for mice inoculated with Gli2-Rep transfected cells derived from single cell clones (Figure 22).

In addition to radiographic analyses, tibiae were examined by *ex vivo* microCT. There was a significant decrease in trabecular bone volume in the MDA-MB-231-cntrl inoculated mice compared to the MDA-MB-231-Gli2-Rep inoculated mice (Figure 23A), although there were no other significant changes in microCT parameters such as trabecular number, trabecular thickness, or connectivity density (Figure 23B-D). Bone volume of mice inoculated with MDA-MB-231-Gli2-Rep cells was not significantly different from non-tumor bearing age- and sex-matched mice (BV/TV approx. 0.0448-.1518). These data indicate that Gli2 inhibition in MDA-MB-231 cells decreased the ability of the tumor cells to induce bone destruction.

Consistent with disrupting TGF-β induced propagation of tumor-induced osteolysis, histomorphometric analyses of the tibiae revealed a significant decrease in tumor burden in Gli2-Rep tumor bearing mice relative to empty-vector control tumor-bearing mice (Figure 23E), and this was accompanied by a reduction in detectable PTHrP protein expression identified by immunohistochemistry (Figure 23F).

Interestingly, we observed a decrease in tumor burden at sites of bone metastases in the Gli2-Rep intracardiac model, although tumor growth was unaltered in the Gli2-Rep orthotopic mammary fat pad model as shown in Figure 11C. Since our previous data indicate

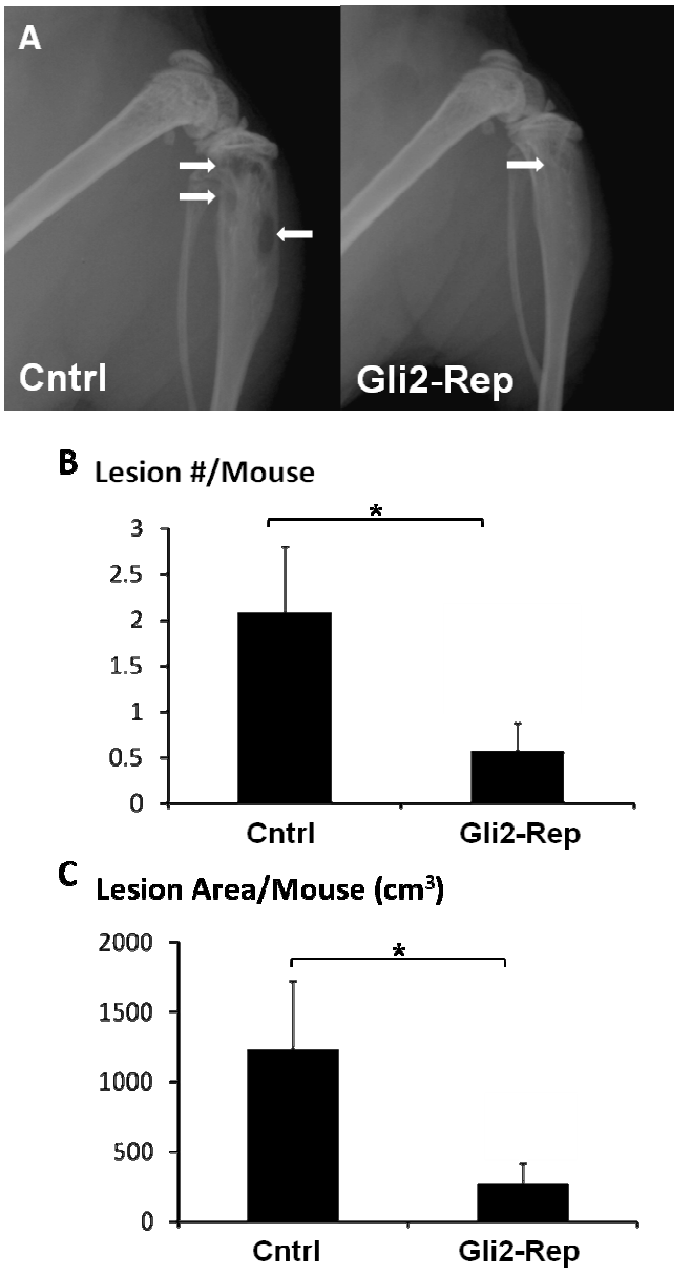

Figure 21. Gli2-Rep blocks tumor-induced bone disease. Mice inoculated with MDA-MB-231-Gli2-Rep (n=7) or MDA-MB-231-cntrl (n=10) cells via intracardiac injection were imaged radiographically weekly. (a) Faxitron images depict fewer lesions in mice inoculated with MDA-MB-231-Gli2-Rep cells. There was a significant reduction in average lesion number/mouse (b) and average lesion area/mouse (c), as measured by region of interest (ROI) analysis. Values = mean ± standard error, and p-values were determined using unpaired t-test. *p< 0.05, **p< 0.01, ***p<0.001.

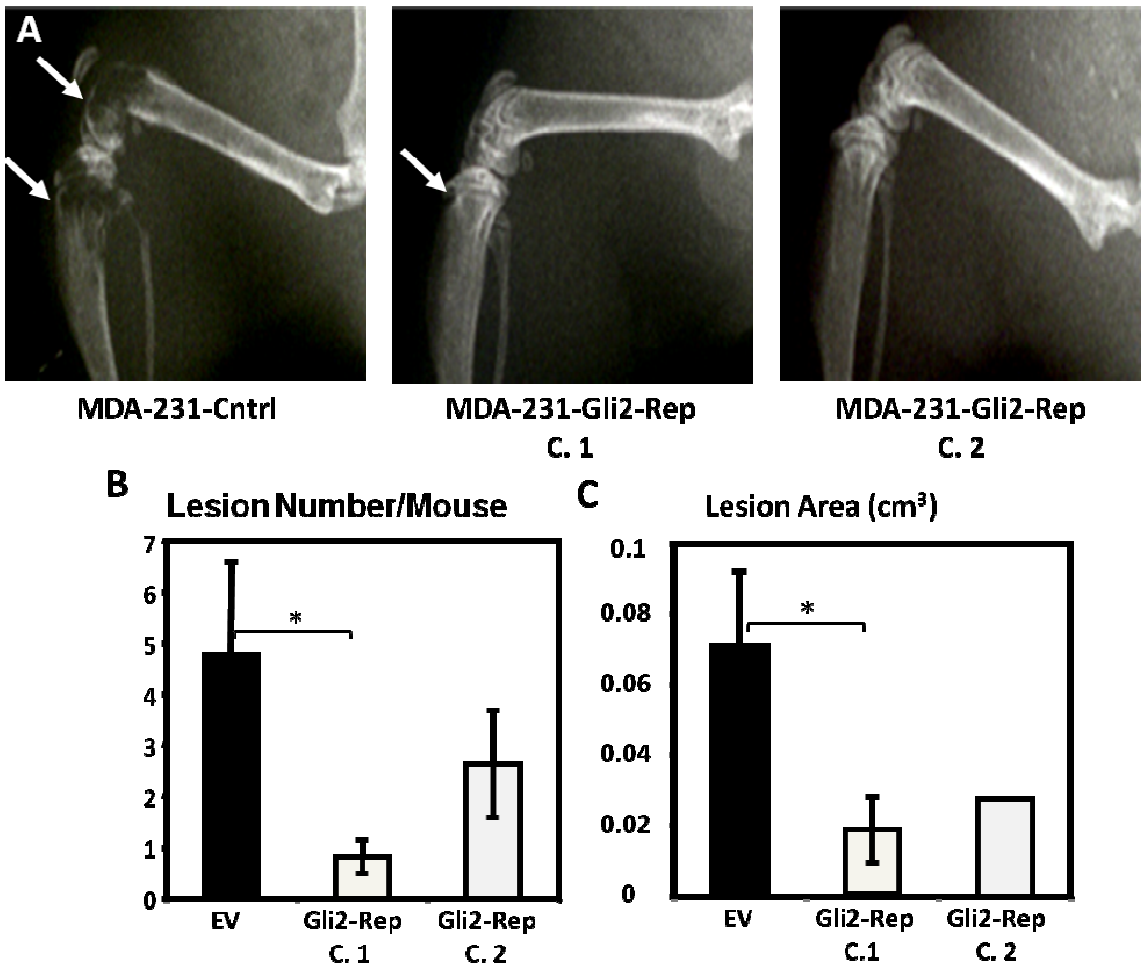

Figure 22. Gli2-Rep reduces tumor-induced bone disease following clonal selection of tumor cells. MDA-MB-231 cells transfected with Gli2-Rep or empty vector control were plated as single cell limiting dilutions, clonally selected for antibiotic resistance (400µg/ml G418 selection), and inoculated into female, athymic nude mice via intracardiac injection (n=10, control; n=9, Gli2-Rep). (a) Faxitron images depict decreased osteolysis in mice inoculated with either clone 1 or clone 2 of the MDA-MB-231-Gli2-Rep cells when compared to MDA-MB-231-cntrl inoculated mice. Quantification of these images using Metamorph shows a significant reduction in (b) average lesion number/mouse and (c) average lesion area/mouse. Values = mean ± standard error, and p-values were determined using unpaired t-test. *p< 0.05, **p< 0.01, ***p<0.001.

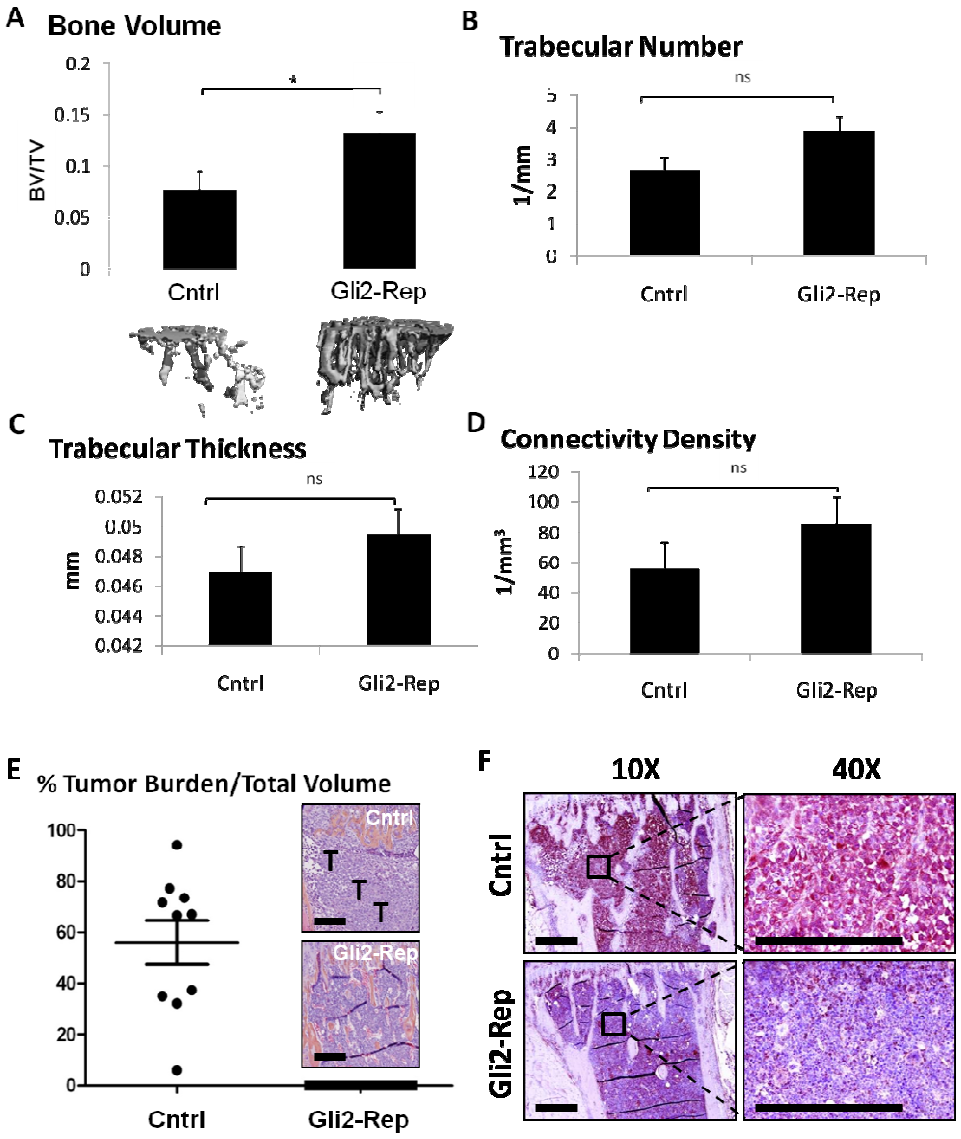

Figure 23. Gli2-Rep reduces osteolysis and tumor burden. (A) *Ex vivo* microCT (Scanco) analyses indicate a significant reduction in osteolysis in MDA-MB-231-Gli2-Rep inoculated mice (n=7 tibiae) compared to MDA-MB-231-Cntrl inoculated mice (n=10 tibiae). *Ex vivo* microCT (Scanco) analyses do not indicate any significant difference in additional microCT parameters beyond bone volume in MDA-MB-231-Gli2-Rep inoculated mice (n=7 tibiae) compared to MDA-MB-231-Cntrl inoculated mice (n=10 tibiae). (B) Trabecular number, (C) Trabecular thickness, and (D) Connectivity density. Histomorphometric analyses of bone sections from these mice show (E) significant inhibition of tumor burden in MDA-MB-231-Gli2-Rep inoculated mice, and (F) decreased immunohistochemical staining for PTHrP in sections from MDA-MB-231-Gli2-Rep mice. The black bar on the histological sections represents a length of 500µM. Values = mean ± standard error, and p-values were determined using unpaired t-test. *p< 0.05, **p< 0.01, ***p<0.001.

that Tgf-β at least in part regulates Gli2 signaling, we reason that the observed decrease in tumor growth was caused by indirect blockade of Tgf-β stimulation of PTHrP, and overall blockade of the vicious cycle. Our *in vitro* studies demonstrated that Gli2 is in fact required for Tgf-β to increase PTHrP expression, suggesting that when Gli2 is not activated, Tgf-β in the bone matrix will no longer have a stimulatory effect on PTHrP secretion from breast cancer tumor cells and consequently tumor cell growth and bone resorption will be inhibited.

GANT inhibits PTHrP expression but not osteolysis

The GANT compounds (GANT58 and GANT61) were initially discovered in a cell-based screen to find inhibitors of the Hh transcription factor Gli1, which is known to be important in tumorigenesis at the primary site of disease (62); however, due to the homology between Gli1 and Gli2, these compounds effectively block the function of both molecules. Both compounds are believed to inhibit Hh downstream of Smo by causing a conformational change in nuclear Gli which compromises DNA binding (62).

In an effort to block Gli2 signaling in osteolytic tumor cells, we treated MDA-MB-231 cells with 10μmol GANT58 and found that it significantly blocked PTHrP mRNA expression *in vitro* (Figure 24A), and similar to our Gli2-Rep data, found that GANT58 had no effect on tumor cell growth at the primary site when MDA-MB-231 cells were inoculated into the mammary fat pad (Figure 24B).

Since GANT 58 successfully reduced PTHrP expression *in* vitro, we tested its effectiveness in a mouse model of breast cancer metastasis to bone, where we inoculated 4-week old athymic nude mice with MDA-MB-231-GFP cells via intracardiac injection and treated mice with 25mg/kg/day of GANT58 by i.p. injection. When we examined GANT58 effects on tumor burden, we found that although GANT58 treatment trended toward a decrease in tumor

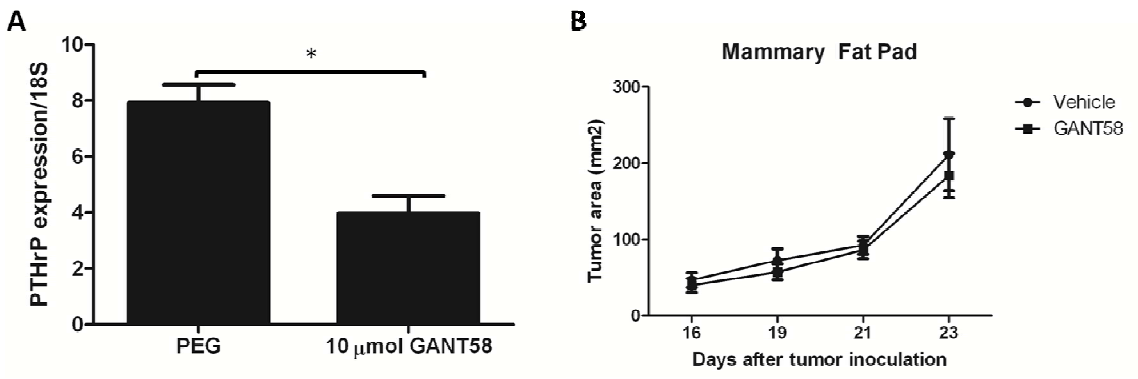

Figure 24. GANT58 reduces PTHrP expression but does not alter tumor growth *in vivo*. (A) MDA-MB-231 cells were treated with 10μmol GANT58 for 24 hours and harvested for RNA. (B) 4-week old athymic nude mice were inoculated with 1×10^7 MDA-MB-231 cells directly into the mammary fat pad, treated with 25mg/kg/day GANT58 (n=6) or PEG (n=8) and allowed to grow for 23 days. Tumor size was determined by caliper measurement throughout experiment. Values = mean ± standard error, and p-values were determined using unpaired t-test. *p< 0.05, **p< 0.01, ***p<0.001.

burden by histomorphometric analyses (Figure 25A), tumor cell fluorescence revealed no significant changes in tumor burden (Figure 25B). Analyses of GANT58 treatment on bone volume in the same tumor bearing animals indicated that although GANT58 treatment trended toward increased bone volume and trabecular number by *ex vivo* microCT (Figure 25F&G), it did not did not alter bone volume as measured by histomorphometry (Figure 25C), nor did it affect the microCT parameters of trabecular spacing, trabecular thickness (Figure 25H&I), or lesion area or lesion number as measured by Faxitron analyses (Figure 25D&E). Similar negative results were found when mice were inoculated with MDA-MB-231 cells directly into the tibia (Figure 26), and when treated with GANT61 (data not shown).

Although Gli proteins are not expressed in adult mice, the unanticipated results from the GANT58 intracardiac and intratibial studies prompted us to test GANT58 effects on normal bone modeling. When we treated normal mice with 25mg/kg/day of GANT58, we found that GANT58 treatment resulted in decreased bone volume and trabecular number, and increased trabecular spacing by microCT analyses (Figure 27A-C), but did not affect trabecular thickness (Figure 27D). In order to determine if the data was due to an increase in osteoclast number, histological sections were stained for TRAP positive osteoclasts, where we found that neither osteoclast number nor osteoclast surface/bone surface were elevated (Figure 27E&F). Since GANT58 disrupts downstream Hh signaling, which is important for growth plate regulation during development (279), and our breast tumor model uses 4-week old mice, we tested whether GANT58 affects the overall height or organization of the growth plate. We found that GANT58 treatment did not affect the overall height of the growth plate (Figure 27G), but significantly reduced the size of the proliferation zone (Figure 27H), and disrupted its organization as seen in Figure 28I.

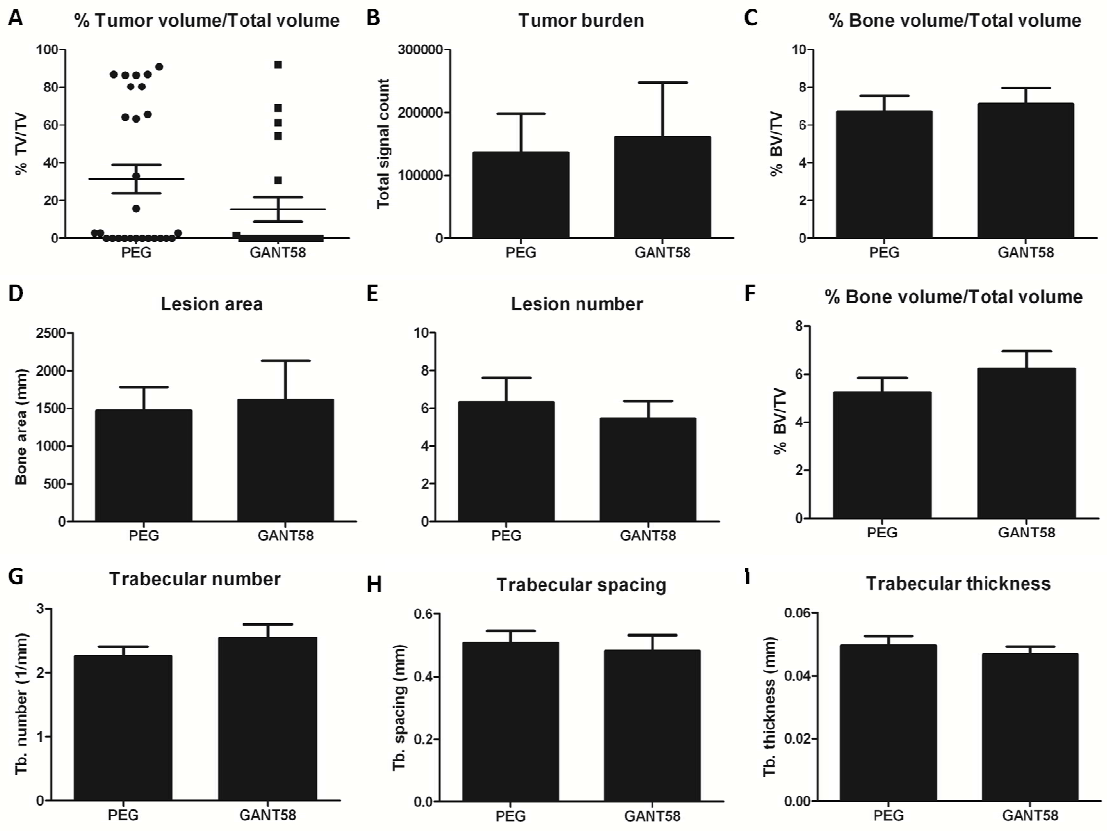

Figure 25. GANT58 does not block osteolysis as measured by trabecular analyses. 4-week old athymic nude mice were inoculated with 1×10^6 MDA-MB-231 cells via intracardiac injection, treated with 25mg/kg/day GANT58 (n=11) or PEG (n=13), and sacrificed after 4 weeks, with imaging throughout. (A) Histomorphometric analyses of H+E stained slides reveal a trend toward decreased tumor burden with GANT58 treatment. (B) Tumor cell fluorescence imaging by Maestro shows no change in tumor burden. (C) Histomorphometric analyses show no change in bone volume. (D,E) Faxitron analyses show no changes at end-point between PEG and GANT58 treatment. (F-I) *Ex vivo* microCT analyses indicate a trend toward increased bone volume (F) and Tb. Number (G), but no significant changes were detected in any parameters with any imaging modality. Values = mean ± standard error, and p-values were determined using unpaired t-test.

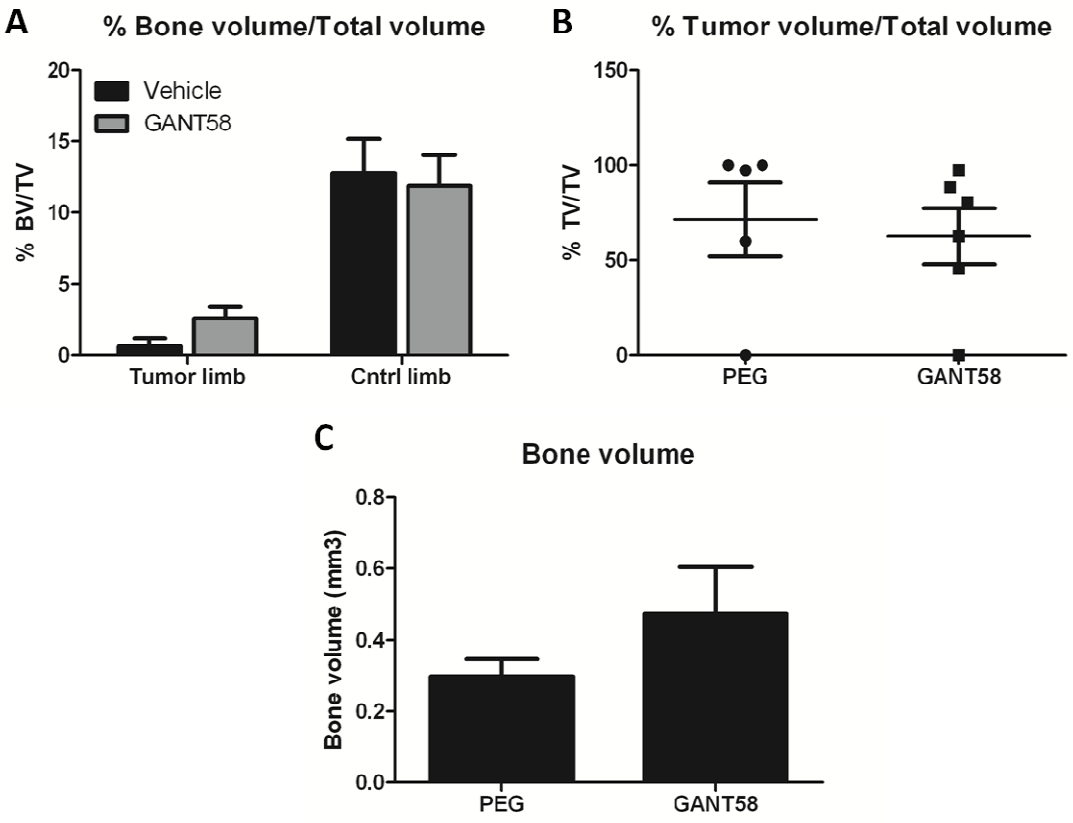

Figure 26. GANT58 does not alter bone volume or tumor burden in the mouse intratibial model. 4-week old athymic nude mice were inoculated with 1×10^5 MDA-MB-231 cells directly into the tibia, treated with 25mg/kg/day GANT58 (n=7) or PEG (n=5) and sacrificed after 4 weeks, with imaging throughout. (A) Histomorphometry analyses reveal that GANT58 treatment slightly prevented osteolysis in the tumor limb and had no affect on the control limb. Neither of the results were significant. (B) Histomorphometry analyses showed that GANT58 did not decrease tumor burden, although there was a slight trend toward decreasead tumor burden with GANT58 treatment. (C) MicroCT analysis of the tumor bearing limb showed that PEG treated mice had lower bone volume than GANT58 treated mice, but these results were not significant. Values = mean ± standard error, and p-values were determined using unpaired t-test.

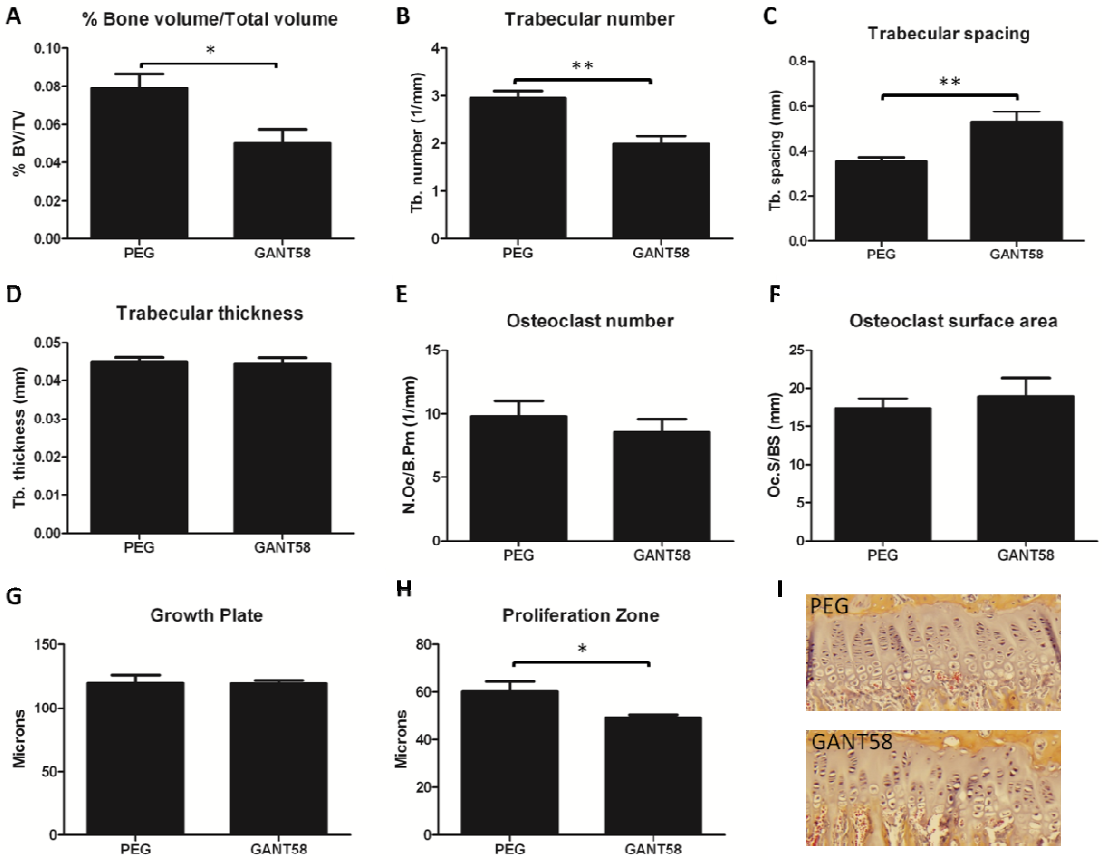

Figure 27. GANT58 decreases bone volume through disruption of the growth plate. 4-week old athymic nude mice were treated with GANT58 (n=4) or PEG (n=5) for 4 weeks until sacrifice. (A) MicroCT analyses reveal that GANT58 treatment significantly reduced bone volume, (B) Tb. Number, and (C) Tb. Spacing, but did not affect (D) Tb. thickness. Histomorphometric analyses show that (E) Oc number and (F) surface area were unaffected by GANT58 treatment, and that (G) the height of the growth plate was not altered. (H, I) Further analysis of the growth plate shows that the proliferating zone of chondrocytes was disrupted with GANT58 treatment. Values = mean ± standard error, and p-values were determined using unpaired t-test. *p< 0.05, **p< 0.01, ***p<0.001.

We believe that this phenotype can be largely attributed to limitations of the tumor model, in that 4-week old mice with an open growth plate are required for efficient tumor take. Gli2 is essential for normal growth plate development, and bones harvested from Gli2-/- embryos show decreased Ihh, Ptch, and PTHrP expression (59), which fits well with the observed reduction in the size of the growth plate proliferating zone after GANT58 treatment and also suggests that the significant decrease in bone volume occurs because there is less foundation for bone being made in the presence of GANT58. In addition to the observed effects of GANT treatment on chondrocyte maturation, disruption of downstream Ihh signaling by GANT may also elicit an effect on osteoblast differentiation. Indeed, Ihh produced by prehypertrophic chondrocytes, in addition to signaling back to proliferating chondrocytes, also signals to the perichondrium to stimulate osteoblast differentiation (279). This correlates well with our Gli2-Rep data, in which we disrupted Gli signaling in the tumor cells only and observed a reduction in tumor burden and osteolysis. Therefore, we believe that Gli2 is still an effective target, but that the limitations of our tumor model make this difficult to explore therapeutically. We hope to develop a tumor model in the future which will allow us to test the effects of GANT in a mouse model of breast cancer metastasis to bone in which the growth plate is closed.

Conclusions

The inhibition of bone destruction and tumor growth observed in the Gli2-Rep tumor bearing mice identifies Gli2 as a promising target for developing therapeutic approaches in the prevention and treatment of tumor-induced bone disease. Postnatal expression of Gli2 is primarily limited to the growth plate (59) and the hair follicle (280, 281), making Gli2 an ideal clinical target with low potential for significant off target effects in adult patients.

This work demonstrates that Gli2 genetic inhibition reduces tumor growth and bone destruction, suggesting that targeting Gli2 may be a valid approach to inhibit bone metastases; however, our GANT *in vivo* results indicate that inhibiting Gli signaling in adolescents would reduce the anti-osteolytic effect of Gli inhibition. Therefore, we would only recommend using Gli inhibitors in adults, where we believe that osteolysis and tumor burden would be reduced. This seems quite reasonable clinically, since breast cancer does not affect pre-adolescents.

Accordingly, the guanosine nucleotide 6-TG is used clinically in leukemia patients and has been shown to effectively block osteolysis and reduce tumor burden in a mouse model of breast cancer metastasis to bone (27). Since 6-TG was not reported to affect the growth plate in these mice, we investigated whether 6-TG inhibition of PTHrP is mediated through Gli2, and perhaps preferentially affects tumor cells since they are rapidly dividing. These data are presented in the following section.

Acknowledgements

A portion of these data were published in *Cancer Research* as follows: Rachelle W. Johnson, Mai P. Nguyen, Susan S. Padalecki, Barry G. Grubbs, Alyssa R. Merkel, Babatunde O. Oyajobi, Lynn M. Matrisian, Gregory R. Mundy, Julie A. Sterling. TGF-beta promotion of Gli2-induced expression of parathyroid hormone-related protein, an important osteolytic factor in bone metastasis, is independent of canonical Hedgehog signaling. Cancer Res. 2011 Feb 1;71(3):822-31. Epub 2010 Dec 28 (61).

Ms. Alyssa Merkel provided excellent technical support, animal work, and data analysis for the Gli2-Rep and GANT studies. Dr. Dan Perrien provided technical support with microCT scanning, osteoclast, and growth plate analyses. Dr. Julie Sterling, Dr. Lynn Matrisian, Dr. T. John Martin and the late Dr. Greg Mundy provided scientific critiques and guidance.

6-Thioguanine inhibition of PTHrP is mediated through Gli2

Introduction

The release of PTHrP into the tumor-bone micro-environment contributes to increased osteoclastogenesis and the excessive release of active Tgf-β at the site of skeletal metastasis. Our group has previously demonstrated that GLI2 overexpression in osteolytic breast cancer cells increases osteolysis *in vivo* (36), and here we have shown that transfection with Gli2-Rep inhibits PTHrP mRNA expression *in vitro* and *in vivo*. In addition, others have shown that PTHrP inhibition by neutralizing antibody prevents tumor-induced bone destruction in a murine model of breast cancer metastasis to bone (28).

Guanosine metabolites have been clinically utilized for the treatment of acute leukemia, where the purine analogs incorporate into DNA and disrupt its replication and subsequent cellular proliferation (224), resulting in a modest antitumor effect. 6-Thioguanine (6-TG) was initially identified during a cell-based screen for compounds that inhibit PTHrP promoter activation, and has been shown to specifically inhibit PTHrP expression at low doses and with little cytotoxicity (27). 6-TG has also been shown to inhibit PTHrP activity in human breast cancer cells *in vitro* and tumor growth and osteolysis *in vivo* in a murine model of breast cancer metastasis to bone (27); however, the mechanism through which 6-TG inhibits PTHrP remains unknown.

Based on these data, we hypothesized that the inhibitory effects of 6-TG on PTHrP occur in a Gli2-dependent manner. In this study, we treated human osteolytic MDA-MB-231 breast cancer cells and human RWGT2 squamous-cell lung carcinoma cells with 6-TG and examined GLI2 mRNA transcription and stability by Q-PCR. In addition, we transfected osteolytic breast cancer cells with a GLI2 promoter construct and examined the ability of 6-TG to directly inhibit

GLI2 promoter activity. Lastly, GLI2 was constitutively expressed under the CMV promoter to block the inhibitory effect of 6-TG on PTHrP mRNA expression.

Low doses of 6-TG do not inhibit cell proliferation

It has previously been shown that low doses of 6-TG specifically inhibit PTHrP in tumor cells, but do not alter tumor growth *in vivo* (27). In order to more directly examine the effect of low-dose 6-TG treatment on tumor cell growth, we determined whether the general cytotoxic effects of 6-TG were abolished at low-dose treatment *in vitro*. In order to determine the effect of low dose 6-TG on cell proliferation, MDA-MB-231 or RWGT2 cells were treated with 100 µmol 6-TG and examined for changes in cellular metabolism via MTS assay. We found that at low doses, 6-TG does not inhibit tumor cell growth of MDA-MB-231 (Figure 28A) or RWGT2 cells (Figure 28B), indicating that the effects of 6-TG on PTHrP are not due to changes in cell proliferation.

6-TG exhibits inhibitory effects on GLI2 mRNA and protein expression

We have shown here that both RWGT2 and MDA-MB-231 cells express detectable levels of GLI2, and that TMC23 cells express GLI2 and the Hh signaling receptors PTCH and SMO. Since it is well-established that Gli2 regulates PTHrP in some osteolytic breast cancer cells (36, 61), we rationalized that 6-TG may therefore inhibit PTHrP through Gli2 regulation. To determine the effect of 6-TG on GLI2 and PTHrP mRNA expression in tumor cells, we treated MDA-MB-231 human breast cancer cells, RWGT2 human squamous-cell lung carcinoma cells, and control TMC23 proliferating chondrocytes with 100 µmol 6-TG and harvested cells after 24 or 48 hours for RNA, which was reverse transcribed for Q-PCR. We found that 6-TG significantly inhibited expression of GLI2 and PTHrP mRNA in MDA-MB-231 cells at both 24 and 48 hours post-treatment, and modestly inhibited these in RWGT2 and control TMC23 cells (Figure 29A&B), and

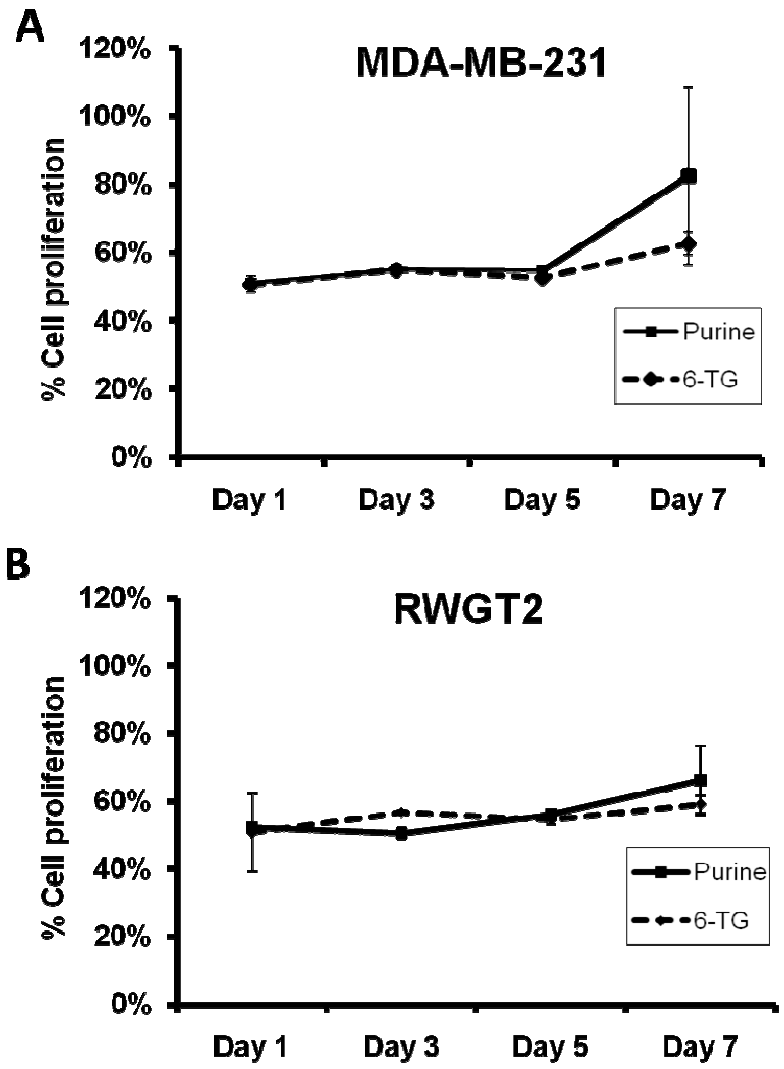

Figure 28. Low-dose treatment of 6-TG does not alter viability of osteolytic tumor cells. Osteolytic tumor cells were treated with 100 µmol 6-TG for 24 hours. Treatment did alter tumor cell viability *via* MTS assay of (A) MDA-MB-231 human osteolytic breast cancer cells, nor of (B) RWGT2 human osteolytic squamous-cell lung carcinoma cell line. Values are the mean ± standard error (n=4). No significant differences in data were detected using unpaired *t*-test.

these effects were observed as early as 4 hours post-treatment in MDA-MB-231 cells (Figure 29C). To determine whether 6-TG also has inhibitory effects at the protein level, we analyzed MDA-MB-231 and RWGT2 cell lysates by Western blot for Gli2 protein expression. We found that 6-TG treatment reduced Gli2 protein expression (Figure 29D) in both MDA-MB-231 and RWGT2 cells, indicating that 6-TG functions at multiple levels to inhibit Gli2 expression.

6-TG does not affect mRNA stability at low doses

Since previous reports show that 6-TG inhibits steady-state PTHrP mRNA expression at later time points of incubation (27) and our data suggest that 6-TG inhibits GLI2 mRNA expression, we also determined its effects on mRNA stability. MDA-MB-231 and RWGT2 cells were treated with the transcriptional inhibitor actinomycin D as previously described (282) two hours post-6-TG treatment and cells were harvested every two hours for RNA and subsequent reverse transcription for real-time PCR. We found that 6-TG treatment had no effect on GLI2 or PTHrP mRNA degradation in either MDA-MB-231 breast cancer cells (Figure 30A) or RWGT2 squamous-cell lung carcinoma cells (Figure 30B). Indeed, the data indicated that there may in fact be a slight trend towards PTHrP and GLI2 mRNA stabilization in the presence of 6-TG. Although the effects of actinomycin D in blocking transcription are not specific for GLI2, these data exclude the possibility that 6-TG blocks expression of Gli2 and PTHrP through a post-transcriptional effect, and strongly suggest that the specific inhibitory effect of 6-TG on Gli2 and PTHrP indeed occurs at the transcriptional level.

Previous work by our group indicated that 6-TG affects steady-state *PTHrP* mRNA expression (27); however, the data presented here suggest that GLI2 and PTHrP mRNA are not in fact de-stabilized in the presence of 6-TG, but rather that 6-TG treatment may cause a modest increase in GLI2 and PTHrP mRNA stability in MDA-MB-231 cells. Despite this effect, PTHrP and

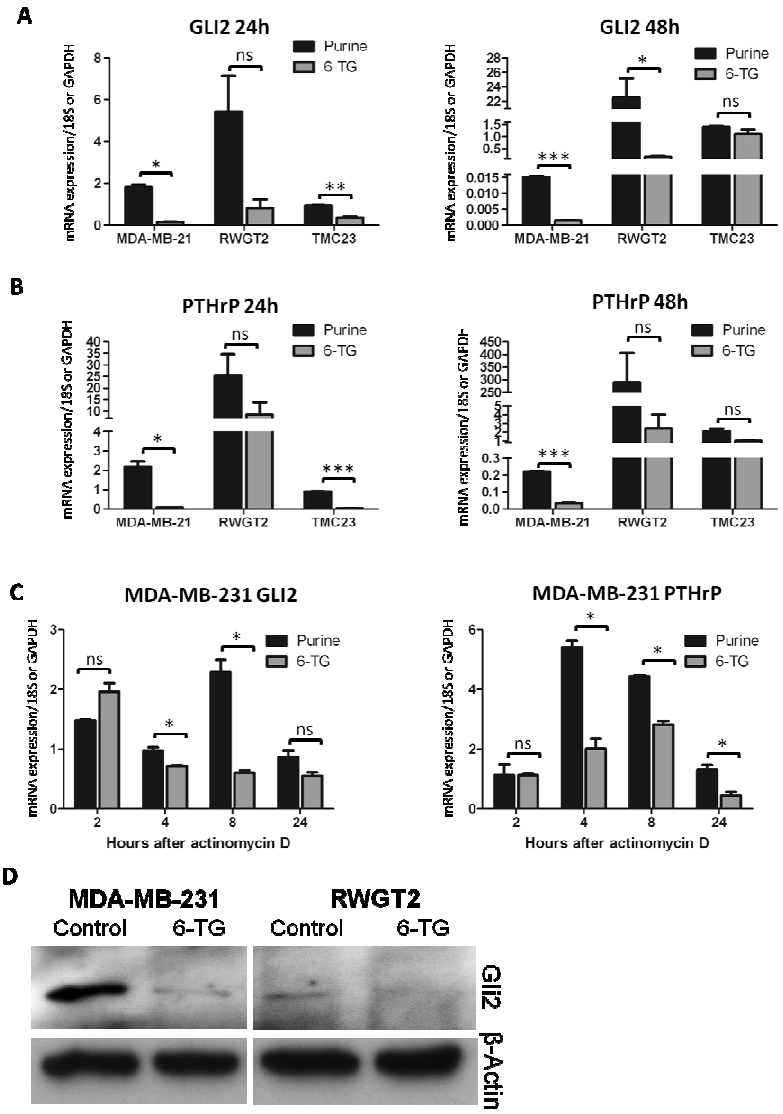

Figure 29. 6-TG redcuces GLI2 and PTHrP expression at multiple time points in osteolytic tumor cells. Osteolytic tumor cells were treated with 100µmol 6-TG for either 24 or 48 hours and GLI2 and PTHrP mRNA expression was determined at each time point. (A) MDA-MB-231 breast cancer cells, RWGT2 squamous-cell lung carcinoma cells, and TMC23 proliferating chondrocytes exhibited reduced GLI2 expression at both 24 and 48 hours after treatment when compared to purine treatment. (B) As a control, PTHrP expression was examined following 6-TG treatment and was found to be down-regulated in MDA-MB-231 cells. (C) MDA-MB-231 breast cancer cells were treated in a time-course experiment to determine the earliest time point at which 6-TG has a significant effect on GLI2 and PTHrP mRNA expression. Values are the mean ± standard error (n=3/column), and p-values were determined using unpaired t-test. *p<0.05, **p<0.01, ***p<0.001. (D) GLI2 protein expression was examined by Western blot following 24 hour treatment with 100 µmol 6-TG.

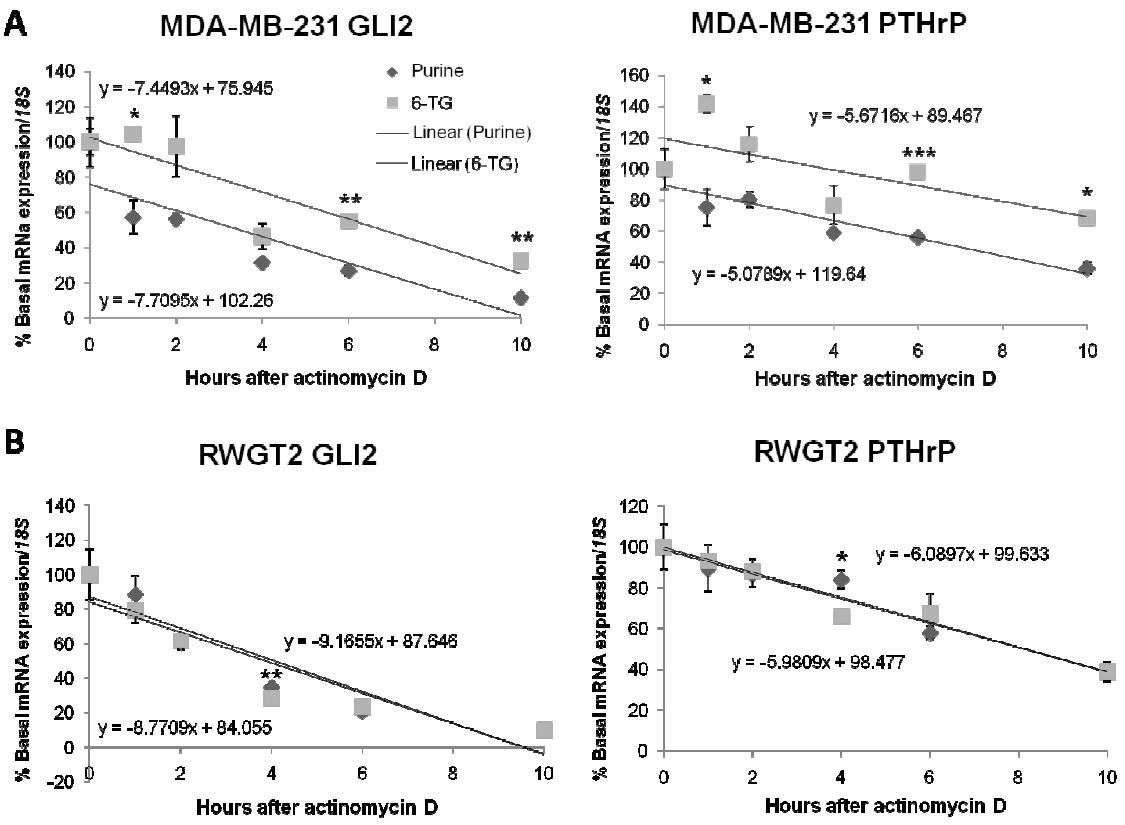

Figure 30. 6-TG effects on GLI2 expression are independent of mRNA stability. Osteolytic tumor cells were first treated with 100 µmol 6-TG or purine control for 4 hours, then tumor cells were treated with 0.8 µM actinomycin D and harvested at various time points for (A) MDA-MB-231 breast cancer cells, or (b) RWGT2 squamous-cell lung carcinoma cells. Plot points indicate average mRNA expression normalized to 18S as a percentage of the mean at zero hour, and regression lines indicate overall trend of mRNA expression. Regression equations for 6-TG and purine are represented on the upper and lower half of each graph, respectively. Values are the mean ± standard error (n=3/time point), and *p*-values were determined using unpaired t-test. *P*-values indicate significant difference between purine and 6-TG treatment groups at individual time points. **p*<0.05, ***p*<0.01, ****p*<0.001.

GLI2 mRNA expression levels are down-regulated in the presence of 6-TG, suggesting that 6-TG overcomes mRNA stabilization to dramatically inhibit transcription. These data were surprising considering our group's previously published data showing 6-TG stabilization of PTHrP mRNA (27), but we believe these differences stem from the techniques used in determining mRNA stability. Differences may also be attributed to variance in time points, since our group previously focused on later time points (48 hours) for steady-state mRNA expression (27), and our studies here focus on earlier time points.

6-TG directly reduces GLI2 promoter activity

Since our work has demonstrated that 6-TG inhibits GLI2 expression and leads to PTHrP inhibition, we determined whether 6-TG directly regulates GLI2 promoter activity using a GLI2 promoter construct (60). MDA-MB-231 cells were transiently transfected with the GLI2 WT promoter construct and harvested for luciferase assay 24 hours following 1mmol 6-TG treatment. We found that 6-TG significantly inhibited GLI2 promoter activity when compared to MDA-MB-231 cells expressing a control vector in both serum-free medium (Figure 31A) and in the presence of recombinant human Tgf-β1 (Figure 31B). Recent reports have indicated that the GLI2 promoter contains a SMAD-binding element (SBE) and T-cell factor (TCF)-binding element (TBE), indicative of both Tgf-β and β-catenin signaling regulation of GLI2 transcription (60). Interestingly, 6-TG inhibited the GLI2 promoter even when the SBE or TBE was mutated (Figure 31), suggesting that these elements are not essential for 6-TG regulation of GLI2.

Circumventing the GLI2 promoter abrogates 6-TG inhibitory effect on PTHrP transcription

In order to determine whether Gli2 acts upstream of PTHrP to elicit 6-TG inhibitory effects on transcription, we reasoned that the blockade of the GLI2 promoter should prevent 6-TG inhibition of PTHrP mRNA expression. We therefore transfected MDA-MB-231 cells with a

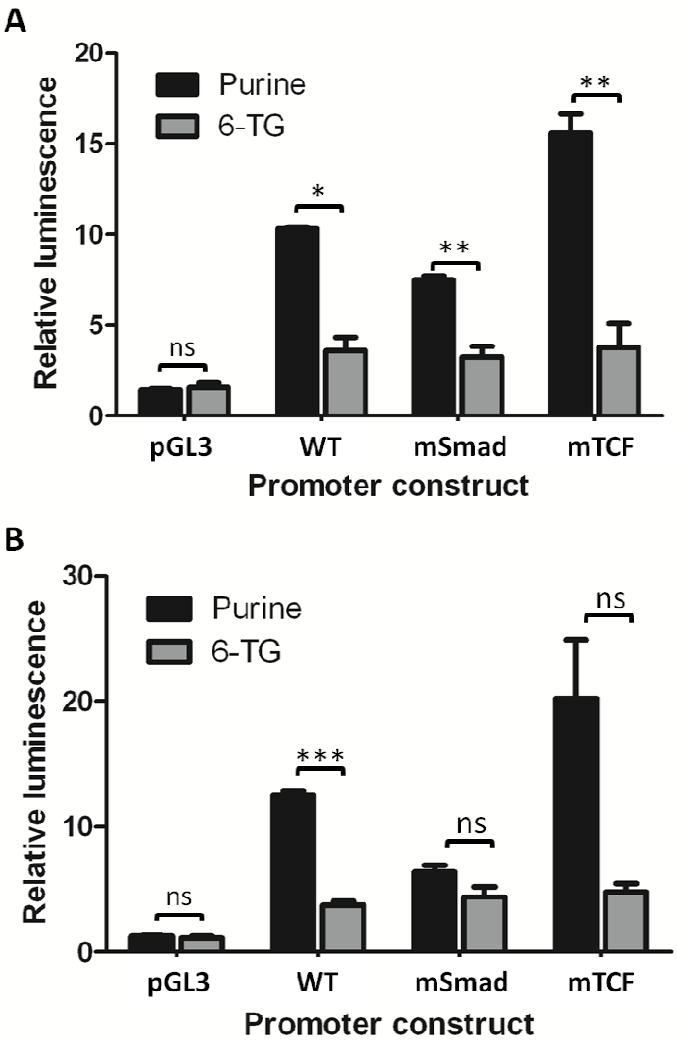

Figure 31. 6-TG directly inhibits GLI2 promoter activation. MDA-MB-231 cells were transfected with GLI2 wild-type (WT), SBE mutant (mSmad), or TBE mutant (mTCF) promoter constructs and treated with 1 mmol 6-TG or purine for 24 hours. Control cells were transfected with pGL3 and also treated with 1 mmol 6-TG. (A) Cells were treated in serum-free DMEM, and (B) cells were treated in DMEM supplemented with 5ng/ml recombinant human Tgf-β. Values are the mean ± standard error (n=3/column), and *p*-values were determined using unpaired *t*-test. **p*<0.05, ***p*<0.01, ****p*<0.001.

GLI2 construct constitutively expressed under the CMV promoter. Since we have shown that 6-TG regulates GLI2 expression at the mRNA level, 6-TG treatment should affect endogenous GLI2, but will be unable to inhibit GLI2 expressed under a constitutive promoter such as CMV (Figure 32A). Therefore, constitutive expression of GLI2 should prevent the inhibitory effects of 6-TG on PTHrP expression that work through stimulation of the GLI2 promoter. Following transfection with CMV-GLI2 and 6-TG treatment, we found that PTHrP mRNA expression was no longer affected by 6-TG in the MDA-MB-231 cells overexpressing GLI2 under control of the CMV promoter (Figure 32B).

Conclusions

While we have demonstrated that 6-TG targets GLI2 mRNA and protein expression, it remains unclear whether 6-TG directly targets GLI2, or if the effects of 6-TG on GLI2 are driven by signaling upstream of GLI2. An essential role of GLI2 is regulating PTHrP expression and subsequent osteolysis by tumor cells, which underlines the importance of finding the mechanism through which GLI2 transcription is activated. For example, our group and others have previously published that Tgf-β signaling plays a key regulatory role in GLI2 transactivation (60, 61, 114). Our data presented in Figure 32A are in serum-free conditions, and do not contain excess human Tgf-β1, which can elevate GLI2 promoter activity above basal levels; however, when we repeated this experiment in the presence of recombinant human Tgf-β1, we saw similar results (Figure 31B), indicating that there are Tgf-β independent pathways regulating GLI2.

Given the clinical success of 6-TG treatment in cancers such as leukemia, and that 6-TG appears to specifically inhibit Gli2 upstream of PTHrP, the use of 6-TG against tumor types in which GLI2 is up-regulated may be a potential therapeutic option. GLI proteins have been

demonstrated to be up-regulated in a number of tumor types, including medulloblastoma and tumorigenesis (66). However, due to the cytotoxic and off-target effects of 6-TG in the clinical setting, other groups are investigating alternative guanidine-related compounds (283). Similar to 6-TG, these drugs are effective inhibitors of PTHrP, but the mechanism has not been investigated. It is likely that these drugs work in part through Gli2 inhibition, similar to 6-TG. However, *in vitro* they appear more potent and possibly more specific to PTHrP (283).

Taken together, our data indicate that low-dose 6-TG effects on PTHrP are driven at least in part though Gli2 inhibition, and are independent of tumor cell growth. Therefore, Gli2 inhibition by low-dose 6-TG may be a novel therapy in cancer patients expressing elevated levels of Gli proteins.

Acknowledgements

These data were published in *Anticancer Research* as follows: Rachelle W. Johnson, Alyssa R. Merkel, Sabrina Danilin, Mai P. Nguyen, Gregory R. Mundy, Julie A. Sterling. 6-Thioguanine Inhibition of Parathyroid Hormone-related Protein Expression Is Mediated by GLI2. Anticancer Res. 2011 *in press*.

Ms. Alyssa Merkel and Dr. Mai Nguyen contributed technical expertise in the tumor cell growth and expression experiments. Dr. Sabrina Danilin provided technical expertise and analysis in the 6-TG mRNA stability experiments. Dr. Julie Sterling, Dr. Lynn Matrisian and the late Dr. Greg Mundy provided scientific critiques and guidance.

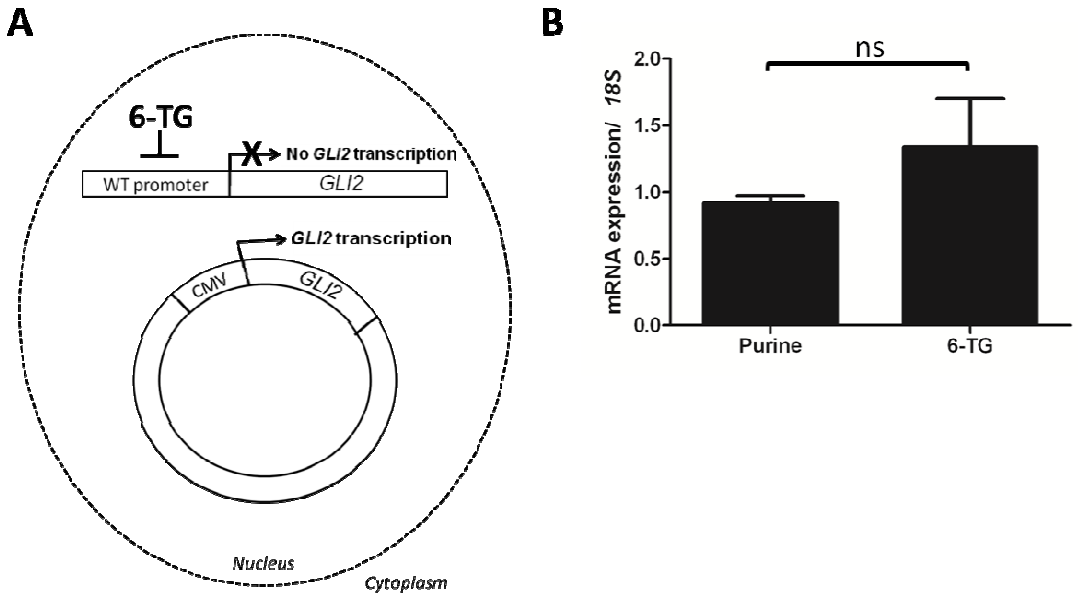

Figure 32. Endogenous GLI2 promoter is required for 6-TG inhibitory effects on PTHrP expression. (A) Diagram indicating MDA-MB-231 cells were transfected with a GLI2 expression vector under control of a constitutively active CMV promoter or an empty vector as a control. (B) PTHrP mRNA expression in MDA-MB-231 cells when GLI2 was constitutively expressed under the CMV promoter. Cells were treated with 100 µmol 6-TG or purine as a control. Values are the mean ± standard error (n=3/column). No significant differences in data were detected using unpaired *t*-test.

CHAPTER IV

DISCUSSION AND SIGNIFICANCE

Despite advances in the treatment of tumor-induced bone disease, primarily through the introduction of anti-resorptives such as bisphosphonates and denosumab, significant advancements are still needed to alter the course of the disease from terminal to chronic, or to eradicate it altogether. In order to advance the field, improvements in both our technologies and our understanding of interactions between the tumor cells and the bone micro-environment are critical.

Advances in imaging technology

The data presented here indicate that there are still advancements to be made in monitoring tumor and bone interactions through multiple imaging modalities. Although we have frequently relied on Faxitron and fluorescence imaging to monitor tumor cells and resulting bone destruction in the past, our data indicate that there are more effective methods for monitoring these interactions such as through *in vivo* microCT, PET, or SPECT. The largest obstacle to overcome with these technologies is the low throughput and associated costliness. The low efficiency of new imaging technologies like *in vivo* microCT is likely to be improved rapidly as the importance of imaging modalities that can detect bone destruction earlier and with greater sensitivity than current standards becomes more appreciated. In addition to computed tomography, NIR technology holds great promise as a tool for monitoring tumor growth in bone and the localization of proteins to sites of skeletal metastasis (164-166). Additional studies by our group have utilized NIR-tagged antibody to monitor drug distribution in tumor metastasis models, where uptake of the antibody in bone indicates more rapid turnover and correlates with tumor burden (unpublished data).

Tgf-β signaling in the vicious cycle

Our understanding of the molecular mechanisms which drive tumor cell growth in bone is as important as our ability to visualize tumor-bone interactions. Our data indicate that in breast tumor cells that cause osteolysis, factors which regulate the production of osteolytic molecules are essential for tumor-induced bone destruction. Specifically, our data indicate that Tgf-β regulates the transcription factor GLI2 in osteolytic tumor cells, instead of the Hh signaling pathway, which regulates Gli2 production during development. This novel finding is of particaul importance to pre-clinical studies, since drug companies are actively pursuing cyclopamine analogues as inhibitors of Hh signaling and the Gli proteins in particular. Our data indicate that although these analogues may be less toxic than cyclopamine, they will likely be ineffective in blocking breast tumor-induced osteolysis. Tgf-β stimulation of Gli2 enhances PTHrP production and the resulting bone destruction, and accordingly, Gli2 inhibition reduces osteolysis. These data confirm the previously published finding that GLI2 is regulated in part by a Smad binding element within the promoter (60). The mineralized bone matrix is a significant reservoir for Tgf-β, which is released in its active form upon bone resorption by activated osteoclasts (26); however, the timing of Tgf-β signaling in promoting tumor-induced bone disease has been debated since copious amounts of active Tgf-β will likely not be released from the bone matrix until the tumor cells are well established in bone and had adequate time to activate RANK/RANKL signaling and enhance osteoclastogenesis.

Tumor-matrix interactions

It is currently unknown whether osteolytic tumor cells up-regulate the expression of Gli2 prior to, during the metastatic cascade, or after establishment in bone, but our group has observed that the physical bone micro-environment plays a significant role in activating GLI2

and PTHrP transcription (97), and our data presented here indicate that bone stiffness may also activate Wnt signaling, which has been linked to mechanotransduction pathways like Src (255-258). Although it is difficult to distinguish the timing of these pathways in the establishment of tumor-induced bone disease, our data suggest that when tumor cells metastasize to bone, they sense the physical stiffness of the bone micro-environment, which may or may not be through direct interactions between the tumor cells and bone matrix. Histology indicates that tumor cells may reside in direct contact with the bone matrix in certain planes, but it is difficult to determine whether this is an artifact of histological processing or a biological phenomenon. Even if tumor cells do not come in direct contact with the bone but rather come in physical contact with bone lining cells, we believe that tumor cells are still able to sense bone stiffness, since our *in vitro* data indicates that there is a direct effect of matrix stiffness on tumor cell gene expression. Whether bone stroma such as osteoblasts or fibroblasts contribute to tumor cells sensing bone stiffness *in vivo* remains to be determined.

Our group has previously shown that increasing matrix stiffness up-regulates expression of the Tgf-β1 ligand and activates Tgf-β signaling as measured by 3TP-lux (97), and our data presented here indicate that Wnt signaling is also activated with increased matrix stiffness, as measured by TOPFlash activation (Figure 14A) and PCR array (Table 1). This was further supported by enhanced nuclear localization of β-catenin when tumor cells were seeded onto stiff TCPS (Figure 14B). Wnt signaling has been previously shown to crosstalk with mechanotransduction pathways (257-260), and our data suggest that this activation may also trigger downstream effects on Gli2 and PTHrP. This also opens up the possibility that Src signaling may regulate Gli2 and PTHrP. In combination, these data suggest that when tumor cells sense the stiffness of bone, they activate both the Tgf-β and Wnt signaling pathways in

osteolytic tumor cells, which in turn activate GLI2 transcription, as indicated by our promoter and mRNA expression data (Figures 15, 16, and 20) in MDA-MB-231 cells.

Proposed timing of the vicious cycle

We propose that Tgf-β signaling is important early in the vicious cycle for the activation of Gli2 and PTHrP, and late in the vicious cycle, to maintain this up-regulation and tumor cell proliferation. It is also likely that the stiffness of bone regulates the initial Tgf-β response, but it is the continuous release of active Tgf-β from the mineralized bone matrix which maintains the vicious cycle, since the rigidity of bone will diminish as the cycle continues and bone is degraded. Accordingly, we propose that Wnt signaling is also important early in the vicious cycle for complete activation of GLI2 transcription, but that the copious amounts of Tgf-β present in the tumor-bone micro-environment late in the vicious cycle are sufficient to continue Gli2 expression and PTHrP production. As bone degrades and its rigidity is diminished with decreasing bone volume, the mechanotransduction pathways that crosstalk with Wnt signaling through Src and β-catenin interactions and with Tgf-β signaling through ROCK are likely also reduced. At this point late in the vicious cycle, the role of the surrounding stroma may become increasingly important (Figure 33). Indeed, data from our group suggests that both normal and cancer-associated fibroblasts can enhance Gli2 and PTHrP production in MDA-MB-231 cells through an unknown soluble factor. Conditioned media harvested from a number of primary human fibroblast cultures were found to increase GLI2 and PTHrP mRNA expression, and MDA-MB-231 cells co-inoculated with primary human fibroblasts directly into the tibia resulted in enhanced bone destruction (unpublished data). These effects may be mediated through Tgf-β, Wnt signaling, or both. Further studies are required to determine fibroblast contribution to osteolysis. It is important to note that these effects would be separate from stiffness activation

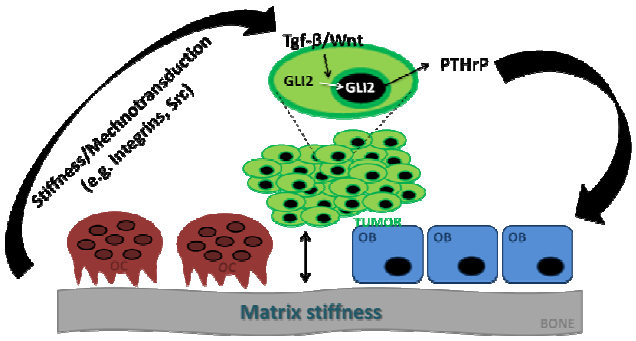

Early Vicious Cycle

Tumor cells metastasize to bone and sense bone stiffness. Mechanotransduction pathways activate Tgf-β/Wnt signaling pathways and GLI2/PTHrP downstream.

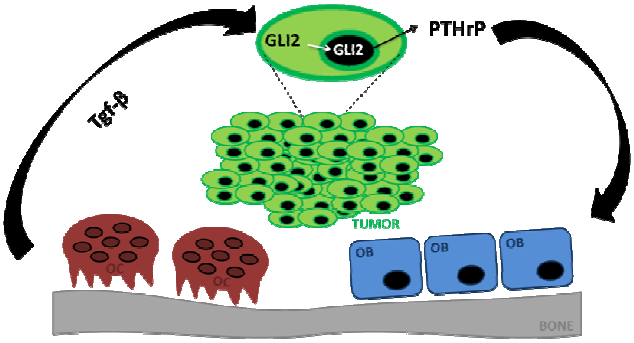

Mid Vicious Cycle

GLI2/PTHrP production is elevated and Tgf-β is actively being released from the bone matrix to stimulate GLI2 transcription.

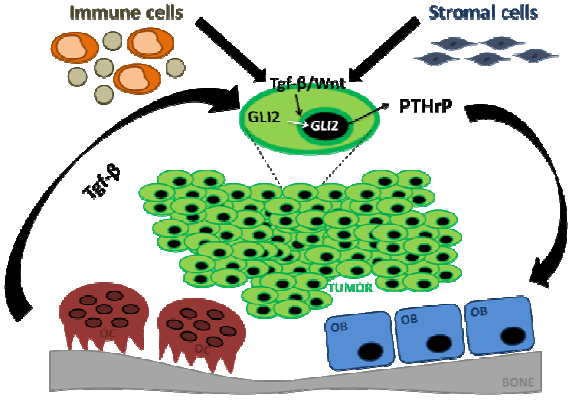

Late Vicious Cycle

Bone destruction reduces bone stiffness and mechanotransduction pathways are down-regulated. Residual Tgf-β and stroma/immune cells in the bone marrow maintain the vicious cycle.

Figure 33. Proposed timing of stiffness, Tgf-β, and Wnt signaling on GLI2/PTHrP activation and tumor-induced bone destruction.

of Wnt or Tgf-β signaling activity since increasing rigidity alone is sufficient to enhance both of these signaling pathways.

Inhibiting Tgf-β/Wnt signaling in osteolysis

In addition to its extensive role in tumor-induced bone disease, Tgf-β signaling is important for maintenance of normal bone homeostasis, which is evidenced by mouse models of TGF-β blockade which result in enhanced bone mineral density and bone volume due to increased osteoblast and decreased osteoclast numbers (12, 13). Unpublished data from our group (*Biswas et al.,* submitted) also suggests that inhibition of Tgf-β signaling may be beneficial in blocking breast tumor-induced bone disease. Our *in vitro* data supports these findings in preclinical models. However, our most accurate mouse model available for studying human tumor-induced bone disease relies on intracardiac injection and does not take into account the biphasic effect of Tgf-β on the primary tumor. Patients with residual tumor at the primary site could experience increased metastasis with Tgf-β inhibition, due to the protective effects of Tgf-β in tumorigenesis (216). Therefore, Tgf-β blockade would only be recommended in patients in whom the primary tumor has been completely removed, as in such cases where the patient has undergone a mastectomy.

Similarly, there are caveats to consider in blocking Wnt signaling in osteolysis, namely the anabolic effects of Wnt signaling through osteoblast differentiation. LRP5-/- mice exhibit a low bone mass phenotype and disrupted preosteoblast differentiation (120), suggesting that Wnt inhibition could have catabolic effects in bone metastasis patients. Furthermore, our *in vitro* data do not directly indicate that Wnt inhibition would inhibit Gli2 or PTHrP production, since blocking Wnt through small molecule antagonists was ineffective. It remains unclear whether this was due to low endogenous levels of β-catenin in the MDA-MB-231 cells or

because Tgf-β is compensatory, but it is unlikely to be the latter since we have tested TGF-β activity when MDA-MB-231 cells are treated with a Wnt inhibitor and observe no detectable changes in 3TP-lux activation (data not shown). If further studies warrant the use of Wnt signaling *in vivo* to block tumor-induced osteolysis, it would need to also be tested with an anti-resorptive drug such as a bisphosphonate to counteract the catabolic effect it may have on bone.

Gli inhibition and tumor-induced bone destruction

There are a number of complications associated with Tgf-β and Wnt inhibition for the treatment of osteolysis, but our data indicate that Gli2 is an effective target in blocking tumor-induced bone disease, particularly based on our evidence from the Gli2-Rep construct in which Gli2 is preferentially repressed in tumor cells only (Figures 21-23). Due to limitations in our tumor model, we were unable to repeat these data using the small molecule inhibitor GANT58, but we were able to show that 6-TG, which at low concentrations specifically inhibits PTHrP (27), also inhibits GLI2 activity. These data are still somewhat puzzling since the mouse tumor model using 4-week old mice was used in both the GANT58 studies and the previously published 6-TG studies (27), but 6-TG was not reported to have any detrimental effects on bone volume or the growth plate. We believe these results may be attributed to the targeting of 6-TG to tumor cells, since presumably a chemotherapeutic agent such as 6-TG would likely be incorporated much faster and more efficiently into rapidly dividing tumor cells than into chondrocytes of the growth plate in late stages of development. Conversely, GANT58 appears to show no specificity to tumor cells over any other cell expressing Gli1 or Gli2. The differential effect could also be due to 6-TG specificity for Gli2 in particular, whereas GANT58 inhibits both Gli1 and Gli2. Furthermore, Gli1 may compensate for the loss of Gli2 in the growth plate during 6-TG

treatment. Therefore, we still conclude that Gli2 may be an effective target in tumor-induced osteolysis, but that better inhibitors are needed. Fortunately, interest still lies in developing inhibitors against the Gli proteins due to their up-regulation in numerous tumor types (66). For example the *E. agallocha* compounds which were extracted from Japanese herbals are currently under investigation as Gli inhibitors in pancreatic and prostate cancer cells (63), and our group intends to test these compounds in primary breast cancer and breast tumor metastasis to bone, as well investigating any skeletal effects on normal mice.

Taken together, our data indicate that the stiffness of bone activates both Tgf-β and Wnt signaling to up-regulate GLI2 transcription early in the vicious cycle, and that Gli2 may therefore be a more specific therapeutic target than Tgf-β or Wnt signaling in blocking tumor-induced bone disease. We believe that patients suffering from tumors in which the Gli proteins are up-regulated could benefit significantly from Gli inhibition, and studies will continue in an effort to find accurate preclinical models which accurately reflect the human condition. In the future, our advances in imaging technology will allow us to better explore Gli2 as a clinical target and more accurately examine the signaling pathways that regulate Gli2.

REFERENCES

1. Boxer DI, Todd CE, Coleman R, Fogelman I. Bone secondaries in breast cancer: the solitary metastasis. J Nucl Med. 1989;30:1318-20.
2. Body JJ, Bartl R, Burckhardt P, Delmas PD, Diel IJ, Fleisch H, et al. Current use of bisphosphonates in oncology. International Bone and Cancer Study Group. J Clin Oncol. 1998;16:3890-9.
3. Legrand SB. Modern Management of Malignant Hypercalcemia. Am J Hosp Palliat Care. 2011.
4. Body JJ. New developments for treatment and prevention of bone metastases. Curr Opin Oncol. 2011;23:338-42.
5. Schilcher J, Michaelsson K, Aspenberg P. Bisphosphonate use and atypical fractures of the femoral shaft. N Engl J Med. 2011;364:1728-37.
6. Feng X, McDonald JM. Disorders of bone remodeling. Annu Rev Pathol. 2011;6:121-45.
7. Otto F, Thornell AP, Crompton T, Denzel A, Gilmour KC, Rosewell IR, et al. Cbfa1, a candidate gene for cleidocranial dysplasia syndrome, is essential for osteoblast differentiation and bone development. Cell. 1997;89:765-71.
8. St-Jacques B, Hammerschmidt M, McMahon AP. Indian hedgehog signaling regulates proliferation and differentiation of chondrocytes and is essential for bone formation. Genes Dev. 1999;13:2072-86.
9. Long F, Chung UI, Ohba S, McMahon J, Kronenberg HM, McMahon AP. Ihh signaling is directly required for the osteoblast lineage in the endochondral skeleton. Development. 2004;131:1309-18.
10. Chen D, Zhao M, Mundy GR. Bone morphogenetic proteins. Growth Factors. 2004;22:233-41.
11. Sowa H, Kaji H, Yamaguchi T, Sugimoto T, Chihara K. Smad3 promotes alkaline phosphatase activity and mineralization of osteoblastic MC3T3-E1 cells. J Bone Miner Res. 2002;17:1190-9.
12. Edwards JR, Nyman JS, Lwin ST, Moore MM, Esparza J, O'Quinn EC, et al. Inhibition of TGF-beta signaling by 1D11 antibody treatment increases bone mass and quality in vivo. J Bone Miner Res. 2010;25:2419-26.
13. Mohammad KS, Chen CG, Balooch G, Stebbins E, McKenna CR, Davis H, et al. Pharmacologic inhibition of the TGF-beta type I receptor kinase has anabolic and anti-catabolic effects on bone. PLoS One. 2009;4:e5275.
14. Karaplis AC, Luz A, Glowacki J, Bronson RT, Tybulewicz VL, Kronenberg HM, et al. Lethal skeletal dysplasia from targeted disruption of the parathyroid hormone-related peptide gene. Genes Dev. 1994;8:277-89.
15. Weir EC, Philbrick WM, Amling M, Neff LA, Baron R, Broadus AE. Targeted overexpression of parathyroid hormone-related peptide in chondrocytes causes chondrodysplasia and delayed endochondral bone formation. Proc Natl Acad Sci U S A. 1996;93:10240-5.
16. Day TF, Guo X, Garrett-Beal L, Yang Y. Wnt/beta-catenin signaling in mesenchymal progenitors controls osteoblast and chondrocyte differentiation during vertebrate skeletogenesis. Dev Cell. 2005;8:739-50.
17. Hill TP, Spater D, Taketo MM, Birchmeier W, Hartmann C. Canonical Wnt/beta-catenin signaling prevents osteoblasts from differentiating into chondrocytes. Dev Cell. 2005;8:727-38.

18. Boyden LM, Mao J, Belsky J, Mitzner L, Farhi A, Mitnick MA, et al. High bone density due to a mutation in LDL-receptor-related protein 5. N Engl J Med. 2002;346:1513-21.
19. Little RD, Carulli JP, Del Mastro RG, Dupuis J, Osborne M, Folz C, et al. A mutation in the LDL receptor-related protein 5 gene results in the autosomal dominant high-bone-mass trait. Am J Hum Genet. 2002;70:11-9.
20. Van Wesenbeeck L, Cleiren E, Gram J, Beals RK, Benichou O, Scopelliti D, et al. Six novel missense mutations in the LDL receptor-related protein 5 (LRP5) gene in different conditions with an increased bone density. Am J Hum Genet. 2003;72:763-71.
21. Takayanagi H. Mechanistic insight into osteoclast differentiation in osteoimmunology. J Mol Med (Berl). 2005;83:170-9.
22. Key LL, Jr., Rodriguiz RM, Willi SM, Wright NM, Hatcher HC, Eyre DR, et al. Long-term treatment of osteopetrosis with recombinant human interferon gamma. N Engl J Med. 1995;332:1594-9.
23. Cenci S, Toraldo G, Weitzmann MN, Roggia C, Gao Y, Qian WP, et al. Estrogen deficiency induces bone loss by increasing T cell proliferation and lifespan through IFN-gamma-induced class II transactivator. Proc Natl Acad Sci U S A. 2003;100:10405-10.
24. Kostenuik PJ, Shalhoub V. Osteoprotegerin: a physiological and pharmacological inhibitor of bone resorption. Curr Pharm Des. 2001;7:613-35.
25. Goltzman D, Miao D, Panda DK, Hendy GN. Effects of calcium and of the Vitamin D system on skeletal and calcium homeostasis: lessons from genetic models. J Steroid Biochem Mol Biol. 2004;89-90:485-9.
26. Mundy GR. Mechanisms of bone metastasis. Cancer. 1997;80:1546-56.
27. Gallwitz WE, Guise TA, Mundy GR. Guanosine nucleotides inhibit different syndromes of PTHrP excess caused by human cancers in vivo. J Clin Invest. 2002;110:1559-72.
28. Guise TA, Yin JJ, Taylor SD, Kumagai Y, Dallas M, Boyce BF, et al. Evidence for a causal role of parathyroid hormone-related protein in the pathogenesis of human breast cancer-mediated osteolysis. J Clin Invest. 1996;98:1544-9.
29. Shiirevnyamba A, Takahashi T, Shan H, Ogawa H, Yano S, Kanayama H, et al. Enhancement of osteoclastogenic activity in osteolytic prostate cancer cells by physical contact with osteoblasts. Br J Cancer. 2011;104:505-13.
30. Sieh S, Lubik AA, Clements JA, Nelson CC, Hutmacher DW. Interactions between human osteoblasts and prostate cancer cells in a novel 3D in vitro model. Organogenesis. 2010;6:181-8.
31. Roodman GD. Osteoblast function in myeloma. Bone. 2011;48:135-40.
32. Langley RR, Fidler IJ. The seed and soil hypothesis revisited--the role of tumor-stroma interactions in metastasis to different organs. Int J Cancer. 2011;128:2527-35.
33. Schmid MC, Varner JA. Myeloid cells in the tumor microenvironment: modulation of tumor angiogenesis and tumor inflammation. J Oncol. 2010;2010:201026.
34. Tadmor T, Attias D, Polliack A. Myeloid-derived suppressor cells--their role in haemato-oncological malignancies and other cancers and possible implications for therapy. Br J Haematol. 2011;153:557-67.
35. Sterling JA, Edwards JR, Martin TJ, Mundy GR. Advances in the biology of bone metastasis: How the skeleton affects tumor behavior. Bone. 2010.
36. Sterling JA, Oyajobi BO, Grubbs B, Padalecki SS, Munoz SA, Gupta A, et al. The hedgehog signaling molecule Gli2 induces parathyroid hormone-related peptide expression and osteolysis in metastatic human breast cancer cells. Cancer Res. 2006;66:7548-53.
37. Martin TJ, Suva LJ. Parathyroid hormone-related protein: a novel gene product. Baillieres Clin Endocrinol Metab. 1988;2:1003-29.

38. Martin TJ, Allan EH, Caple IW, Care AD, Danks JA, Diefenbach-Jagger H, et al. Parathyroid hormone-related protein: isolation, molecular cloning, and mechanism of action. Recent Prog Horm Res. 1989;45:467-502; discussion -6.
39. Martin TJ, Danks JA. A novel parathyroid hormone-related gene product. Henry Ford Hosp Med J. 1989;37:187-9.
40. Martin TJ, Suva LJ. Parathyroid hormone-related protein in hypercalcaemia of malignancy. Clin Endocrinol (Oxf). 1989;31:631-47.
41. Suva LJ, Mather KA, Gillespie MT, Webb GC, Ng KW, Winslow GA, et al. Structure of the 5' flanking region of the gene encoding human parathyroid-hormone-related protein (PTHrP). Gene. 1989;77:95-105.
42. Gillespie MT, Martin TJ. The parathyroid hormone-related protein gene and its expression. Mol Cell Endocrinol. 1994;100:143-7.
43. Burtis WJ, Brady TG, Orloff JJ, Ersbak JB, Warrell RP, Jr., Olson BR, et al. Immunochemical characterization of circulating parathyroid hormone-related protein in patients with humoral hypercalcemia of cancer. N Engl J Med. 1990;322:1106-12.
44. Guise TA, Yin JJ, Thomas RJ, Dallas M, Cui Y, Gillespie MT. Parathyroid hormone-related protein (PTHrP)-(1-139) isoform is efficiently secreted in vitro and enhances breast cancer metastasis to bone in vivo. Bone. 2002;30:670-6.
45. Southby J, Kissin MW, Danks JA, Hayman JA, Moseley JM, Henderson MA, et al. Immunohistochemical localization of parathyroid hormone-related protein in human breast cancer. Cancer Res. 1990;50:7710-6.
46. Powell GJ, Southby J, Danks JA, Stillwell RG, Hayman JA, Henderson MA, et al. Localization of parathyroid hormone-related protein in breast cancer metastases: increased incidence in bone compared with other sites. Cancer Res. 1991;51:3059-61.
47. Bouizar Z, Spyratos F, De vernejoul MC. The parathyroid hormone-related protein (PTHrP) gene: use of downstream TATA promotor and PTHrP 1-139 coding pathways in primary breast cancers vary with the occurrence of bone metastasis. J Bone Miner Res. 1999;14:406-14.
48. Bundred NJ, Walker RA, Ratcliffe WA, Warwick J, Morrison JM, Ratcliffe JG. Parathyroid hormone related protein and skeletal morbidity in breast cancer. Eur J Cancer. 1992;28:690-2.
49. Kissin MW, Henderson MA, Danks JA, Hayman JA, Bennett RC, Martin TJ. Parathyroid hormone related protein in breast cancers of widely varying prognosis. Eur J Surg Oncol. 1993;19:134-42.
50. Liapis H, Crouch EC, Roby J, Rader JS. In situ localization of parathyroid hormone-like protein and mRNA in intraepithelial neoplasia and invasive carcinoma of the uterine cervix. Hum Pathol. 1993;24:1058-66.
51. Kronenberg HM. Developmental regulation of the growth plate. Nature. 2003;423:332-6.
52. Kronenberg HM. PTHrP and skeletal development. Ann N Y Acad Sci. 2006;1068:1-13.
53. Thiede MA, Rodan GA. Expression of a calcium-mobilizing parathyroid hormone-like peptide in lactating mammary tissue. Science. 1988;242:278-80.
54. Budayr AA, Halloran BP, King JC, Diep D, Nissenson RA, Strewler GJ. High levels of a parathyroid hormone-like protein in milk. Proc Natl Acad Sci U S A. 1989;86:7183-5.
55. Hens JR, Wysolmerski JJ. Key stages of mammary gland development: molecular mechanisms involved in the formation of the embryonic mammary gland. Breast Cancer Res. 2005;7:220-4.
56. Foley J, Dann P, Hong J, Cosgrove J, Dreyer B, Rimm D, et al. Parathyroid hormone-related protein maintains mammary epithelial fate and triggers nipple skin differentiation during embryonic breast development. Development. 2001;128:513-25.

57. VanHouten JN, Dann P, Stewart AF, Watson CJ, Pollak M, Karaplis AC, et al. Mammary-specific deletion of parathyroid hormone-related protein preserves bone mass during lactation. J Clin Invest. 2003;112:1429-36.
58. VanHouten J, Dann P, McGeoch G, Brown EM, Krapcho K, Neville M, et al. The calcium-sensing receptor regulates mammary gland parathyroid hormone-related protein production and calcium transport. J Clin Invest. 2004;113:598-608.
59. Miao D, Liu H, Plut P, Niu M, Huo R, Goltzman D, et al. Impaired endochondral bone development and osteopenia in Gli2-deficient mice. Exp Cell Res. 2004;294:210-22.
60. Dennler S, Andre J, Verrecchia F, Mauviel A. Cloning of the human GLI2 Promoter: transcriptional activation by transforming growth factor-beta via SMAD3/beta-catenin cooperation. J Biol Chem. 2009;284:31523-31.
61. Johnson RW, Nguyen MP, Padalecki SS, Grubbs BG, Merkel AR, Oyajobi BO, et al. TGF-beta promotion of Gli2-induced expression of parathyroid hormone-related protein, an important osteolytic factor in bone metastasis, is independent of canonical Hedgehog signaling. Cancer Res. 2011;71:822-31.
62. Lauth M, Bergstrom A, Shimokawa T, Toftgard R. Inhibition of GLI-mediated transcription and tumor cell growth by small-molecule antagonists. Proc Natl Acad Sci U S A. 2007;104:8455-60.
63. Rifai Y, Arai MA, Sadhu SK, Ahmed F, Ishibashi M. New Hedgehog/GLI signaling inhibitors from Excoecaria agallocha. Bioorg Med Chem Lett. 2011;21:718-22.
64. Kang Y, Siegel PM, Shu W, Drobnjak M, Kakonen SM, Cordon-Cardo C, et al. A multigenic program mediating breast cancer metastasis to bone. Cancer Cell. 2003;3:537-49.
65. Stanton BZ, Peng LF. Small-molecule modulators of the Sonic Hedgehog signaling pathway. Mol Biosyst. 2010;6:44-54.
66. Lauth M, Toftgard R. Non-canonical activation of GLI transcription factors: implications for targeted anti-cancer therapy. Cell Cycle. 2007;6:2458-63.
67. Taipale J, Chen JK, Cooper MK, Wang B, Mann RK, Milenkovic L, et al. Effects of oncogenic mutations in Smoothened and Patched can be reversed by cyclopamine. Nature. 2000;406:1005-9.
68. Chen JK, Taipale J, Cooper MK, Beachy PA. Inhibition of Hedgehog signaling by direct binding of cyclopamine to Smoothened. Genes Dev. 2002;16:2743-8.
69. Yin JJ, Selander K, Chirgwin JM, Dallas M, Grubbs BG, Wieser R, et al. TGF-beta signaling blockade inhibits PTHrP secretion by breast cancer cells and bone metastases development. J Clin Invest. 1999;103:197-206.
70. Dibrov A, Kashour T, Amara FM. The role of transforming growth factor beta signaling in messenger RNA stability. Growth Factors. 2006;24:1-11.
71. Kumar R, Thompson JR. The regulation of parathyroid hormone secretion and synthesis. J Am Soc Nephrol. 2011;22:216-24.
72. Bhatia V, Mula RV, Falzon M. 1,25-Dihydroxyvitamin D(3) regulates PTHrP expression via transcriptional, post-transcriptional and post-translational pathways. Mol Cell Endocrinol. 2011.
73. Massfelder T, Lang H, Schordan E, Lindner V, Rothhut S, Welsch S, et al. Parathyroid hormone-related protein is an essential growth factor for human clear cell renal carcinoma and a target for the von Hippel-Lindau tumor suppressor gene. Cancer Res. 2004;64:180-8.
74. Danilin S, Sourbier C, Thomas L, Rothhut S, Lindner V, Helwig JJ, et al. von Hippel-Lindau tumor suppressor gene-dependent mRNA stabilization of the survival factor parathyroid hormone-related protein in human renal cell carcinoma by the RNA-binding protein HuR. Carcinogenesis. 2009;30:387-96.

75. Kiriyama T, Gillespie MT, Glatz JA, Fukumoto S, Moseley JM, Martin TJ. Transforming growth factor beta stimulation of parathyroid hormone-related protein (PTHrP): a paracrine regulator? Mol Cell Endocrinol. 1993;92:55-62.
76. Werkmeister JR, Blomme EA, Weckmann MT, Grone A, McCauley LK, Wade AB, et al. Effect of transforming growth factor-beta1 on parathyroid hormone-related protein secretion and mRNA expression by normal human keratinocytes in vitro. Endocrine. 1998;8:291-9.
77. Benitez-Verguizas J, Loarte D, de Miguel F, Esbrit P. Effects of transforming growth factor beta1 on cell growth and parathyroid hormone-related protein in Walker 256 tumor cells. Life Sci. 1999;65:1807-16.
78. Sellers RS, Luchin AI, Richard V, Brena RM, Lima D, Rosol TJ. Alternative splicing of parathyroid hormone-related protein mRNA: expression and stability. J Mol Endocrinol. 2004;33:227-41.
79. Tannehill-Gregg S, Kergosien E, Rosol TJ. Feline head and neck squamous cell carcinoma cell line: characterization, production of parathyroid hormone-related protein, and regulation by transforming growth factor-beta. In Vitro Cell Dev Biol Anim. 2001;37:676-83.
80. Sellers RS, Capen CC, Rosol TJ. Messenger RNA stability of parathyroid hormone-related protein regulated by transforming growth factor-beta1. Mol Cell Endocrinol. 2002;188:37-46.
81. Yaccoby S, Ling W, Zhan F, Walker R, Barlogie B, Shaughnessy JD, Jr. Antibody-based inhibition of DKK1 suppresses tumor-induced bone resorption and multiple myeloma growth in vivo. Blood. 2007;109:2106-11.
82. Oshima T, Abe M, Asano J, Hara T, Kitazoe K, Sekimoto E, et al. Myeloma cells suppress bone formation by secreting a soluble Wnt inhibitor, sFRP-2. Blood. 2005;106:3160-5.
83. Jost E, Gezer D, Wilop S, Suzuki H, Herman JG, Osieka R, et al. Epigenetic dysregulation of secreted Frizzled-related proteins in multiple myeloma. Cancer Lett. 2009;281:24-31.
84. Callander NS, Roodman GD. Myeloma bone disease. Semin Hematol. 2001;38:276-85.
85. Bendre MS, Gaddy-Kurten D, Mon-Foote T, Akel NS, Skinner RA, Nicholas RW, et al. Expression of interleukin 8 and not parathyroid hormone-related protein by human breast cancer cells correlates with bone metastasis in vivo. Cancer Res. 2002;62:5571-9.
86. Bendre MS, Montague DC, Peery T, Akel NS, Gaddy D, Suva LJ. Interleukin-8 stimulation of osteoclastogenesis and bone resorption is a mechanism for the increased osteolysis of metastatic bone disease. Bone. 2003;33:28-37.
87. Bendre MS, Margulies AG, Walser B, Akel NS, Bhattacharrya S, Skinner RA, et al. Tumor-derived interleukin-8 stimulates osteolysis independent of the receptor activator of nuclear factor-kappaB ligand pathway. Cancer Res. 2005;65:11001-9.
88. Pratap J, Lian JB, Javed A, Barnes GL, van Wijnen AJ, Stein JL, et al. Regulatory roles of Runx2 in metastatic tumor and cancer cell interactions with bone. Cancer Metastasis Rev. 2006;25:589-600.
89. Pratap J, Javed A, Languino LR, van Wijnen AJ, Stein JL, Stein GS, et al. The Runx2 osteogenic transcription factor regulates matrix metalloproteinase 9 in bone metastatic cancer cells and controls cell invasion. Mol Cell Biol. 2005;25:8581-91.
90. Lynch CC, Hikosaka A, Acuff HB, Martin MD, Kawai N, Singh RK, et al. MMP-7 promotes prostate cancer-induced osteolysis via the solubilization of RANKL. Cancer Cell. 2005;7:485-96.
91. Thiolloy S, Halpern J, Holt GE, Schwartz HS, Mundy GR, Matrisian LM, et al. Osteoclast-derived matrix metalloproteinase-7, but not matrix metalloproteinase-9, contributes to tumor-induced osteolysis. Cancer Res. 2009;69:6747-55.
92. Saad F, Gleason DM, Murray R, Tchekmedyian S, Venner P, Lacombe L, et al. A randomized, placebo-controlled trial of zoledronic acid in patients with hormone-refractory metastatic prostate carcinoma. J Natl Cancer Inst. 2002;94:1458-68.

93. Thudi NK, Martin CK, Murahari S, Shu ST, Lanigan LG, Werbeck JL, et al. Dickkopf-1 (DKK-1) stimulated prostate cancer growth and metastasis and inhibited bone formation in osteoblastic bone metastases. Prostate. 2011;71:615-25.
94. Clines GA, Mohammad KS, Bao Y, Stephens OW, Suva LJ, Shaughnessy JD, Jr., et al. Dickkopf homolog 1 mediates endothelin-1-stimulated new bone formation. Mol Endocrinol. 2007;21:486-98.
95. Sterling JA, Guelcher SA. Bone structural components regulating sites of tumor metastasis. Curr Osteoporos Rep. 2011;9:89-95.
96. Levental KR, Yu H, Kass L, Lakins JN, Egeblad M, Erler JT, et al. Matrix crosslinking forces tumor progression by enhancing integrin signaling. Cell. 2009;139:891-906.
97. Ruppender NS, Merkel AR, Martin TJ, Mundy GR, Sterling JA, Guelcher SA. Matrix rigidity induces osteolytic gene expression of metastatic breast cancer cells. PLoS One. 2010;5:e15451.
98. Hayward SW, Cunha GR. The prostate: development and physiology. Radiol Clin North Am. 2000;38:1-14.
99. Hayward SW, Cunha GR, Dahiya R. Normal development and carcinogenesis of the prostate. A unifying hypothesis. Ann N Y Acad Sci. 1996;784:50-62.
100. Onishi T, Hayashi N, Theriault RL, Hortobagyi GN, Ueno NT. Future directions of bone-targeted therapy for metastatic breast cancer. Nat Rev Clin Oncol. 2010;7:641-51.
101. Nannuru KC, Singh RK. Tumor-stromal interactions in bone metastasis. Curr Osteoporos Rep. 2010;8:105-13.
102. Taichman RS, Cooper C, Keller ET, Pienta KJ, Taichman NS, McCauley LK. Use of the stromal cell-derived factor-1/CXCR4 pathway in prostate cancer metastasis to bone. Cancer Res. 2002;62:1832-7.
103. Muller A, Homey B, Soto H, Ge N, Catron D, Buchanan ME, et al. Involvement of chemokine receptors in breast cancer metastasis. Nature. 2001;410:50-6.
104. Studebaker AW, Storci G, Werbeck JL, Sansone P, Sasser AK, Tavolari S, et al. Fibroblasts isolated from common sites of breast cancer metastasis enhance cancer cell growth rates and invasiveness in an interleukin-6-dependent manner. Cancer Res. 2008;68:9087-95.
105. Karnoub AE, Dash AB, Vo AP, Sullivan A, Brooks MW, Bell GW, et al. Mesenchymal stem cells within tumour stroma promote breast cancer metastasis. Nature. 2007;449:557-63.
106. Sasser AK, Mundy BL, Smith KM, Studebaker AW, Axel AE, Haidet AM, et al. Human bone marrow stromal cells enhance breast cancer cell growth rates in a cell line-dependent manner when evaluated in 3D tumor environments. Cancer Lett. 2007;254:255-64.
107. Delany AM, Canalis E. The metastasis-associated metalloproteinase stromelysin-3 is induced by transforming growth factor-beta in osteoblasts and fibroblasts. Endocrinology. 2001;142:1561-6.
108. Guo X, Wang XF. Signaling cross-talk between TGF-beta/BMP and other pathways. Cell Res. 2009;19:71-88.
109. Barker N. The canonical Wnt/beta-catenin signalling pathway. Methods Mol Biol. 2008;468:5-15.
110. Placencio VR, Sharif-Afshar AR, Li X, Huang H, Uwamariya C, Neilson EG, et al. Stromal transforming growth factor-beta signaling mediates prostatic response to androgen ablation by paracrine Wnt activity. Cancer Res. 2008;68:4709-18.
111. Mullor JL, Dahmane N, Sun T, Ruiz i Altaba A. Wnt signals are targets and mediators of Gli function. Curr Biol. 2001;11:769-73.
112. Yazawa S, Umesono Y, Hayashi T, Tarui H, Agata K. Planarian Hedgehog/Patched establishes anterior-posterior polarity by regulating Wnt signaling. Proc Natl Acad Sci U S A. 2009;106:22329-34.

113. Alvarez-Medina R, Le Dreau G, Ros M, Marti E. Hedgehog activation is required upstream of Wnt signalling to control neural progenitor proliferation. Development. 2009;136:3301-9.
114. Dennler S, Andre J, Alexaki I, Li A, Magnaldo T, ten Dijke P, et al. Induction of sonic hedgehog mediators by transforming growth factor-beta: Smad3-dependent activation of Gli2 and Gli1 expression in vitro and in vivo. Cancer Res. 2007;67:6981-6.
115. Mohinta S, Wu H, Chaurasia P, Watabe K. Wnt pathway and breast cancer. Front Biosci. 2007;12:4020-33.
116. Spencer GJ, Utting JC, Etheridge SL, Arnett TR, Genever PG. Wnt signalling in osteoblasts regulates expression of the receptor activator of NFkappaB ligand and inhibits osteoclastogenesis in vitro. J Cell Sci. 2006;119:1283-96.
117. Howe LR, Brown AM. Wnt signaling and breast cancer. Cancer Biol Ther. 2004;3:36-41.
118. Michaelson JS, Leder P. beta-catenin is a downstream effector of Wnt-mediated tumorigenesis in the mammary gland. Oncogene. 2001;20:5093-9.
119. Yao H, Ashihara E, Maekawa T. Targeting the Wnt/beta-catenin signaling pathway in human cancers. Expert Opin Ther Targets. 2011;15:873-87.
120. Kato M, Patel MS, Levasseur R, Lobov I, Chang BH, Glass DA, 2nd, et al. Cbfa1-independent decrease in osteoblast proliferation, osteopenia, and persistent embryonic eye vascularization in mice deficient in Lrp5, a Wnt coreceptor. J Cell Biol. 2002;157:303-14.
121. Takahashi N, Maeda K, Ishihara A, Uehara S, Kobayashi Y. Regulatory mechanism of osteoclastogenesis by RANKL and Wnt signals. Front Biosci. 2011;16:21-30.
122. Holmen SL, Zylstra CR, Mukherjee A, Sigler RE, Faugere MC, Bouxsein ML, et al. Essential role of beta-catenin in postnatal bone acquisition. J Biol Chem. 2005;280:21162-8.
123. Mbalaviele G, Sheikh S, Stains JP, Salazar VS, Cheng SL, Chen D, et al. Beta-catenin and BMP-2 synergize to promote osteoblast differentiation and new bone formation. J Cell Biochem. 2005;94:403-18.
124. Zhang M, Yan Y, Lim YB, Tang D, Xie R, Chen A, et al. BMP-2 modulates beta-catenin signaling through stimulation of Lrp5 expression and inhibition of beta-TrCP expression in osteoblasts. J Cell Biochem. 2009;108:896-905.
125. Fukuda T, Kokabu S, Ohte S, Sasanuma H, Kanomata K, Yoneyama K, et al. Canonical Wnts and BMPs cooperatively induce osteoblastic differentiation through a GSK3beta-dependent and beta-catenin-independent mechanism. Differentiation. 2010;80:46-52.
126. Komori T. Signaling networks in RUNX2-dependent bone development. J Cell Biochem. 2011;112:750-5.
127. Komiya Y, Habas R. Wnt signal transduction pathways. Organogenesis. 2008;4:68-75.
128. Takada I, Mihara M, Suzawa M, Ohtake F, Kobayashi S, Igarashi M, et al. A histone lysine methyltransferase activated by non-canonical Wnt signalling suppresses PPAR-gamma transactivation. Nat Cell Biol. 2007;9:1273-85.
129. Kertesz N, Krasnoperov V, Reddy R, Leshanski L, Kumar SR, Zozulya S, et al. The soluble extracellular domain of EphB4 (sEphB4) antagonizes EphB4-EphrinB2 interaction, modulates angiogenesis, and inhibits tumor growth. Blood. 2006;107:2330-8.
130. Krasnoperov V, Kumar SR, Ley E, Li X, Scehnet J, Liu R, et al. Novel EphB4 monoclonal antibodies modulate angiogenesis and inhibit tumor growth. Am J Pathol. 2010;176:2029-38.
131. Compagni A, Logan M, Klein R, Adams RH. Control of skeletal patterning by ephrinB1-EphB interactions. Dev Cell. 2003;5:217-30.
132. Martin TJ, Allan EH, Ho PW, Gooi JH, Quinn JM, Gillespie MT, et al. Communication Between EphrinB2 and EphB4 Within the Osteoblast Lineage. Adv Exp Med Biol. 2010;658:51-60.

133. Allan EH, Hausler KD, Wei T, Gooi JH, Quinn JM, Crimeen-Irwin B, et al. EphrinB2 regulation by PTH and PTHrP revealed by molecular profiling in differentiating osteoblasts. J Bone Miner Res. 2008;23:1170-81.
134. Yang L, Edwards CM, Mundy GR. Gr-1+CD11b+ myeloid-derived suppressor cells: formidable partners in tumor metastasis. J Bone Miner Res. 2010;25:1701-6.
135. Zhang K, Kim S, Cremasco V, Hirbe A, Novack D, Weilbaecher K, et al. CD8+ T cells Regulate Bone Tumor Burden Independent of Osteoclast Resorption. Cancer Res. 2011.
136. Fowler JA, Mundy GR, Lwin ST, Lynch CC, Edwards CM. A murine model of myeloma that allows genetic manipulation of the host microenvironment. Dis Model Mech. 2009;2:604-11.
137. Edwards CM, Lwin ST, Fowler JA, Oyajobi BO, Zhuang J, Bates AL, et al. Myeloma cells exhibit an increase in proteasome activity and an enhanced response to proteasome inhibition in the bone marrow microenvironment in vivo. Am J Hematol. 2009;84:268-72.
138. Edwards CM, Edwards JR, Lwin ST, Esparza J, Oyajobi BO, McCluskey B, et al. Increasing Wnt signaling in the bone marrow microenvironment inhibits the development of myeloma bone disease and reduces tumor burden in bone in vivo. Blood. 2008;111:2833-42.
139. Oyajobi BO, Garrett IR, Gupta A, Flores A, Esparza J, Munoz S, et al. Stimulation of new bone formation by the proteasome inhibitor, bortezomib: implications for myeloma bone disease. Br J Haematol. 2007;139:434-8.
140. Hiraga T, Myoui A, Choi ME, Yoshikawa H, Yoneda T. Stimulation of cyclooxygenase-2 expression by bone-derived transforming growth factor-beta enhances bone metastases in breast cancer. Cancer Res. 2006;66:2067-73.
141. Johnson LC, Johnson RW, Munoz SA, Mundy GR, Peterson TE, Sterling JA. Longitudinal live animal microCT allows for quantitative analysis of tumor-induced bone destruction. Bone. 2010.
142. Morrissey C, Dowell A, Koreckij TD, Nguyen H, Lakely B, Fanslow WC, et al. Inhibition of angiopoietin-2 in LuCaP 23.1 prostate cancer tumors decreases tumor growth and viability. Prostate. 2010;70:1799-808.
143. Nagae M, Hiraga T, Yoneda T. Acidic microenvironment created by osteoclasts causes bone pain associated with tumor colonization. J Bone Miner Metab. 2007;25:99-104.
144. Hiraga T, Hata K, Ikeda F, Kitagaki J, Fujimoto-Ouchi K, Tanaka Y, et al. Preferential inhibition of bone metastases by 5'-deoxy-5-fluorouridine and capecitabine in the 4T1/luc mouse breast cancer model. Oncol Rep. 2005;14:695-9.
145. Rose AA, Pepin F, Russo C, Abou Khalil JE, Hallett M, Siegel PM. Osteoactivin promotes breast cancer metastasis to bone. Mol Cancer Res. 2007;5:1001-14.
146. Thalmann GN, Anezinis PE, Chang SM, Zhau HE, Kim EE, Hopwood VL, et al. Androgen-independent cancer progression and bone metastasis in the LNCaP model of human prostate cancer. Cancer Res. 1994;54:2577-81.
147. Thalmann GN, Sikes RA, Wu TT, Degeorges A, Chang SM, Ozen M, et al. LNCaP progression model of human prostate cancer: androgen-independence and osseous metastasis. Prostate. 2000;44:91-103 Jul 1;44(2).
148. Corey E, Quinn JE, Buhler KR, Nelson PS, Macoska JA, True LD, et al. LuCaP 35: a new model of prostate cancer progression to androgen independence. Prostate. 2003;55:239-46.
149. Guise TA, Yoneda T, Yates AJ, Mundy GR. The combined effect of tumor-produced parathyroid hormone-related protein and transforming growth factor-alpha enhance hypercalcemia in vivo and bone resorption in vitro. J Clin Endocrinol Metab. 1993;77:40-5.
150. Dunn EJ, Bowes DW, Rothert SW, Greer RB, 3rd. Letter: Microradiography of bone, a new use for the versatile Faxitron. Arch Pathol. 1975;99:62.

151. Rajarubendra N, Bolton D, Lawrentschuk N. Diagnosis of bone metastases in urological malignancies--an update. Urology. 2010;76:782-90.
152. Alexaki VI, Javelaud D, Van Kempen LC, Mohammad KS, Dennler S, Luciani F, et al. GLI2-mediated melanoma invasion and metastasis. J Natl Cancer Inst. 2010;102:1148-59.
153. Oyajobi BO, Munoz S, Kakonen R, Williams PJ, Gupta A, Wideman CL, et al. Detection of myeloma in skeleton of mice by whole-body optical fluorescence imaging. Mol Cancer Ther. 2007;6:1701-8.
154. Hall DC, Johnson-Pais TL, Grubbs B, Bernal R, Leach RJ, Padalecki SS. Maspin reduces prostate cancer metastasis to bone. Urol Oncol. 2008;26:652-8.
155. Chishima T, Miyagi Y, Li L, Tan Y, Baranov E, Yang M, et al. Use of histoculture and green fluorescent protein to visualize tumor cell host interaction. In Vitro Cell Dev Biol Anim. 1997;33:745-7.
156. Hoffman RM. Recent advances on in vivo imaging with fluorescent proteins. Methods Cell Biol. 2008;85:485-95.
157. Cai W, Shin DW, Chen K, Gheysens O, Cao Q, Wang SX, et al. Peptide-labeled near-infrared quantum dots for imaging tumor vasculature in living subjects. Nano Lett. 2006;6:669-76.
158. Edinger M, Cao YA, Hornig YS, Jenkins DE, Verneris MR, Bachmann MH, et al. Advancing animal models of neoplasia through in vivo bioluminescence imaging. Eur J Cancer. 2002;38:2128-36.
159. Murray LJ, Abrams TJ, Long KR, Ngai TJ, Olson LM, Hong W, et al. SU11248 inhibits tumor growth and CSF-1R-dependent osteolysis in an experimental breast cancer bone metastasis model. Clin Exp Metastasis. 2003;20:757-66.
160. Minn AJ, Kang Y, Serganova I, Gupta GP, Giri DD, Doubrovin M, et al. Distinct organ-specific metastatic potential of individual breast cancer cells and primary tumors. J Clin Invest. 2005;115:44-55.
161. Drake JM, Gabriel CL, Henry MD. Assessing tumor growth and distribution in a model of prostate cancer metastasis using bioluminescence imaging. Clin Exp Metastasis. 2005;22:674-84.
162. Stripecke R, Carmen Villacres M, Skelton D, Satake N, Halene S, Kohn D. Immune response to green fluorescent protein: implications for gene therapy. Gene Ther. 1999;6:1305-12.
163. Jeon YH, Choi Y, Kang JH, Kim CW, Jeong JM, Lee DS, et al. Immune response to firefly luciferase as a naked DNA. Cancer Biol Ther. 2007;6:781-6.
164. Shcherbo D, Shemiakina, II, Ryabova AV, Luker KE, Schmidt BT, Souslova EA, et al. Near-infrared fluorescent proteins. Nat Methods. 2010;7:827-9.
165. Sexton M, Woodruff G, Cudaback E, Kreitzer FR, Xu C, Lin YH, et al. Binding of NIR-conPK and NIR-6T to astrocytomas and microglial cells: evidence for a protein related to TSPO. PLoS One. 2009;4:e8271.
166. Wyatt SK, Manning HC, Bai M, Bailey SN, Gallant P, Ma G, et al. Molecular imaging of the translocator protein (TSPO) in a pre-clinical model of breast cancer. Mol Imaging Biol. 2010;12:349-58.
167. Deane NG, Manning HC, Foutch AC, Washington MK, Aronow BJ, Bornhop DJ, et al. Targeted imaging of colonic tumors in smad3-/- mice discriminates cancer and inflammation. Mol Cancer Res. 2007;5:341-9.
168. Bonnet N, Laroche N, Vico L, Dolleans E, Courteix D, Benhamou CL. Assessment of trabecular bone microarchitecture by two different x-ray microcomputed tomographs: a comparative study of the rat distal tibia using Skyscan and Scanco devices. Med Phys. 2009;36:1286-97.

169. Cohen A, Dempster DW, Muller R, Guo XE, Nickolas TL, Liu XS, et al. Assessment of trabecular and cortical architecture and mechanical competence of bone by high-resolution peripheral computed tomography: comparison with transiliac bone biopsy. Osteoporos Int. 2010;21:263-73.
170. Nazarian A, Snyder BD, Zurakowski D, Muller R. Quantitative micro-computed tomography: a non-invasive method to assess equivalent bone mineral density. Bone. 2008;43:302-11.
171. MacNeil JA, Boyd SK. Accuracy of high-resolution peripheral quantitative computed tomography for measurement of bone quality. Med Eng Phys. 2007;29:1096-105.
172. Kurth AA, Muller R. The effect of an osteolytic tumor on the three-dimensional trabecular bone morphology in an animal model. Skeletal Radiol. 2001;30:94-8.
173. Thorpe MP, Valentine RJ, Moulton CJ, Johnson AJ, Evans EM, Layman DK. Breast tumors induced by N-methyl-N-nitrosourea are damaging to bone strength, structure and mineralization in the absence of metastasis in rats. J Bone Miner Res. 2010.
174. Tu Q, Zhang J, Fix A, Brewer E, Li YP, Zhang ZY, et al. Targeted overexpression of BSP in osteoclasts promotes bone metastasis of breast cancer cells. J Cell Physiol. 2009;218:135-45.
175. Chanda D, Isayeva T, Kumar S, Siegal GP, Szafran AA, Zinn KR, et al. Systemic osteoprotegerin gene therapy restores tumor-induced bone loss in a therapeutic model of breast cancer bone metastasis. Mol Ther. 2008;16:871-8.
176. Li Z, Schem C, Shi YH, Medina D, Zhang M. Increased COX2 expression enhances tumor-induced osteoclastic lesions in breast cancer bone metastasis. Clin Exp Metastasis. 2008;25:389-400.
177. Cowey S, Szafran AA, Kappes J, Zinn KR, Siegal GP, Desmond RA, et al. Breast cancer metastasis to bone: evaluation of bioluminescent imaging and microSPECT/CT for detecting bone metastasis in immunodeficient mice. Clin Exp Metastasis. 2007;24:389-401.
178. Hojjat SP, Hardisty MR, Whyne CM. Micro-computed tomography-based highly automated 3D segmentation of the rat spine for quantitative analysis of metastatic disease. J Neurosurg Spine. 2010;13:367-70.
179. Hojjat SP, Whyne CM. Automated quantitative microstructural analysis of metastatically involved vertebrae: Effects of stereologic model and spatial resolution. Med Eng Phys. 2010.
180. Peterson TE, Manning HC. Molecular imaging: 18F-FDG PET and a whole lot more. J Nucl Med Technol. 2009;37:151-61.
181. Marom EM, Erasmus JJ, Pass HI, Patz EF, Jr. The role of imaging in malignant pleural mesothelioma. Semin Oncol. 2002;29:26-35.
182. Marom EM, Sarvis S, Herndon JE, 2nd, Patz EF, Jr. T1 lung cancers: sensitivity of diagnosis with fluorodeoxyglucose PET. Radiology. 2002;223:453-9.
183. Cheran SK, Nielsen ND, Patz EF, Jr. False-negative findings for primary lung tumors on FDG positron emission tomography: staging and prognostic implications. AJR Am J Roentgenol. 2004;182:1129-32.
184. Tateishi U, Gamez C, Dawood S, Yeung HW, Cristofanilli M, Macapinlac HA. Bone metastases in patients with metastatic breast cancer: morphologic and metabolic monitoring of response to systemic therapy with integrated PET/CT. Radiology. 2008;247:189-96.
185. De Giorgi U, Mego M, Rohren EM, Liu P, Handy BC, Reuben JM, et al. 18F-FDG PET/CT findings and circulating tumor cell counts in the monitoring of systemic therapies for bone metastases from breast cancer. J Nucl Med. 2010;51:1213-8.
186. Gambhir SS. Molecular imaging of cancer with positron emission tomography. Nat Rev Cancer. 2002;2:683-93.

187. Jones MD, Liu JC, Barthel TK, Hussain S, Lovria E, Cheng D, et al. A proteasome inhibitor, bortezomib, inhibits breast cancer growth and reduces osteolysis by downregulating metastatic genes. Clin Cancer Res. 2010;16:4978-89.
188. Winkelmann CT, Figueroa SD, Rold TL, Volkert WA, Hoffman TJ. Microimaging characterization of a B16-F10 melanoma metastasis mouse model. Mol Imaging. 2006;5:105-14.
189. Buck JR, McKinley ET, Hight MR, Fu A, Tang D, Smith RA, et al. Quantitative, preclinical PET of translocator protein expression in glioma using 18F-N-fluoroacetyl-N-(2,5-dimethoxybenzyl)-2-phenoxyaniline. J Nucl Med. 2011;52:107-14.
190. Tang D, Buck JR, Hight MR, Manning HC. Microwave-assisted Organic Synthesis of a High-affinity Pyrazolo-pyrimidinyl TSPO Ligand. Tetrahedron Lett. 2010;51:4595-8.
191. Beheshti M, Langsteger W, Fogelman I. Prostate cancer: role of SPECT and PET in imaging bone metastases. Semin Nucl Med. 2009;39:396-407.
192. Delbeke D, Schoder H, Martin WH, Wahl RL. Hybrid imaging (SPECT/CT and PET/CT): improving therapeutic decisions. Semin Nucl Med. 2009;39:308-40.
193. Song H, Shahverdi K, Huso DL, Wang Y, Fox JJ, Hobbs RF, et al. An immunotolerant HER-2/neu transgenic mouse model of metastatic breast cancer. Clin Cancer Res. 2008;14:6116-24.
194. Yankeelov TE, Gore JC. Dynamic Contrast Enhanced Magnetic Resonance Imaging in Oncology: Theory, Data Acquisition, Analysis, and Examples. Curr Med Imaging Rev. 2009;3:91-107.
195. Liu T, Cheng T, Xu W, Yan WL, Liu J, Yang HL. A meta-analysis of (18)FDG-PET, MRI and bone scintigraphy for diagnosis of bone metastases in patients with breast cancer. Skeletal Radiol. 2010.
196. Reitan NK, Thuen M, Goa PE, de Lange Davies C. Characterization of tumor microvascular structure and permeability: comparison between magnetic resonance imaging and intravital confocal imaging. J Biomed Opt. 2010;15:036004.
197. Loveless ME, Whisenant JG, Wilson K, Lyshchik A, Sinha TK, Gore JC, et al. Coregistration of ultrasonography and magnetic resonance imaging with a preliminary investigation of the spatial colocalization of vascular endothelial growth factor receptor 2 expression and tumor perfusion in a murine tumor model. Mol Imaging. 2009;8:187-98.
198. Li X, Yankeelov TE, Rosen GD, Gore JC, Dawant BM. Enhancement of histological volumes through averaging and their use for the analysis of magnetic resonance images. Magn Reson Imaging. 2009;27:401-16.
199. Martiniova L, Kotys MS, Thomasson D, Schimel D, Lai EW, Bernardo M, et al. Noninvasive monitoring of a murine model of metastatic pheochromocytoma: a comparison of contrast-enhanced microCT and nonenhanced MRI. J Magn Reson Imaging. 2009;29:685-91.
200. Rozel S, Galban CJ, Nicolay K, Lee KC, Sud S, Neeley C, et al. Synergy between anti-CCL2 and docetaxel as determined by DW-MRI in a metastatic bone cancer model. J Cell Biochem. 2009;107:58-64.
201. Merz M, Komljenovic D, Zwick S, Semmler W, Bauerle T. Sorafenib tosylate and paclitaxel induce anti-angiogenic, anti-tumour and anti-resorptive effects in experimental breast cancer bone metastases. Eur J Cancer. 2010.
202. Bauerle T, Komljenovic D, Merz M, Berger MR, Goodman SL, Semmler W. Cilengitide inhibits progression of experimental breast cancer bone metastases as imaged noninvasively using VCT, MRI and DCE-MRI in a longitudinal in vivo study. Int J Cancer. 2010.
203. Roach PJ, Gradinscak DJ, Schembri GP, Bailey EA, Willowson KP, Bailey DL. SPECT/CT in V/Q scanning. Semin Nucl Med. 2010;40:455-66.

204. Aide N, Desmonts C, Beauregard JM, Beyer T, Kinross K, Roselt P, et al. High throughput static and dynamic small animal imaging using clinical PET/CT: potential preclinical applications. Eur J Nucl Med Mol Imaging. 2010;37:991-1001.
205. Sinha TK, Khatib-Shahidi S, Yankeelov TE, Mapara K, Ehtesham M, Cornett DS, et al. Integrating spatially resolved three-dimensional MALDI IMS with in vivo magnetic resonance imaging. Nat Methods. 2008;5:57-9.
206. Beyer T, Weigert M, Quick HH, Pietrzyk U, Vogt F, Palm C, et al. MR-based attenuation correction for torso-PET/MR imaging: pitfalls in mapping MR to CT data. Eur J Nucl Med Mol Imaging. 2008;35:1142-6.
207. Shane E. Evolving data about subtrochanteric fractures and bisphosphonates. N Engl J Med. 2010;362:1825-7.
208. Fizazi K, Carducci M, Smith M, Damiao R, Brown J, Karsh L, et al. Denosumab versus zoledronic acid for treatment of bone metastases in men with castration-resistant prostate cancer: a randomised, double-blind study. Lancet. 2011;377:813-22.
209. Coleman R, Woodward E, Brown J, Cameron D, Bell R, Dodwell D, et al. Safety of zoledronic acid and incidence of osteonecrosis of the jaw (ONJ) during adjuvant therapy in a randomised phase III trial (AZURE: BIG 01-04) for women with stage II/III breast cancer. Breast Cancer Res Treat. 2011;127:429-38.
210. Black DM, Kelly MP, Genant HK, Palermo L, Eastell R, Bucci-Rechtweg C, et al. Bisphosphonates and fractures of the subtrochanteric or diaphyseal femur. N Engl J Med. 2010;362:1761-71.
211. McClung MR. Inhibition of RANKL as a treatment for osteoporosis: preclinical and early clinical studies. Curr Osteoporos Rep. 2006;4:28-33.
212. Gonzalez-Suarez E, Jacob AP, Jones J, Miller R, Roudier-Meyer MP, Erwert R, et al. RANK ligand mediates progestin-induced mammary epithelial proliferation and carcinogenesis. Nature. 2010;468:103-7.
213. Biswas S, Guix M, Rinehart C, Dugger TC, Chytil A, Moses HL, et al. Inhibition of TGF-beta with neutralizing antibodies prevents radiation-induced acceleration of metastatic cancer progression. J Clin Invest. 2007;117:1305-13.
214. Ganapathy V, Ge R, Grazioli A, Xie W, Banach-Petrosky W, Kang Y, et al. Targeting the Transforming Growth Factor-beta pathway inhibits human basal-like breast cancer metastasis. Mol Cancer. 2010;9:122.
215. Mohammad KS, Javelaud D, Fournier PG, Niewolna M, McKenna CR, Peng XH, et al. TGF-beta-RI kinase inhibitor SD-208 reduces the development and progression of melanoma bone metastases. Cancer Res. 2011;71:175-84.
216. Tan AR, Alexe G, Reiss M. Transforming growth factor-beta signaling: emerging stem cell target in metastatic breast cancer? Breast Cancer Res Treat. 2009;115:453-95.
217. Schneider JG, Amend SR, Weilbaecher KN. Integrins and bone metastasis: integrating tumor cell and stromal cell interactions. Bone. 2011;48:54-65.
218. Hirbe AC, Morgan EA, Weilbaecher KN. The CXCR4/SDF-1 chemokine axis: a potential therapeutic target for bone metastases? Curr Pharm Des. 2010;16:1284-90.
219. Liu S, Goldstein RH, Scepansky EM, Rosenblatt M. Inhibition of rho-associated kinase signaling prevents breast cancer metastasis to human bone. Cancer Res. 2009;69:8742-51.
220. Yang JC, Bai L, Yap S, Gao AC, Kung HJ, Evans CP. Effect of the specific Src family kinase inhibitor saracatinib on osteolytic lesions using the PC-3 bone model. Mol Cancer Ther. 2010;9:1629-37.
221. Araujo J, Logothetis C. Dasatinib: a potent SRC inhibitor in clinical development for the treatment of solid tumors. Cancer Treat Rev. 2010;36:492-500.

222. Pratap J, Akech J, Wixted JJ, Szabo G, Hussain S, McGee-Lawrence ME, et al. The histone deacetylase inhibitor, vorinostat, reduces tumor growth at the metastatic bone site and associated osteolysis, but promotes normal bone loss. Mol Cancer Ther. 2010;9:3210-20.
223. Furugaki K, Moriya Y, Iwai T, Yorozu K, Yanagisawa M, Kondoh K, et al. Erlotinib inhibits osteolytic bone invasion of human non-small-cell lung cancer cell line NCI-H292. Clin Exp Metastasis. 2011.
224. Nelson JA, Carpenter JW, Rose LM, Adamson DJ. Mechanisms of action of 6-thioguanine, 6-mercaptopurine, and 8-azaguanine. Cancer Res. 1975;35:2872-8.
225. Ogawa T, Shimokawa H, Fukada K, Suzuki S, Shibata S, Ohya K, et al. Localization and inhibitory effect of basic fibroblast growth factor on chondrogenesis in cultured mouse mandibular condyle. J Bone Miner Metab. 2003;21:145-53.
226. Agren M, Kogerman P, Kleman MI, Wessling M, Toftgard R. Expression of the PTCH1 tumor suppressor gene is regulated by alternative promoters and a single functional Gli-binding site. Gene. 2004;330:101-14.
227. Petropoulos H, Gianakopoulos PJ, Ridgeway AG, Skerjanc IS. Disruption of Meox or Gli activity ablates skeletal myogenesis in P19 cells. J Biol Chem. 2004;279:23874-81.
228. Jamieson C, Sharma M, Henderson BR. Regulation of beta-Catenin Nuclear Dynamics by GSK-3beta Involves a LEF-1 Positive Feedback Loop. Traffic. 2011.
229. Stambolic V, Ruel L, Woodgett JR. Lithium inhibits glycogen synthase kinase-3 activity and mimics wingless signalling in intact cells. Curr Biol. 1996;6:1664-8.
230. Karhadkar SS, Bova GS, Abdallah N, Dhara S, Gardner D, Maitra A, et al. Hedgehog signalling in prostate regeneration, neoplasia and metastasis. Nature. 2004;431:707-12.
231. Coleman RE. Metastatic bone disease: clinical features, pathophysiology and treatment strategies. Cancer Treat Rev. 2001;27:165-76.
232. Yoneda T, Michigami T, Yi B, Williams PJ, Niewolna M, Hiraga T. Use of bisphosphonates for the treatment of bone metastasis in experimental animal models. Cancer Treat Rev. 1999;25:293-9.
233. Fisher JL, Schmitt JF, Howard ML, Mackie PS, Choong PF, Risbridger GP. An in vivo model of prostate carcinoma growth and invasion in bone. Cell Tissue Res. 2002;307:337-45.
234. Rosol TJ, Tannehill-Gregg SH, LeRoy BE, Mandl S, Contag CH. Animal models of bone metastasis. Cancer. 2003;97:748-57.
235. Rajarubendra N, Bolton D, Lawrentschuk N. Diagnosis of Bone Metastases in Urological Malignancies-An Update. Urology. 2010.
236. Bussard KM, Mastro AM. Ex-vivo analysis of the bone microenvironment in bone metastatic breast cancer. J Mammary Gland Biol Neoplasia. 2009;14:387-95.
237. Missbach-Guentner J, Dullin C, Zientkowska M, Domeyer-Missbach M, Kimmina S, Obenauer S, et al. Flat-panel detector-based volume computed tomography: a novel 3D imaging technique to monitor osteolytic bone lesions in a mouse tumor metastasis model. Neoplasia. 2007;9:755-65.
238. Costa L, Major PP. Effect of bisphosphonates on pain and quality of life in patients with bone metastases. Nat Clin Pract Oncol. 2009;6:163-74.
239. Yamada T, Muguruma H, Yano S, Ikuta K, Ogino H, Kakiuchi S, et al. Intensification therapy with anti-parathyroid hormone-related protein antibody plus zoledronic acid for bone metastases of small cell lung cancer cells in severe combined immunodeficient mice. Mol Cancer Ther. 2009;8:119-26.
240. Sato K, Onuma E, Yocum RC, Ogata E. Treatment of malignancy-associated hypercalcemia and cachexia with humanized anti-parathyroid hormone-related protein antibody. Semin Oncol. 2003;30:167-73.

241. Saito H, Tsunenari T, Onuma E, Sato K, Ogata E, Yamada-Okabe H. Humanized monoclonal antibody against parathyroid hormone-related protein suppresses osteolytic bone metastasis of human breast cancer cells derived from MDA-MB-231. Anticancer Res. 2005;25:3817-23.
242. Sasaki H, Nishizaki Y, Hui C, Nakafuku M, Kondoh H. Regulation of Gli2 and Gli3 activities by an amino-terminal repression domain: implication of Gli2 and Gli3 as primary mediators of Shh signaling. Development. 1999;126:3915-24.
243. Sanchez P, Ruiz i Altaba A. In vivo inhibition of endogenous brain tumors through systemic interference of Hedgehog signaling in mice. Mech Dev. 2005;122:223-30.
244. Chung UI, Lanske B, Lee K, Li E, Kronenberg H. The parathyroid hormone/parathyroid hormone-related peptide receptor coordinates endochondral bone development by directly controlling chondrocyte differentiation. Proc Natl Acad Sci U S A. 1998;95:13030-5.
245. Zhang X, Harrington N, Moraes RC, Wu MF, Hilsenbeck SG, Lewis MT. Cyclopamine inhibition of human breast cancer cell growth independent of Smoothened (Smo). Breast Cancer Res Treat. 2009;115:505-21.
246. Zhao C, Chen A, Jamieson CH, Fereshteh M, Abrahamsson A, Blum J, et al. Hedgehog signalling is essential for maintenance of cancer stem cells in myeloid leukaemia. Nature. 2009;458:776-9.
247. Dierks C, Beigi R, Guo GR, Zirlik K, Stegert MR, Manley P, et al. Expansion of Bcr-Abl-positive leukemic stem cells is dependent on Hedgehog pathway activation. Cancer Cell. 2008;14:238-49.
248. Bar EE, Chaudhry A, Lin A, Fan X, Schreck K, Matsui W, et al. Cyclopamine-mediated hedgehog pathway inhibition depletes stem-like cancer cells in glioblastoma. Stem Cells. 2007;25:2524-33.
249. Peacock CD, Wang Q, Gesell GS, Corcoran-Schwartz IM, Jones E, Kim J, et al. Hedgehog signaling maintains a tumor stem cell compartment in multiple myeloma. Proc Natl Acad Sci U S A. 2007;104:4048-53.
250. Trowbridge JJ, Scott MP, Bhatia M. Hedgehog modulates cell cycle regulators in stem cells to control hematopoietic regeneration. Proc Natl Acad Sci U S A. 2006;103:14134-9.
251. Sterling JA, Edwards JR, Martin TJ, Mundy GR. Advances in the biology of bone metastasis: how the skeleton affects tumor behavior. Bone. 2011;48:6-15.
252. Yu H, Mouw JK, Weaver VM. Forcing form and function: biomechanical regulation of tumor evolution. Trends Cell Biol. 2011;21:47-56.
253. Provenzano PP, Keely PJ. Mechanical signaling through the cytoskeleton regulates cell proliferation by coordinated focal adhesion and Rho GTPase signaling. J Cell Sci. 2011;124:1195-205.
254. Schrader J, Gordon-Walker TT, Aucott RL, van Deemter M, Quaas A, Walsh S, et al. Matrix stiffness modulates proliferation, chemotherapeutic response, and dormancy in hepatocellular carcinoma cells. Hepatology. 2011;53:1192-205.
255. Previdi S, Maroni P, Matteucci E, Broggini M, Bendinelli P, Desiderio MA. Interaction between human-breast cancer metastasis and bone microenvironment through activated hepatocyte growth factor/Met and beta-catenin/Wnt pathways. Eur J Cancer. 2010;46:1679-91.
256. Hamaguchi M, Matsuyoshi N, Ohnishi Y, Gotoh B, Takeichi M, Nagai Y. p60v-src causes tyrosine phosphorylation and inactivation of the N-cadherin-catenin cell adhesion system. EMBO J. 1993;12:307-14.
257. Lilien J, Balsamo J. The regulation of cadherin-mediated adhesion by tyrosine phosphorylation/dephosphorylation of beta-catenin. Curr Opin Cell Biol. 2005;17:459-65.

258. Lim SK, Orhant-Prioux M, Toy W, Tan KY, Lim YP. Tyrosine phosphorylation of transcriptional coactivator WW-domain binding protein 2 regulates estrogen receptor {alpha} function in breast cancer via the Wnt pathway. FASEB J. 2011.
259. Zeljko M, Pecina-Slaus N, Martic TN, Kusec V, Beros V, Tomas D. Molecular alterations of E-cadherin and beta-catenin in brain metastases. Front Biosci (Elite Ed). 2011;3:616-24.
260. Klemm F, Bleckmann A, Siam L, Chuang HN, Rietkotter E, Behme D, et al. beta-catenin-independent WNT signaling in basal-like breast cancer and brain metastasis. Carcinogenesis. 2011;32:434-42.
261. Turner CH. Bone strength: current concepts. Ann N Y Acad Sci. 2006;1068:429-46.
262. Sawakami K, Robling AG, Ai M, Pitner ND, Liu D, Warden SJ, et al. The Wnt co-receptor LRP5 is essential for skeletal mechanotransduction but not for the anabolic bone response to parathyroid hormone treatment. J Biol Chem. 2006;281:23698-711.
263. Yao H, Ashihara E, Maekawa T. Targeting the Wnt/beta-catenin signaling pathway in human cancers. Expert Opin Ther Targets. 2011.
264. Najdi R, Holcombe RF, Waterman ML. Wnt signaling and colon carcinogenesis: beyond APC. J Carcinog. 2011;10:5.
265. Kharaishvili G, Simkova D, Makharoblidze E, Trtkova K, Kolar Z, Bouchal J. Wnt signaling in prostate development and carcinogenesis. Biomed Pap Med Fac Univ Palacky Olomouc Czech Repub. 2011;155:11-8.
266. Kim Y, Reifenberger G, Lu D, Endo T, Carson DA, Gast SM, et al. Influencing the Wnt signaling pathway in multiple myeloma. Anticancer Res. 2011;31:725-30.
267. Cornella H, Alsinet C, Villanueva A. Molecular pathogenesis of hepatocellular carcinoma. Alcohol Clin Exp Res. 2011;35:821-5.
268. Serra R, Easter SL, Jiang W, Baxley SE. Wnt5a as an Effector of TGFbeta in Mammary Development and Cancer. J Mammary Gland Biol Neoplasia. 2011;16:157-67.
269. Huang SM, Mishina YM, Liu S, Cheung A, Stegmeier F, Michaud GA, et al. Tankyrase inhibition stabilizes axin and antagonizes Wnt signalling. Nature. 2009;461:614-20.
270. Saraswati S, Alfaro MP, Thorne CA, Atkinson J, Lee E, Young PP. Pyrvinium, a potent small molecule Wnt inhibitor, promotes wound repair and post-MI cardiac remodeling. PLoS One. 2010;5:e15521.
271. Liu CC, Prior J, Piwnica-Worms D, Bu G. LRP6 overexpression defines a class of breast cancer subtype and is a target for therapy. Proc Natl Acad Sci U S A. 2010;107:5136-41.
272. Portal-Nunez S, Lozano D, de Castro LF, de Gortazar AR, Nogues X, Esbrit P. Alterations of the Wnt/beta-catenin pathway and its target genes for the N- and C-terminal domains of parathyroid hormone-related protein in bone from diabetic mice. FEBS Lett. 2010;584:3095-100.
273. Baum B, Georgiou M. Dynamics of adherens junctions in epithelial establishment, maintenance, and remodeling. J Cell Biol. 2011;192:907-17.
274. Letamendia A, Labbe E, Attisano L. Transcriptional regulation by Smads: crosstalk between the TGF-beta and Wnt pathways. J Bone Joint Surg Am. 2001;83-A Suppl 1:S31-9.
275. Fuxe J, Vincent T, Garcia de Herreros A. Transcriptional crosstalk between TGFbeta and stem cell pathways in tumor cell invasion: Role of EMT promoting Smad complexes. Cell Cycle. 2010;9:2363-74.
276. Ressler S, Mlineritsch B, Greil R. Zoledronic acid for adjuvant use in patients with breast cancer. Expert Rev Anticancer Ther. 2011;11:333-49.
277. Santini D, Fratto ME, Vincenzi B, Napoli N, Galluzzo S, Tantardini M, et al. Denosumab: the era of targeted therapies in bone metastatic diseases. Curr Cancer Drug Targets. 2009;9:834-42.

278. Desch P, Asslaber D, Kern D, Schnidar H, Mangelberger D, Alinger B, et al. Inhibition of GLI, but not Smoothened, induces apoptosis in chronic lymphocytic leukemia cells. Oncogene. 2010.
279. Mak KK, Chen MH, Day TF, Chuang PT, Yang Y. Wnt/beta-catenin signaling interacts differentially with Ihh signaling in controlling endochondral bone and synovial joint formation. Development. 2006;133:3695-707.
280. Mill P, Mo R, Fu H, Grachtchouk M, Kim PC, Dlugosz AA, et al. Sonic hedgehog-dependent activation of Gli2 is essential for embryonic hair follicle development. Genes Dev. 2003;17:282-94.
281. Eichberger T, Kaser A, Pixner C, Schmid C, Klingler S, Winklmayr M, et al. GLI2-specific transcriptional activation of the bone morphogenetic protein/activin antagonist follistatin in human epidermal cells. J Biol Chem. 2008;283:12426-37.
282. Heath JK, Southby J, Fukumoto S, O'Keeffe LM, Martin TJ, Gillespie MT. Epidermal growth factor-stimulated parathyroid hormone-related protein expression involves increased gene transcription and mRNA stability. Biochem J. 1995;307 (Pt 1):159-67.
283. Hastings RH, Burton DW, Nefzi A, Montgrain PR, Quintana R, Deftos LJ. Combinatorial library discovery of small molecule inhibitors of lung cancer proliferation and parathyroid hormone-related protein expression. Cancer Biol Ther. 2010;10.